Aspects of Vortices and Hyperbolic Monopoles

COCKBURN, ALEXANDER,HUGH

Aspects of Vortices and Hyperbolic Monopoles

Alexander H. Cockburn

A thesis presented for the degree of
Doctor of Philosophy

Centre for Particle Theory
Department of Mathematical Sciences
University of Durham

May 2015

Dedicated to

Patrick Cockburn, Janet Montefiore, and Henry Cockburn

Aspects of Vortices and Hyperbolic Monopoles

Alexander H. Cockburn

Submitted for the degree of Doctor of Philosophy
May 2015

Abstract

This thesis discusses BPS monopoles in hyperbolic space and BPS vortices in the presence of magnetic impurities. We prove explicit formulae for the spectral curve and rational map of a JNR-type hyperbolic monopole, and we use these to study some Platonic examples as well as some new 1-parameter families analogous to Euclidean monopole scattering. Explicit fields and Braam-Austin data for axial hyperbolic monopoles of a particular mass are derived using a correspondence to 1-monopoles, and this data is deformed to give new 1-parameter families. Numerical techniques are used to study the effect of magnetic impurities on vortices on a flat background. Analytic results for vortices with magnetic impurities are found by adapting previous results on vortices on the hyperbolic plane and the 2-sphere.

Declaration

The work carried out in this thesis is based on research carried out in the Centre for Particle Theory, Department of Mathematical Sciences, in the University of Durham, UK. No part of this thesis has been submitted elsewhere for any other degree or qualification and it is all my own work unless referenced to the contrary in the text.

Chapters 1 and 2 contain introductory information which is used to place the rest of the thesis into context. Chapter 3 is based on work published in Nonlinearity in collaboration with Dr S. Bolognesi and Prof. P. M. Sutcliffe [BCS15], and care has been taken to indicate my own contribution. The work in Chapter 4 is my own, and has been published in J. Phys. A [Coc14]. Chapter 5 is also my own work, and is pending publication.

Acknowledgements

I would like to thank my supervisor Richard Ward for his guidance, encouragement, and constant support throughout my PhD. I am also particularly indebted to Paul Sutcliffe for patiently answering my monopole-related questions and kindly giving me the opportunity to participate in a very enjoyable collaboration. I am fortunate to have been at Durham at the same time as Stefano Bolognesi, to whom I am grateful both for our collaboration and for many stimulating discussions. Many thanks are also due to Derek Harland for helpful and encouraging conversations. Thanks to Andrew Iskauskas for proof-reading this thesis.

Many thanks to all the friends who have made Durham such an enjoyable place to live and study. Most importantly, special thanks go to my family for all their love and support over the years.

I am grateful to the UK Science and Technology Facilities Council for a studentship.

Contents

List of Figures

1

Introduction

1.1 Overview of the thesis

This thesis focuses on two separate topics: hyperbolic monopoles and vortices with magnetic impurities. The purpose of this Chapter is to provide background for the Chapters 3 and 4 on hyperbolic monopoles. The next Chapter will set the scene for the work on vortices and impurities in Chapter 5 by giving a brief introduction to vortices.

The first new results are presented in Chapter 3. In this Chapter we use the JNR ansatz for instantons to find new hyperbolic monopole solutions. This approach is shown to be very fruitful, and we present many explicit hyperbolic analogues of Euclidean monopoles, as well as some new examples. The work in Chapter 3 has been published as *Hyperbolic monopoles, JNR data, and spectral curves* [BCS15].

Chapter 4 addresses the problem of finding hyperbolic monopole solutions from a slightly different perspective. The work in this Chapter has been published as the sole-author paper *Symmetric hyperbolic monopoles* [Coc14]. As we will describe in this introductory Chapter, certain hyperbolic monopoles are equivalent to matrices satisfying algebraic constraints. The approach of Chapter 4 is to impose symmetry directly on these matrices. This gives many new examples of hyperbolic monopoles, some of which are generalisations of the examples presented in Chapter 3.

A way to introduce electric and magnetic impurities into the vortex Lagrangian while preserving a moduli space of solutions has recently been suggested [TW14]. While electric impurities were thoroughly explored in [TW14],

there remained some open questions regarding the effect of magnetic impurities on vortex solutions and dynamics. Chapter 5 answers some of these using a combination of numerical and analytical techniques.

1.2 INSTANTONS

Monopoles on both Euclidean and hyperbolic space are related to different dimensional reductions of the instanton equations, so we begin with a review of instantons before moving on to monopoles. Our exposition will draw both from [MS04] and the original papers.

We start with the Yang-Mills action on Euclidean $\mathbf{R}^4$ for an $SU(2)$-connection defined by the 1-form gauge potential A, which is

$$S = -\frac{1}{8}\int_{\mathbf{R}^4} \mathrm{Tr}(F \wedge *F), \tag{1.1}$$

where $F = dA + A \wedge A$ is the curvature of A. Applying an argument of a type due to Bogomolny gives:

$$S = \pm\frac{1}{8}\int_{\mathbf{R}^4} \mathrm{Tr}(F \wedge F) - \frac{1}{16}\int_{\mathbf{R}^4} \mathrm{Tr}((F \pm *F) \wedge *(F \pm *F)). \tag{1.2}$$

The second term is positive definite, which implies that the action is bounded below by the first term. The second Chern class I of the connection A is given by the integral formula

$$I = -\frac{1}{8\pi^2}\int_{\mathbf{R}^4} \mathrm{Tr}(F \wedge F),$$

so we have the topological lower bound

$$S \geq \pi^2 |I|.$$

We are interested in field configurations minimising S, and we see from (1.2) that this inequality is saturated if and only if

$$F = \pm * F. \tag{1.3}$$

These are the famous self-dual Yang-Mills equations (SDYM), and a finite action solution to these is called an instanton. The Yang-Mills equations originated in quantum field theory, where they describe quantum tunnelling effects

between topologically distinct vacua.

There has been an enormous amount of interest in solutions to SDYM and its dimensional reductions since they were introduced. A natural first question is to ask how many distinct instanton solutions there are for each I. Index theorems by Atiyah, Hitchin, and Singer [AHS77] and Schwartz [Sch77] show that the number of parameters needed to specify an I-instanton solution up to gauge equivalence is $8I$. The space of gauge-equivalent instanton solutions is called the moduli space.

The first explicit solution was the 1-instanton found by Belavin *et al.* [BPST75]. The BPST instanton is spherically-symmetric with action density localised around the centre of the sphere (these configurations were called 'pseudoparticles' in the older physical literature). There are 8 parameters describing a BPST instanton: 4 give the spatial position, 1 is an overall scale, and 3 give the orientation in the gauge group $SU(2)$, so dimension counting suggests that every 1-instanton is a BPST instanton, and in fact this is the case. For $I > 1$, the configuration generically resembles a superposition of I BPST instantons, each with 8 parameters describing position, scale, and gauge orientation, but this interpretation breaks down if the separation of the instantons is of the same order as their scale.

The BPST instanton was later shown to be a special case of a more general ansatz due to Corrigan, Fairlie, and 't Hooft [tH] [CF77]. In coordinates, the Corrigan-Fairlie-'t Hooft (CF'tH) ansatz is

$$A_\mu = \frac{i}{2}\sigma_{\mu\nu}\partial_\nu \log \rho, \tag{1.4}$$

where $\sigma_{i4} = \tau_i$, $\sigma_{ij} = \varepsilon_{ijk}\tau_k$, and τ_i $(i = 1, 2, 3)$ are the Pauli matrices. Inserting this ansatz into (1.3) gives the condition that the 'superpotential' ρ be harmonic. A family of I-vortex solutions is given by

$$\rho = 1 + \sum_{j=1}^{I} \frac{\lambda_j^2}{|x - \gamma_j|^2}, \tag{1.5}$$

where the weights $\{\lambda_j\}$ are positive real numbers and the poles $\{\gamma_j\}$ are points in $\mathbf{R}^4$. The apparent singularities at the poles are only an artefact of the gauge choice, and all gauge-invariant quantities are smooth. Naively this space of solutions is parametrised by $5I + 3$ real numbers (after including global $SU(2)$ orientations), and in fact different values of the parameters do lead to gauge-inequivalent solutions.

A fundamental feature of the SDYM equations, which we shall make use of at several points throughout this introduction, is their conformal invariance. This property was used by Jackiw, Nohl and Rebbi [JNR77] to extend the CF'tH ansatz by taking the superpotential

$$\rho = \sum_{j=0}^{I} \frac{\lambda_j^2}{|x - \gamma_j|^2}. \tag{1.6}$$

The logarithmic derivative in (1.4) removes one degree of freedom, so there are $5I + 7$ independent parameters. In contrast to the CF'tH ansatz there is no simple relation between the JNR parameters and the corresponding instanton. If $I = 1, 2$ then the number of parameters in the JNR ansatz appears to exceed the dimension of the moduli space, but it turns out that these extra parameters correspond to gauge degrees of freedom. For $I > 2$ dimension counting implies that there are other instanton solutions not obtainable from the JNR ansatz, and we need more sophisticated methods to find these.

1.3 The ADHM construction

A major breakthrough in the study of instantons was made by Ward [War77], who showed that instantons are in 1-1 correspondence with certain holomorphic bundles over the space of oriented lines in $\mathbf{R}^4$, called the twistor space. A complete classification of these bundles was given by Atiyah *et al.* [AHDM78]. By choosing suitable coordinates one can show that these bundles are equivalent to quaternionic matrices satisfying algebraic constraints, called the ADHM data. This is the version of the ADHM construction we shall describe below.

We use an identification of $\mathbf{R}^4$ with the quaternions $\mathbf{H}$, so that a point $x \in \mathbf{R}^4$ is written as $x_1 + ix_2 + jx_3 + kx_4$. The ADHM data for a charge I instanton is given by a pair of quaternionic matrices L and M, where L is an I-component row vector, and M is a symmetric $I \times I$ matrix. These are combined into

$$\widehat{M} = \begin{pmatrix} L \\ M \end{pmatrix}. \tag{1.7}$$

The ADHM constraint is

$$\widehat{M}^\dagger \widehat{M} = R_I, \tag{1.8}$$

where R_I is a non-singular, real $I \times I$ matrix. The advantage of the ADHM construction is that it replaces SDYM with a non-linear algebraic system, which is easier to solve than a complicated set of PDEs.

Note that there is a redundancy in the ADHM data

$$\widehat{M} \to \begin{pmatrix} q & 0 \\ 0 & \mathcal{O} \end{pmatrix} \widehat{M}\mathcal{O}^{-1}, \tag{1.9}$$

where q is a unit quaternion and $\mathcal{O} \in \mathrm{O}(I)$. A count of the free parameters which includes this redundancy and the constraint (1.8) gives the expected dimension of the moduli space $8I$.

To find the gauge field, one constructs the ADHM operator

$$\Delta(x) = \begin{pmatrix} L \\ M \end{pmatrix} - \begin{pmatrix} 0 \\ 1_I \end{pmatrix} x. \tag{1.10}$$

One then needs to find an $(I+1)$-component column vector Ψ with $\Psi^\dagger\Psi = 1$ that solves

$$\Psi^\dagger\Delta(x) = 0.$$

The gauge potential is given by

$$A_\mu = \Psi^\dagger\partial_\mu\Psi,$$

where the pure quaternion is regarded as an element of $su(2)$.

The ADHM constraints are more tractable than the SDYM equations, but they are still difficult and the general solution is not known. We can easily obtain a family of solutions by setting M to be diagonal and the elements of L to be positive and real, and it turns out that this is equivalent to the CF'tH ansatz. The i-th diagonal entry in M will be a pole in the CF'tH ansatz with weight L_i. Instanton solutions outside the 't Hooft/JNR ansätze have been found by completely solving for the ADHM constraints in the $I = 3$ case [CWS78] [KS83] or by imposing discrete symmetries acting in both 3 [SS99] and 4 [AS13] dimensions.

1.4 Magnetic monopoles

In this Section we review BPS monopoles, which are the major focus of this thesis. Dirac was the first to realise that magnetic monopoles could be sensibly introduced into electromagnetism, and that their charge has a topological nature [Dir31]. A non-zero magnetic charge would seem to rule out the existence of an electromagnetic gauge potential, but Dirac realised that the gauge potential need only be defined on local patches related by a gauge transformation on the overlap. The requirement that this gauge transformation be single-valued translates into a quantization condition for the magnetic charge. In mathematical terms, the gauge potential for a Dirac monopole corresponds to a connection on a principal $U(1)$-bundle over $\mathbf{R}^3 \setminus \{0\}$ with non-zero degree.

In the 70's 't Hooft and Polyakov discovered that magnetic monopoles occur in non-abelian Yang-Mills-Higgs theories and that unlike the Dirac monopole, which necessarily has a singularity, these solutions are completely smooth. The instantons of the previous Section are usually considered to be static objects, but for monopoles we are ultimately interested in their dynamics in theories with a time direction. The Yang-Mills-Higgs action on $\mathbf{R}^{1,3}$ with metric $(1,-1,-1,-1)$ is

$$S = \int \left(\frac{1}{8}\mathrm{Tr}(F_{\mu\nu}F^{\mu\nu}) - \frac{1}{4}\mathrm{Tr}(D_\mu \Phi D^\mu \Phi) + \frac{\lambda}{4}(1 - ||\Phi||^2)^2 \right) d^4x \qquad (1.11)$$

Here Φ is an adjoint scalar Higgs field valued in $su(2)$ and F is the curvature of an $SU(2)$-connection A.

The Lagrangian $L = \int \mathcal{L}\, d^3x$ can be split into kinetic and potential terms $L = T - V$ where

$$T = \int \left(-\frac{1}{4}\mathrm{Tr}(F_{i0}F_{i0}) - \frac{1}{4}\mathrm{Tr}(D_0\Phi D_0\Phi) \right) d^3x, \qquad (1.12)$$

and

$$V = \int \left(-\frac{1}{8}\mathrm{Tr}(F_{ij}F_{ij}) - \frac{1}{4}\mathrm{Tr}(D_i\Phi D_i\Phi) + \frac{\lambda}{4}(1 - ||\Phi||^2)^2 \right) d^3x. \qquad (1.13)$$

where $||\Phi||^2 = -\frac{1}{2}\mathrm{Tr}(\Phi^2)$. Ideally we would like to find the general solution of the second-order field equations coming from the variation of (1.11), but this is currently beyond analytical and numerical techniques. The first progress was made by 't Hooft and Polyakov, who gave numerical evidence of the existence

of a spherically-symmetric static solution minimising the potential (1.13) for all $\lambda \geq 0$. The interpretation of minimisers of V as magnetic monopoles comes from considering the projection $f = -\frac{1}{2}\mathrm{Tr}(F\Phi)/||\Phi||$ of the curvature in the direction of the Higgs field. Away from the monopole core the spatial part of this tensor exponentially approaches the field due to a magnetic point source.

Like the Dirac monopole, the charge of a non-abelian monopole has a topological nature which leads to its quantization. For physically reasonable solutions we require finite V, which implies that $||\Phi|| \to 1$ at spatial infinity. The asymptotic value of Φ along oriented lines through the origin therefore defines a map of of 2-spheres from the space of directions in $\mathbf{R}^3$ to the 2-sphere of unit-norm elements in $su(2)$. The total magnetic charge g of the monopole, defined as the flux of f through the 2-sphere at infinity, is related to the degree N of this map by $g = -2\pi N$. Smooth variations of the fields cannot change N, so the magnetic charge is conserved.

The most mathematically interesting case is when $\lambda = 0$, which is called the BPS limit. The static Yang-Mills-Higgs energy functional is then

$$E = \int_{\mathbf{R}^3} \mathcal{E}\,\mathrm{vol},$$

where

$$\mathcal{E}\,\mathrm{vol} = -\frac{1}{4}\mathrm{Tr}\left(F \wedge *F + D\Phi \wedge *D\Phi\right). \tag{1.14}$$

We retain the boundary condition that $||\Phi|| \to 1$ at spatial infinity. In the BPS limit we can again apply a Bogomolny argument:

$$-\frac{1}{4}\int_{\mathbf{R}^3} \mathrm{Tr}((F + *D\Phi) \wedge *(F + *D\Phi) - 2F \wedge D\Phi). \tag{1.15}$$

Note that we can rewrite $F \wedge D\Phi = D(F\Phi)$ because of the Bianchi identity $DF = 0$. Furthermore $\mathrm{Tr}(D(F\Phi)) = d\,\mathrm{Tr}(F\Phi)$, and since $\mathrm{Tr}(F\Phi)$ tends to the abelian projection f at infinity, we have

$$\frac{1}{2}\int_{\mathbf{R}^3} \mathrm{Tr}(F \wedge D\Phi) = \int_{S^2_\infty} f$$

by Stokes' theorem. The first term of (1.15) is positive, so we have the inequality

$$E \geq 2\pi N,$$

where N is the winding number of the Higgs field at infinity. This bound is saturated if and only if the Bogomolny equation

$$* F = D\Phi \tag{1.16}$$

is satisfied. Note that for solutions of the Bogomolny equation the asymptotic length of the Higgs field will have the form

$$||\Phi|| = 1 - \frac{N}{2r} + \mathcal{O}(r^{-2}).$$

We will also need Ward's formula [War82] for the energy density of BPS monopoles

$$\mathcal{E} = \frac{1}{2}\nabla^2||\Phi||^2. \tag{1.17}$$

To derive this formula first note that for solutions of the Bogomolny equation both terms in (1.14) are equal, so $\mathcal{E}\,\mathrm{vol} = -\frac{1}{2}\mathrm{Tr}(D\Phi \wedge *D\Phi)$. The Bianchi identity and the Bogomolny equation imply that $D * D\Phi = DF = 0$, and we have

$$-\frac{1}{2}\mathrm{Tr}(D\Phi \wedge *D\Phi) = -\frac{1}{2}\mathrm{Tr}(D(\Phi * D\Phi)) = d(-\frac{1}{2}\mathrm{Tr}(\Phi * D\Phi)) = -\frac{1}{2}d * d||\Phi||^2$$

which proves Ward's formula (1.17) since $\nabla^2 = - * d * d$ for functions on 3-manifolds.

Much of this thesis is ultimately motivated by the difficulty of solving the Bogomolny equation (1.16), which is far harder than SDYM. The dimension of the moduli space can be determined by index theorems to be $4N$ [Wei79b]; the interpretation is that, for each monopole, three moduli specify a position and one specifies a phase. Despite the fact that the space of solutions is known to be very large, only a few explicit ones are known. The first solution to be discovered was the $N = 1$ monopole by Prasad and Sommerfeld [PS75]. Their spherically-symmetric ansatz for the fields is

$$A_i^a = \frac{p(r) - 1}{2r^2}\varepsilon_{iak}x^k \text{ and } \Phi^a = \frac{q(r)x^a}{r}. \tag{1.18}$$

The resulting pair of ODEs has solution

$$p(r) = \coth 2r - \frac{1}{2r}$$
$$q(r) = \frac{2r}{\sinh 2r}.$$

The Prasad-Sommerfeld solution illustrates that even in the charge 1 sector monopole solutions are more complicated than instantons: the magnitude of the Higgs field involves a hyperbolic function of the spatial coordinates, while for instantons the ADHM construction implies that all gauge-invariant quantities can be given by rational functions. It turns out that there are no spherically-symmetric monopole solutions for $N > 1$ [WG76]. An explicit construction of an axial $N = 2$ monopole was given by Ward [War82] using twistor methods and later Prasad gave a general construction of axial monopoles of arbitrary charge [Pra81]. One of the first attempts to solve the Bogomolny equation was to exploit the fact that the Bogomolny equation (1.16) is related to the SDYM equations by dimensionally reducing in the x_4-direction and setting $A_4 = \Phi$, but initially only the Prasad-Sommmerfeld monopole could be rederived in this way [Man78].

Static monopole solutions are of course interesting in their own right, but an additional important motivation comes from a conjecture of Manton [Man82] that the geometry of the moduli space determines the low-energy monopole dynamics. In Manton's approximation, slow-moving monopoles are assumed to be close to static solutions so that the potential term (1.13) can be taken to be constant, and the dynamics are determined by the kinetic term (1.12). If we work in the gauge $A_0 = 0$ then this term is simply the standard L^2 norm of the tangent vector $(\dot{\Phi}, \dot{A}_\mu)$ to the configuration space at the point (Φ, A_μ). Since we are supposing that the evolution of the system stays close to the moduli space, this suggests that the dynamics should be governed by the standard L^2 metric on the moduli space, and the evolution of systems of monopoles should correspond to a geodesic of this metric. Stuart has proved this approximation rigorously for vortices [Stu94a] and monopoles [Stu94b]. We will give more details on the moduli space approximation in the case of vortices in Chapter 2.

The difficulty of solving the Bogomolny equation means that progress in finding metrics and geodesics has had to be rather indirect. Atiyah and Hitchin were able to find the metric on the 2-monopole moduli space just from its symmetry properties, while for higher charge monopoles some interesting geodesics have been obtained as fixed point sets of discrete symmetries acting on the moduli space. Many of these geodesics were found using certain correspondences between monopoles and other kinds of data, which we outline in the next Section.

1.5 The Nahm transform, spectral curves, and rational maps

Despite the lack of explicit monopole solutions we can extract a lot of information about the structure of the moduli space and the qualitative nature of some solutions via a number of different correspondences. The next few Sections contain a brief review of these.

1.5.1 The Nahm transform

Probably the most useful method for constructing solutions is Nahm's extension of the ADHM construction to monopoles [Nah80]. Just as for instantons, the construction is a $1-1$ correspondence between solutions to the Bogomolny equation and solutions to a simpler system, which in this case is a triplet of antihermitian $N \times N$ matrices depending on a parameter $s \in [-1, 1]$ and solving the Nahm equation

$$\frac{dT_i}{ds} = \frac{1}{2}\varepsilon_{ijk}[T_j(s), T_k(s)], \tag{1.19}$$

as well as the conditions:

1. $T_i(-s) = T_i^t(s)$;
2. The T_i must be regular on $(-1, 1)$, but have simple poles as $s \to \pm 1$. The residues R_i at the endpoints must form an irreducible representation of $su(2)$.

The fact that the Nahm equations are a set of ODEs makes them easier to solve than the Bogomolny equations. However, the Nahm equations are non-linear and still very difficult to solve, although some solutions which also satisfy conditions 1 and 2 have been found. The Nahm data corresponding to the Prasad-Sommerfeld 1-monopole is simply $T_i = 0$. Other non-trivial solutions have been found by imposing discrete Platonic symmetries, which gives algebraic constraints on the Nahm data [HMM95] [HS96c] [HS96b]. Even if one has a solution to the Nahm equations, performing the inverse transform to obtain the fields is also difficult and must usually be done numerically.

The Nahm transform and the ADHM construction fit into a general, unfinished mathematical programme of finding transforms for spaces of solutions to self-duality equations on different 4-manifolds. From this point of view the simplest version of the problem is to consider the self-duality equations on a

4-torus, which we can think of as the quotient of $\mathbf{R}^4$ by the action of a lattice group Λ. The Nahm transform will map a solution of SDYM on $\mathbf{R}^4/\Lambda$ to a solution on the dual torus $(\mathbf{R}^4)^*/\Lambda^*$ [BvB89]. SDYM on $\mathbf{R}^4$ can be considered to be the limit in which all four radii are sent to infinity, and the ADHM constraints can be considered to be the dimensional reduction of SDYM to zero dimensions. For monopoles three of the radii are taken to be infinite and one is zero, and the Nahm equations are the dimensional reduction of SDYM to one dimension.

1.5.2 Spectral curves

Hitchin introduced another correspondence between monopoles and an object called the spectral curve. The spectral curve is a Riemann surface whose points are defined to be the oriented lines γ along which Hitchin's scattering equation

$$(D_\gamma - i\Phi)v = 0 \tag{1.20}$$

has a normalisable solution. The set of oriented lines in $\mathbf{R}^3$, called the mini-twistor space, has a natural complex manifold structure: to see this, note that we can specify an oriented line uniquely by giving a unit vector $\widehat{\mathbf{v}} \in \mathbf{R}^3$ and a point on the plane perpendicular to $\widehat{\mathbf{v}}$ that the line passes through. This is precisely the same as choosing a point in the tangent bundle to $\mathbf{CP}^1$, and it turns out that the spectral curve is a complex curve in $T\mathbf{CP}^1$. Roughly speaking the points in the spectral curve are the lines passing through the monopole cores, and for multi-monopoles this interpretation improves as the distance between the monopoles increases. For a 1-monopole this is a precisely true statement, and the spectral curve is the set of lines passing through the centre of the monopole, called the 'star' at that point.

Hitchin has given a set of conditions for a complex submanifold of $T\mathbf{CP}^1$ to be the spectral curve corresponding to some monopole [Hit82]. Showing that a given curve satisfies Hitchin's constraints is difficult, but we can obtain explicit spectral curves using a connection to Nahm data. The Nahm equations can be written in Lax form

$$\frac{dT}{ds} = [T, T^+]$$

where

$$T = T_1 + iT_2 - 2iT_3\xi + (T_1 - iT_2)\xi^2$$
$$T^+ = -iT^3 + (T_1 - iT_2)\xi,$$

and ξ is a complex parameter. The existence of this Lax pair implies that the Nahm equations are integrable, and that the characteristic equation

$$P(\xi, \psi) := \det(\psi \mathbf{1}_N + T) = 0 \tag{1.21}$$

is the same for all values of s. If we identify the parameters (ξ, ψ) with coordinates on $T\mathbf{CP}^1$ so that ξ is a complex coordinate on the 2-sphere and ψ is a suitably normalised coordinate on the tangent plane at ξ, then the spectral curve is given by the polynomial (1.21).

Rotations around the origin of $\mathbf{R}^3$ act naturally on the spectral curve, which makes the spectral curve particularly convenient for analysing these symmetries. Another use of the spectral curve is to determine the asymptotic behaviour of submanifolds of the moduli space; if the spectral curve tends to a product as we vary a modulus then we can deduce that the asymptotic configuration consists of well-separated clusters of monopoles.

1.5.3 Rational maps

Another useful correspondence for monopoles was proved by Donaldson, who showed that there is a correspondence between the N-monopole moduli space and the space of based degree N rational maps from the 2-sphere to itself [Don84]. The correspondence is a bijection up to an overall phase for the rational map.

Defining the Donaldson rational map requires a choice of direction in $\mathbf{R}^3$, which is normally taken to be the positive x_3-direction. One then considers the scattering equation (1.20) in this direction. Generic solutions will grow exponentially as $x_3 \to \pm\infty$, but it turns out that there is always a solution that decays exponentially as $x_3 \to \infty$, and that this solution is unique up to a multiplicative constant. If we choose a gauge where $\Phi(0, 0, x_3) \to \tau_3$ as $x_3 \to \infty$ then as $x_3 \to -\infty$ this solution will have the asymptotic form

$$a \begin{pmatrix} 1 \\ 0 \end{pmatrix} |x_3|^{N/2} e^{-x_3} + b \begin{pmatrix} 0 \\ 1 \end{pmatrix} |x_3|^{-N/2} e^{x_3}.$$

We define a map $\mathcal{R} : \mathbf{C} \to \mathbf{C}$ by

$$\mathcal{R}(z, \bar{z}) = \frac{b(z, \bar{z})}{a(z, \bar{z})},$$

where $z = x_1 + ix_2$ is the point where the line intersects with the x_1x_2-plane.

Note that

$$[D_{\bar{z}}, D_3 - i\Phi] = 0,$$

and so the uniqueness of our solution to the scattering equation implies that $D_{\bar{z}}\mathcal{R} = 0$. In this gauge $D_{\bar{z}}$ approaches $\partial_{\bar{z}}$ as $x_3 \to -\infty$, so $\mathcal{R}$ is meromorphic. The boundary condition on Φ implies that we can compactify the x_1x_2-plane with a point at infinity, so we can interpret $\mathcal{R}$ as a function on $\mathbf{CP}^1$. $\mathcal{R}$ must therefore take the form

$$\mathcal{R}(z) = \frac{p(z)}{q(z)}.$$

The poles of $\mathcal{R}$ correspond to lines in the x_3 direction which have a normalisable solution as $x_3 \to \pm\infty$, and these are precisely the spectral lines in the x_3 direction. This shows that the denominator of $\mathcal{R}$ can be obtained from the spectral curve $P(\xi, \psi) = 0$ by $q(\psi) = P(0, \psi)$, so $\deg q = N$. The basing condition is $\mathcal{R}(\infty) = 0$, which implies that $\deg p < N$.

The choice of a direction in the construction of the Donaldson rational map breaks the natural symmetry of $\mathbf{R}^3$, and it is not known how the Donaldson rational maps associated with different choices of direction are related to each other. This means that the Donaldson rational map is not convenient for analysing rotational symmetries, apart from subgroups of the unbroken $SO(2)$ rotation group around the x_3-axis. Jarvis constructed a rational map more adapted to the rotational symmetries of $\mathbf{R}^3$ [Jar00]. To define the Jarvis rational map one chooses a basepoint in $\mathbf{R}^3$ and considers the scattering equation (1.20) along all half-lines terminating at that point. An analysis of the decay properties of the solutions yields a rational map of 2-spheres in a similar way to the Donaldson rational map.

The Jarvis rational map $\mathcal{R}$ corresponding to a given monopole is not unique; acting with a Möbius transformation on the target $\mathbf{CP}^1$ gives a rational map corresponding to the same monopole. This means that the monopole will be symmetric under some rotational symmetry group $K \subset SO(3)$ if to each $k \in K$ there corresponds a Möbius transformation M_k with

$$\mathcal{R}(k(z)) = M_k\mathcal{R}(z)$$

in such a way that the map $k \to M_k$ is a homomorphism from K to the group of Möbius transformations of the Riemann sphere.

A point that should be emphasized is that despite the variety of correspondences for monopoles, there are very few explicit examples of any of them corresponding to a given monopole. As we shall see in Chapters 3 and 4, this situation can be improved by moving to a hyperbolic space background.

1.6 Hyperbolic monopoles

The Bogomolny equation (1.16) makes sense on any Riemannian manifold, with the metric entering through the Hodge star operator. The Bogomolny equation is only integrable on spaces of constant curvature, and these are Euclidean space, hyperbolic space, and the 3-sphere (and their quotients). We will focus on hyperbolic space of curvature -1. In the ball model the metric is

$$ds^2(\mathbf{H}^3) = \frac{4(dX_1^2 + dX_2^2 + dX_3^2)}{(1-R^2)^2}\,, \tag{1.22}$$

where $R^2 = X_1^2 + X_2^2 + X_3^2$ and $R < 1$. We will also use the half-space model with metric

$$ds^2(\mathbf{H}^3) = \frac{1}{r^2}(dx_1^2 + dx_2^2 + dr^2). \tag{1.23}$$

The two models are related by the conformal transformation

$$x_1 + ix_2 = \frac{2X_1 + 2iX_2}{1 + R^2 - 2X_3}, \qquad r = \frac{1 - R^2}{1 + R^2 - 2X_3}. \tag{1.24}$$

Just as for Euclidean monopoles we need to set the magnitude of the Higgs field to be constant on the boundary, so in the ball model we require

$$\lim_{|X|\to 1} ||\Phi(X)|| = p,$$

where p is a positive constant called the Higgs mass. In the ball model the Higgs field again defines a map of 2-spheres $\Phi|_{R=1} : S^2 \mapsto S^2$, and the degree N determines the number of localised lumps of energy in a generic solution. The dimension of the moduli space is also $4N$.

In Euclidean space the freedom to rescale the spatial coordinates means that all Higgs masses are physically equivalent, but in hyperbolic space a rescaling of the Higgs mass $p \to \lambda p$ is equivalent to a rescaling of the curvature K of hyperbolic space $K \to K/\lambda^2$. We shall consider the background metric

to be fixed so that the Higgs mass becomes a modulus. Another important difference from Euclidean monopoles is that the decay conditions imply that the projection f of the gauge field in the Higgs direction defines a non-trivial abelian connection f_∞ on the boundary. In the Euclidean case, only the charge of the monopole can be detected from the connection at infinity.

The study of hyperbolic monopoles was initiated by Atiyah [Ati84], who proved results for hyperbolic monopoles similar to those for Euclidean monopoles described in the previous Section. In particular, there is a correspondence to spectral curves and rational maps of Donaldson type. The spectral curve can again be defined as the set of oriented geodesics along which the scattering equation (1.20) has a normalisable solution.

The space of oriented geodesics in $\mathbf{H}^3$, called the twistor space, has a natural complex manifold structure. Oriented geodesics in hyperbolic space are determined by their endpoints on $\partial\mathbf{H}^3 \cong \mathbf{CP}^1$, and we will choose coordinates so that (η, ζ) represents the oriented geodesic starting at $\widehat{\eta} = -1/\eta$ and ending at ζ. Geodesics cannot start and end at the same point, so the true twistor space is $\mathbf{CP}^1 \times \mathbf{CP}^1 \setminus \Delta$, where $\Delta = (\eta, \widehat{\eta})$ is the antidiagonal. In these coordinates the spectral curve corresponding to a monopole of degree N will take the form

$$P(\eta, \zeta) = \sum_{i=0, j=0}^{N} c_{ij} \eta^i \zeta^j = 0. \tag{1.25}$$

Just as for Euclidean monopoles, Atiyah proved that there is a set of constraints that a Riemann surface must satisfy in order to qualify as the spectral curve corresponding to some monopole. The spectral curve of a 1-monopole in the ball model at the point (X_1, X_2, X_3) is again the star or set of geodesics through the centre of the monopole, which is given by

$$2\eta\zeta(X_1 - iX_2) + \zeta(1 + R^2 - X_3) - \eta(1 + R^2 + X_3) - 2(X_1 + iX_2) = 0, \tag{1.26}$$

and in the half-space model this is

$$\eta\zeta(x_1 - ix_2) + \zeta - \eta(x_1^2 + x_2^2 + r^2) - (x_1 + ix_2) = 0. \tag{1.27}$$

Norbury and Romao have made progress in understanding the hyperbolic monopole moduli space using spectral curves [NR07].

Atiyah also proved an analogue of the Donaldson rational map for hyperbolic monopoles. Instead of choosing a direction, one considers solutions to the Hitchin scattering equation along geodesics starting at some basepoint on

the boundary, which we choose to be the north pole $\widehat{\eta} = \infty$. Along each of these geodesics there is a solution decaying at the $\widehat{\eta} = \infty$ end, and this solution is unique up a scalar multiple. We define $\mathcal{R}(z, \bar{z})$ to be the ratio of the decaying to the growing component at the $\zeta = z$ end. $\mathcal{R}$ again turns out to be meromorphic in z and we have a rational map of Riemann spheres of degree N. $\mathcal{R}$ is based in the sense that $\mathcal{R}(\infty) = 0$ and the denominator is equal, up to a constant multiple, to $P(0, z)$.

Jarvis and Norbury adapted the Jarvis rational map for Euclidean monopoles to a hyperbolic background in [JN97]. Their motivation for this was to investigate the behaviour of the moduli space as the Higgs mass varies. Atiyah conjectured that in the Euclidean limit $p \to \infty$ the moduli space of Euclidean monopoles should be recovered. Jarvis and Norbury proved that if one fixes a rational map and takes the Euclidean limit then the corresponding family of hyperbolic monopoles tends to the corresponding Euclidean monopole, proving Atiyah's conjecture.

In addition to spectral curves and rational maps, hyperbolic monopoles possess a correspondence to another type of holomorphic object that is not available to Euclidean monopoles. Murray, Norbury, and Singer have shown that every monopole of charge N is equivalent to a holomorphic embedding $q : \mathbf{CP}^1 \to \mathbf{CP}^N$ unique up to the action of $U(N + 1)$ on its image [MNS01]. An important property of this 'holomorphic sphere', proved in [MNS01], is that the connection at infinity is given by $f_\infty = q^*\omega$, where ω is the standard Kähler form on $\mathbf{CP}^N$ (the form associated to the Fubini-Study metric, which we shall make use of in a different context in Section 5.3). This has the important consequence that a hyperbolic monopole is determined by f_∞. Another property of the holomorphic sphere is that, in a sense, it ties together all the Donaldson rational maps defined at different basepoints: if $\mathcal{R}_\eta$ is the rational map defined using the basepoint η, then

$$\mathcal{R}_\eta = \pi_\eta \circ q,$$

where π_η is the projection onto a unique line $L_\eta \subset \mathbf{CP}^N$ that contains $q(\eta)$, although it is not known how to determine the line intrinsically from q.

At first sight it might appear that the only motivation for studying hyperbolic monopoles is their rich mathematical structure, but it turns out that in certain circumstances they are much simpler than their Euclidean counterparts. This is because of a connection between circle-invariant instantons and

hyperbolic monopoles. To see this, first note that $\mathbf{R}^4 \setminus \mathbf{R}^2$ and $\mathbf{H}^3 \times S^1$ with the standard metrics are conformally equivalent:

$$\begin{aligned} dx_1^2 + dx_2^2 + dx_3^2 + dx_4^2 &= dx_1^2 + dx_2^2 + dr^2 + r^2 d\chi^2 \\ &= r^2 \left(\frac{1}{r^2}(dx_1^2 + dx_2^2 + dr^2) + d\chi^2 \right), \end{aligned} \tag{1.28}$$

where we have set $(x_3, x_4) = (r\cos\chi, r\sin\chi)$. The conformal invariance of SDYM means that if an instanton is invariant under rotations in the χ direction then we can obtain a solution to the hyperbolic Bogomolny equation by dimensionally reducing in the χ direction and setting $\Phi = A_\chi$. The mass p of the monopole so obtained will necessarily be a half-integer, and the monopole charge is related to the instanton charge by $I = 2pN$. We described a variety of techniques to find explicit instanton solutions in Section (1.2), and in Chapters 3 and 4 we will adapt these to the circle-invariant case in order to find explicit hyperbolic monopole solutions, spectral curves, and rational maps. All of our new solutions will be in the simplest case $p = 1/2$, for which the instanton and monopole charges are equal.

1.7 The Braam-Austin construction

The existence of a Nahm transform for general hyperbolic monopoles is an open question, but from the discussion above we know that monopoles with half-integer mass must correspond to circle-invariant ADHM data. Braam and Austin analysed the circle-equivariant ADHM construction in detail [BA90] and showed that the ADHM data breaks up into a set of difference equations defined on a lattice with $2p$ sites.

To simplify our presentation of the Braam-Austin system we will follow [BA90] and restrict to $2p$ odd. For a monopole of charge N, the data consists of complex $N \times N$ matrices β_i, γ_i, and an N-row vector v. The β_i are defined on the even lattice points $i \in \{-2p+1, -2p+3, \ldots, 2p-1\}$, and the γ_i are defined on the odd lattice points $i \in \{-2p+2, -2p+4, \ldots, 2p-2\}$. This data

must satisfy the Braam-Austin equations

$$\gamma_i - \gamma_{-i}^t = 0 \tag{1.29}$$
$$\beta_i - \beta_{-i}^t = 0 \tag{1.30}$$
$$\beta_{i-1}\gamma_i - \gamma_i\beta_{i+1} = 0 \tag{1.31}$$
$$[\beta_i^\dagger, \beta_i] + \gamma_{i-1}^\dagger\gamma_{i-1} - \gamma_{i+1}\gamma_{i+1}^\dagger = 0 \tag{1.32}$$
$$[\beta_{2p-1}, \beta_{2p-1}^\dagger] + v^t\overline{v} - \gamma_{2p-2}^\dagger\gamma_{2p-2} = 0 \tag{1.33}$$

The Braam-Austin equations have a gauge freedom. Suppose that g_i is a sequence of unitary matrices for $i \in \{-2p+1, -2p+3, \ldots, 2p-1\}$ with $g_i = \overline{g}_{-i}$. Then it is easy to see that the gauge transformations

$$\begin{aligned} \beta_i &\to g_i\beta_i g_i^{-1} \\ \gamma_i &\to g_{i-1}\gamma_i g_{i+1}^{-1} \\ v &\to v g_{-2p+1}^{-1} \end{aligned} \tag{1.34}$$

leave the Braam-Austin equations invariant. We also have the freedom to multiply v by a unit norm complex number.

Solutions to the Braam-Austin equations correspond to a hyperbolic monopole in the half-space model. The complete integrability of these equations was discussed by Murray and Singer in [MS00]. In particular they associate a spectral curve to the evolution equations (1.29)-(1.32). This curve is given in terms of the Braam-Austin data as

$$\det(\eta\zeta - \eta(\gamma_{i-1}^\dagger\gamma_{i-1} + \beta_i^\dagger\beta_i) + \zeta - \beta_i^\dagger) = 0. \tag{1.35}$$

If the boundary condition (1.33) is also satisfied then this spectral curve coincides with the one associated to the corresponding monopole via scattering along geodesics. This is the hyperbolic analogue of the formula (1.21) for the spectral curve of a Euclidean monopole in terms of its Nahm data. Note that if we set $\gamma_{2i+1} = \frac{1}{2}p\mathbf{1}_N + T_3(\frac{2i+1}{p})$ and $\beta_{2i} = \frac{1}{2}(T_1(\frac{2i}{p}) + iT_2(\frac{2i}{p}))$, then in the Euclidean limit $p \to \infty$ we recover the Nahm equations.

For general p the Braam-Austin equations have proven to be even harder to solve than the Nahm equations. The simplest case is $N = 1$. Here we can use the gauge freedom to set $\beta_i = \beta$ and $\gamma_i = \gamma = v$ independent of i, where β is a complex number, and γ is a positive real number. (β, γ) can then be interpreted as coordinates for the 1-monopole in the upper half-plane. Murray

and Singer gave axial $N = 2$ solutions for all p in [MS00], and in [War99] Ward gave the general solution to equations (1.29)-(1.32) for $N = 2$ and all p, but without considering the boundary condition (1.33). Part of the problem seems to be that the Braam-Austin construction is adapted to the half-space model of hyperbolic space where rotational symmetries do not act naturally, so one cannot impose Platonic symmetries as easily as in the Euclidean case to construct higher charge monopoles.

The exception to this is when $p = 1/2$. In this case the Braam-Austin data just consists of a single complex matrix β and a complex row vector v. If we identify these with standard form ADHM data: $L = v$, $M = \beta$, then the Braam-Austin conditions become the usual ADHM constraints (1.8). For ADHM data of this form the spectral curve formula (1.35) becomes:

$$\det\left(\eta\zeta M^\dagger + \zeta - \eta\widehat{M}^\dagger\widehat{M} - M\right) = 0. \tag{1.36}$$

Braam and Austin also gave a general formula for the rational map [BA90] in terms of Braam-Austin data, which in this case is

$$\mathcal{R}(z) = L(z - M)^{-1}L^t. \tag{1.37}$$

1.8 Geometry of the hyperbolic monopole moduli space

The geodesic approximation is not available for hyperbolic monopoles because the usual metric defined using the overlap of zero modes is divergent. Nevertheless the moduli space of hyperbolic monopoles has been shown to possess interesting geometric structure. Hyperbolic monopoles are defined by the connection they induce on the boundary, and the L^2 metric on this space is well-defined. This is the metric we shall consider in Section 3.5.

Hitchin has derived a family of four-dimensional self-dual Einstein metrics parametrised by an integer $k \geq 3$ [Hit96] and showed that for $k > 4$ these are also natural metrics on the moduli space of centred 2-monopoles with $p = (k - 4)/4$. More recently Bielawski and Schwachhöfer, following earlier work of Nash [Nas07], showed that the hyperbolic monopole moduli space has a new kind of geometry they call 'pluricomplex', and Figueroa-O'Farrill and Gharamti have shown [FOG14] that this geometry can be understood as a

consequence of supersymmetry. The relationship of all these constructions to hyperbolic monopole dynamics is an interesting open question.

2

Introduction to vortices

The purpose of this Chapter is to review previous work on vortices in order to introduce chapter 5, which is independent of the work on hyperbolic monopoles of chapters 3 and 4.

The standard action for vortices is:

$$\int \left(-\frac{1}{4} F_{\mu\nu} F^{\mu\nu} + \frac{1}{2} \overline{D_\mu \phi} D^\mu \phi - \frac{\lambda}{8} (1 - |\phi|^2)^2 \right) d^3x, \tag{2.1}$$

where ϕ is a complex scalar field coupled to a $U(1)$ gauge field A_μ, $D_\mu \phi = (\partial_\mu - iA_\mu)\phi$ is the covariant derivative and the gauge field strength is $F_{\mu\nu} = \partial_\mu A_\nu - \partial_\nu A_\mu$. The coupling λ is taken to be positive to ensure that the energy is bounded below. The signature of the metric is taken to be $(1, -1, -1)$.

If we impose the equation of motion associated with the gauge choice $A_0 = 0$ as a constraint:

$$\partial_i \dot{A}_i + \frac{i}{2} (\bar{\phi}\dot{\phi} - \phi\dot{\bar{\phi}}) = 0, \tag{2.2}$$

then the Lagrangian can then be written in terms of kinetic and potential energies as $L = T - V$, where (for $i = 1, 2$):

$$T = \frac{1}{2} \int \left(|\dot{\phi}|^2 + \dot{A}_i \dot{A}_i \right) d^2x, \tag{2.3}$$

$$V = \frac{1}{2} \int \left(D_i \phi \overline{D_i \phi} + B^2 + \frac{\lambda}{4} (|\phi|^2 - 1)^2 \right) d^2x, \tag{2.4}$$

and the total conserved energy is $E = T + V$. We are interested in solutions to the second order field equations coming from the variation of the action (2.1), and as for monopoles the simplest first step is to consider static fields minimising the potential energy (2.4). It is quite straightforward to numerically

solve the field equations coming from (2.4) by choosing an axial ansatz for the fields, and the solution resembles a localised lump of energy. Note that finite energy requires that $|\phi| \to 1$ as $|x| \to \infty$, defining a map $\phi|_\infty : S^1 \to U(1)$. The degree N of this map is related to the magnetic flux through the plane by $2\pi N = \int B\, d^2x$.

The coupling λ determines the qualitative behaviour of the vortex solutions: if $\lambda > 1$ then the vortices repel, and if $\lambda < 1$ then the vortices attract. This can be seen by investigating the stability properties of coincident N-vortex solutions, which have been proved to exist for all $\lambda > 0$ [BC89]. The N-vortex configuration has rigorously been shown to be unstable for $\lambda > 1$ and stable for $\lambda < 1$ [GS00]. One can also obtain qualitative information on the effect of λ by comparing the energy of a superposition of N well-separated vortices with the coincident N-vortex configuration, or by making a point-particle approximation of the vortices [Spe97].

The most mathematically interesting case is when $\lambda = 1$. For this value of the coupling we can apply a standard Bogomolny argument to the potential energy:

$$V = \frac{1}{2}\int \left((D_1 \pm iD_2)\phi\overline{(D_1 \pm iD_2)\phi} + \left(B \mp \frac{1}{2}(1 - |\phi|^2) \right)^2 \pm B \right) d^2x,$$

implying the topological bound

$$E \geq \left| \frac{1}{2}\int B\, d^2x \right| = \pi|N|.$$

For $N > 0$, this bound is saturated when first-order vortex equations are satisfied:

$$D_1\phi + iD_2\phi = 0 \tag{2.5}$$

$$B - \frac{1}{2}(1 - |\phi|^2) = 0. \tag{2.6}$$

The sign of N is reversed by a reflection, so we shall only consider the $N > 0$ case. In contrast to the Bogomolny equation, no non-trivial explicit solutions to the vortex equations are known, even in the $N = 1$ sector.

Given how λ controls the qualitative behaviour of the vortices, one might expect that when $\lambda = 1$ there are no static forces between vortices and that a moduli space of solutions exists. Weinberg took the first step towards showing this by proving that the number of linearised deformations around a given

solution orthogonal to gauge orbits is $2N$ [Wei79a]. Taubes later proved [JT80] that given N points $\{z_r\}_{1\leq r\leq N}$ on $\mathbf{R}^2$ there does indeed exist a solution for which ϕ vanishes precisely at the points z_r, and that this solution is unique up to gauge equivalence.

Taubes also made the important observation that we can rewrite (2.5) and (2.6) as a single equation. If we define the gauge-invariant quantity $f = \log|\phi|^2$, then we can use (2.5) to solve for A_μ in terms of ϕ and substitute this expression into (2.6) to obtain

$$\nabla^2 f + 1 - e^f = 4\pi \sum_{r=1}^{N} \delta^2(z - z_r). \tag{2.7}$$

The moduli space approximation can be applied to BPS vortices in the same way as for BPS monopoles. To implement this we need to find tangent vectors to the moduli space, which corresponds to finding solutions $(\delta\phi, \delta A_i)$ to the linearised version of (2.5) and (2.6). These solutions will only correspond to a tangent vector to the space of field configurations solving the Bogomolny equations; to make sure they represent a tangent vector to the moduli space we also require that $(\delta\phi, \delta A_i)$ be orthogonal to infinitesimal gauge orbits. The inner product of an infinitesimal gauge transformation $(i\varepsilon\phi, \partial_i\varepsilon)$ with $(\delta\phi, \delta A_i)$ is

$$\frac{1}{2}\int \left(\delta A_i \partial_i \varepsilon - \frac{i}{2}\varepsilon(\bar{\phi}\delta\phi - \phi\delta\bar{\phi})\right) d^2x = -\frac{1}{2}\int \left(\partial_i \delta A_i + \frac{i}{2}(\bar{\phi}\delta\phi - \phi\delta\bar{\phi})\right) \varepsilon \, d^2x,$$

so we require that $(\delta\phi, \delta A_i)$ satisfies Gauss's law (2.2). The moduli space metric is then given by

$$g_{ab} = \int \left(\delta_a A_i \delta_b A_i + \delta_a\phi\delta_b\bar{\phi} + \delta_a\bar{\phi}\delta_b\phi\right) d^2x. \tag{2.8}$$

This moduli space metric for vortices was explored in detail by Samols [Sam92] and Strachan [Str92] who showed that the integral (2.8) localises around the vortex zeroes. If we expand f around a zero z_r as

$$f = \log|z - z_r|^2 + a_r + \frac{1}{2}\left(b_r(z - z_r) + \bar{b}_r(\bar{z} - \bar{z}_r)\right) + c_r(z - z_r)^2 + d_r(z - z_r)(\bar{z} - \bar{z}_r) + \bar{c}_r(\bar{z} - \bar{z}_r)^2 + \ldots \tag{2.9}$$

then Samols' formula for the metric is

$$ds^2 = \pi \sum_{r,s=1}^{N} \left(\delta_{rs} + 2\frac{\partial \bar{b}_s}{\partial z_r} \right) dz_r \, d\bar{z}_s. \tag{2.10}$$

Unfortunately the symmetry arguments used by Atiyah and Hitchin for the 2-monopole metric do not extend to the 2-vortex case. Samols was able to calculate the metric (2.10) numerically for $N = 2$ and showed that the moduli space approximation compares well with full numerical solutions of the second-order field equations for vortex impact speeds up to around 0.4 of the speed of light.

Analytic progress can be made by changing the background. The action (2.1) makes sense on any background of the form $X \times \mathbf{R}$, where X is an arbitrary Riemann surface. At critical coupling we can apply a Bogomolny argument to the static energy, and in isothermal coordinates for which the metric takes the diagonal form $ds^2 = \Omega(x_1, x_2)(dx_1^2 + dx_2^2)$, the resulting Bogomolny equations are

$$D_1\phi + iD_2\phi = 0 \tag{2.11}$$

$$B - \frac{\Omega}{2}(1 - |\phi|^2) = 0, \tag{2.12}$$

and Samols' formula generalises to

$$ds^2 = \pi \sum_{r,s=1}^{N} \left(\Omega(z_r)\delta_{rs} + 2\frac{\partial \bar{b}_s}{\partial z_r} \right) dz_r \, d\bar{z}_s. \tag{2.13}$$

.

Witten showed that the vortex equations on a hyperbolic background of curvature $-1/2$ are integrable [Wit76]. Witten's motivation for solving this system was to find instanton solutions. The vortex equations on this background are actually the dimensional reduction of the SDYM equations (1.3) over a 2-sphere, a fact which relies on a conformal equivalence between $\mathbf{R}^4 \setminus \mathbf{R}^1$ and $\mathbf{H}^2 \times S^2$. By solving these hyperbolic vortex equations Witten was able to give the first multi-instanton solutions. Strachan later used these solutions to write down an explicit metric on the space of centred 2-vortices in [Str92].

Bradlow proved a simple obstruction to the existence of vortex solutions on compact surfaces [Bra90]. Integrating the second Bogomolny equation (2.12) over X gives the inequality

$$A \geq 4\pi N. \tag{2.14}$$

This inequality is saturated when $\phi = 0$ everywhere, and the interpretation is that each vortex takes up area 4π. A particularly interesting case is when X is a 2-sphere, which Baptista and Manton have analysed close to the Bradlow bound. Baptista and Manton were able to give approximate vortex solutions and moduli space metrics in this limit [BM03].

In Chapter 5 we will adapt the results on all these different backgrounds to the introduction of magnetic impurities.

3

Hyperbolic monopoles from the JNR ansatz

In Chapter 1 we described how hyperbolic monopoles of half-integer mass can be obtained from circle-invariant instantons, and how instanton solutions can be easily obtained from the JNR ansatz. This Chapter explores the hyperbolic monopoles corresponding to circle-invariant JNR-type instantons. The idea is simply to place the JNR poles on the fixed-point set of the circle action, which corresponds to the boundary of hyperbolic space. The hyperbolic monopole so obtained will have mass 1/2 and will inherit any symmetries enjoyed by the configuration of poles. We will review this construction in Section 3.1 below.

[MS14] used this approach to give explicit expressions for the fields of various Platonic hyperbolic analogues of some well-known Euclidean monopoles which are only known from their Nahm data, showing that in this sense the $p = 1/2$ hyperbolic case is more tractable. In this Chapter we go further by giving explicit Braam-Austin data for JNR-type monopoles in Section 3.2 as well as proving simple formulae for the spectral curves and rational maps in terms of the free JNR data. This allows us to present the spectral curves and rational maps corresponding to previously given Platonic examples in Section 3.3, and in Section 3.4 we derive 1-parameter families of dihedrally-symmetric hyperbolic monopoles, some of which are analogues of known geodesics in the moduli space of Euclidean monopoles.

As we mentioned in the introduction, the L^2-metric on the space of abelian connections defined by hyperbolic monopoles on the boundary gives a finite metric on the hyperbolic monopole moduli space. We will present an integral formula for this metric on the space of JNR data in Section 3.5, and we will also

verify that the moduli space metric for a 1-monopole is again hyperbolic space. The 1-parameter families of this Chapter are geodesics of this metric, because they are fixed point-sets of discrete group actions which are also symmetries of the metric.

The results of this Chapter were published in the journal Nonlinearity with the title *Hyperbolic monopoles, JNR data, and spectral curves* [BCS15]. My own contributions consist of a proof of the rational map formula (3.15) and a proof of the change of basis matrices in appendix A. The figures in this Chapter are due to Paul Sutcliffe.

3.1 HYPERBOLIC MONOPOLES FROM JNR DATA

The circle invariance of the instanton is obtained by placing all the JNR poles in the plane $r = 0$, so that the superpotential (1.6) takes the form

$$\rho = \sum_{j=0}^{N} \frac{\lambda_j^2}{|x_1 + ix_2 - \gamma_j|^2 + r^2}, \tag{3.1}$$

where the poles γ_j are complex constants. We can use the superpotential (3.1) and the expression (1.4) for the gauge potential to obtain an explicit expression for the Higgs field magnitude. Firstly

$$\begin{aligned} A_\chi &= \sigma_{\chi\mu}\partial_\mu \log\rho \\ &= \frac{ir}{2\rho}\left(-(\tau_1\cos\chi + \tau_2\sin\chi)\frac{\partial\rho}{\partial x_1} + (\tau_1\sin\chi - \tau_2\cos\chi)\frac{\partial\rho}{\partial x_2} - \tau_3\frac{\partial\rho}{\partial r}\right). \end{aligned}$$

To dimensionally reduce to $\mathbf{H}^3$ we must transform to a χ-independent gauge. This is achieved by the gauge transformation $A \to gAg^{-1} - dgg^{-1}$ where $g = \exp(i\chi\tau_3/2)$. Then

$$A_\chi \to gA_\chi g^{-1} - \partial_\chi g g^{-1} = -\frac{ir}{2\rho}\left(\tau_1\frac{\partial\rho}{\partial x_1} + \tau_2\frac{\partial\rho}{\partial x_2} + \tau_3\left(\frac{\partial\rho}{\partial r} + \frac{\rho}{r}\right)\right),$$

from which the magnitude squared of the Higgs field $\Phi = A_\chi$ can be read off:

$$||\Phi||^2 = \frac{r^2}{4\rho^2}\left(\left(\frac{\partial\rho}{\partial x_1}\right)^2 + \left(\frac{\partial\rho}{\partial x_2}\right)^2 + \left(\frac{\rho}{r} + \frac{\partial\rho}{\partial r}\right)^2\right). \tag{3.2}$$

Taking the limit of this formula as $r \to 0$ shows that $p = 1/2$ for JNR-type monopoles. Ward's formula (1.17) remains true on any background, since we

derived it covariantly, so we can obtain the energy density by acting with the Laplace-Beltrami operator on $||\Phi||^2$. In coordinates this energy density is:

$$\mathcal{E} = \frac{1}{\sqrt{g}}\partial_i(\sqrt{g}g^{ij}\partial_j||\Phi||^2), \tag{3.3}$$

where g_{ij} are the metric components and $g = \det g_{ij}$.

The symmetries of a hyperbolic monopole are most readily seen in the ball model, where the poles γ_j correspond to the Riemann sphere coordinates of $N+1$ points on the S^2 boundary of $\mathbf{H}^3$. If the weights are chosen to be

$$\lambda_j^2 = 1 + |\gamma_j|^2, \tag{3.4}$$

then they are all equal after a conformal transformation to the unit ball model. We shall refer to the choice (3.4) as canonical weights. For canonical weights the symmetry of the set of points $\{\gamma_j\}$, regarded as points on the Riemann sphere, is inherited as a symmetry of the hyperbolic monopole. This Riemann sphere is the boundary of the unit ball model and spatial rotations act as $SU(2)$ Möbius transformations on the Riemann sphere.

The JNR ansatz (3.1) reduces to the 't Hooft ansatz

$$\rho = 1 + \sum_{j=1}^{N} \frac{\lambda_j^2}{|x_1 + ix_2 - \gamma_j|^2 + r^2} \tag{3.5}$$

by taking the limit $\lambda_0^2 = 1 + |\gamma_0|^2 \to \infty$. Thus in considering the symmetry of a monopole obtained from the 't Hooft form one must bear in mind that there is a pole, with canonical weight, at the point ∞ on the Riemann sphere.

The N-monopole moduli space $\mathbf{M}_N$ has dimension $4N-1$ but the JNR ansatz (3.1) has $3N+3$ real parameters. The associated monopole fields are unchanged if ρ is multiplied by a constant, so only the relative weights are of relevance in the JNR form, which reduces the JNR parameter count by one to $3N+2$. If $N \geq 3$ then all these parameters are independent and the JNR construction produces a $(3N+2)$-dimensional subspace $\mathbf{M}_N^{\mathrm{JNR}}$ of the $(4N-1)$-dimensional monopole moduli space $\mathbf{M}_N$. Note that for $N=3$ this matches the dimension of the full moduli space, and it seems likely that $\mathbf{M}_3^{\mathrm{JNR}} = \mathbf{M}_3$. If $N=1$ then the JNR ansatz is equivalent to the 't Hooft ansatz (3.5), as the two can be related by an action of the conformal group. This reduces the parameter count to 3, which is the correct dimension and $\mathbf{M}_1^{\mathrm{JNR}} = \mathbf{M}_1$. For $N=2$ there are three poles, which therefore automatically lie on a circle.

For poles on a circle there is an action of the conformal group that moves the poles around the circle and acts on their weights [JNR77]. This reduces the number of independent parameters in the JNR ansatz by one, leaving the correct dimension 7.

In summary, for the value $p = \frac{1}{2}$ in hyperbolic space of curvature -1, we have the result that for $N \leq 3$ the dimension of the moduli space of JNR generated N-monopoles is $\dim(\mathbf{M}_N^{\mathrm{JNR}}) = \dim(\mathbf{M}_N) = 4N - 1$, and it seems likely that all these N-monopoles can be obtained using the JNR construction. However, if $N > 3$ then $\dim(\mathbf{M}_N^{\mathrm{JNR}}) = 3N + 2 < 4N - 1 = \dim(\mathbf{M}_N)$, so a large class of monopoles can be obtained using the JNR construction, but certainly not all monopoles. Note that any monopole obtained from the JNR data (3.1) can be acted upon by a spatial rotation to map it to a monopole that is obtained from the 't Hooft data (3.5). The required spatial rotation is simply one that rotates any of the $N + 1$ poles on the Riemann sphere to the point ∞. The fact that this pole has canonical weight in 't Hooft form is no loss of generality, because in JNR form only the relative weights are relevant.

3.2 Spectral curves and rational maps from JNR data

As described in Section 1.3 the 't Hooft form of the instanton (3.5) corresponds to the ADHM matrix

$$\mathcal{M} = \begin{pmatrix} \lambda_1 & \lambda_2 & \cdots & \lambda_N \\ \gamma_1 & & & \\ & \gamma_2 & & \\ & & \ddots & \\ & & & \gamma_N \end{pmatrix}. \tag{3.6}$$

Extending this to the more general JNR form (3.1) is a little more involved because the JNR data does not come in a natural format to fit into the standard form of the ADHM matrix, so an appropriate change of basis needs to be found.

Explicitly, the ADHM matrix is given in terms of the JNR data by

$$\widehat{M} = S\Gamma V, \quad \text{where} \quad \Gamma = \begin{pmatrix} \lambda_1\gamma_0 & \lambda_2\gamma_0 & \cdots & \lambda_N\gamma_0 \\ \lambda_0\gamma_1 & & & \\ & \lambda_0\gamma_2 & & \\ & & \ddots & \\ & & & \lambda_0\gamma_N \end{pmatrix}. \tag{3.7}$$

Here $S \in \mathrm{O}(N+1)$ and $V \in GL(N, \mathbf{R})$ perform the required change of basis and must satisfy the equation

$$S \begin{pmatrix} \lambda_1 & \lambda_2 & \cdots & \lambda_N \\ \lambda_0 & & & \\ & \lambda_0 & & \\ & & \ddots & \\ & & & \lambda_0 \end{pmatrix} V = \begin{pmatrix} 0 & 0 & \cdots & 0 \\ 1 & & & \\ & 1 & & \\ & & \ddots & \\ & & & 1 \end{pmatrix}. \tag{3.8}$$

For $N = 1$ and $N = 2$ the required matrices S and V can be found in [Osb81] and in the special case that all the $N+1$ weights are equal the matrices are presented in [AS13] for arbitrary N. Here we require the general solution, which is

$$V_{ij} = \begin{cases} 0 & \text{if } i > j \\ p_i/(\lambda_0 p_{i-1}) & \text{if } i = j \\ -\lambda_i\lambda_j p_j p_{j-1}/\lambda_0 & \text{if } i < j \end{cases} \tag{3.9}$$

and

$$\begin{aligned} S_{i1} &= \lambda_0\lambda_{i-1}p_{i-1}p_{i-2} && \text{for } \; i = 1, \ldots, N+1 \\ S_{1j} &= -\lambda_{j-1}p_N && \text{for } \; j = 2, \ldots, N+1 \\ S_{ij} &= \lambda_0 V_{j-1,i-1} && \text{for } \; i, j = 2, \ldots, N+1, \end{aligned} \tag{3.10}$$

where we have introduced the notation $p_i = (\sum_{j=0}^{i} \lambda_j^2)^{-1/2}$, for $i = 0, \ldots, N$ together with $p_{-1} = p_N$ and $\lambda_{-1} = \lambda_0$. A proof that S and V perform the required change of basis is given in the Appendix. It can be checked that this general solution reduces to the previously known special cases in [Osb81, AS13]. The 't Hooft case is recovered in the limit $\lambda_0^2 = 1 + |\gamma_0|^2 \to \infty$, where S and $\lambda_0 V$ both become the identity matrix.

Substituting the above expressions into the formula (1.36) provides an explicit construction of the spectral curve in terms of JNR data. Although this appears to be a rather cumbersome procedure, in fact it yields a very elegant result, as we now explain. First of all, for 't Hooft data the diagonal form of M in the ADHM matrix (3.6) allows the determinant formula (1.36) to be easily calculated, producing the result

$$\prod_{j=1}^{N}(\zeta-\gamma_j)(1+\eta\bar{\gamma}_j)-\eta\sum_{j=1}^{N}\lambda_j^2\prod_{\substack{k=1\\k\neq j}}^{N}(\zeta-\gamma_k)(1+\eta\bar{\gamma}_k)=0. \tag{3.11}$$

Note that, as required, this formula is invariant under permutations of the N poles, γ_j for $j=1,\ldots,N$ together with their weights λ_j^2. Next we recall that 't Hooft data is simply JNR data with a pole at ∞ with canonical weight. We know how rotations act on both spectral curves and JNR data, so we can easily generalise (3.11) to arbitrary JNR data $\{(\lambda_j,\gamma_j)\}_{0\leq j\leq N}$. We first rescale all the weights so that the weight of γ_0 is canonical. We can then rotate using the Möbius transformation

$$z\to\frac{\gamma_0 z+1}{-z+\gamma_0} \tag{3.12}$$

to bring γ_0 to ∞. The poles and weights transform as

$$\gamma_k\to\gamma_k'=\frac{\gamma_0\gamma_k+1}{-z+\gamma_k}\quad\text{and}\quad\lambda_j^2\to\lambda_j'^2=\frac{1+|\gamma_j'|^2}{1+|\gamma_j|^2}\lambda_j^2.$$

After the rotation the data is in 't Hooft form, so the spectral curve is (3.11) for the data $\{(\lambda_j',\gamma_j')\}_{1\leq j\leq N}$. We can obtain the spectral curve of the original configuration by performing the inverse of (3.12) on (η,ζ):

$$(\eta,\zeta)\to\left(\frac{\eta\gamma_0+1}{-\eta+\gamma_0},\frac{\zeta\gamma_0+1}{-\zeta+\gamma_0}\right),$$

and the result is

$$\sum_{j=0}^{N}\lambda_j^2\prod_{\substack{k=0\\k\neq j}}^{N}(\zeta-\gamma_k)(1+\eta\bar{\gamma}_k)=0. \tag{3.13}$$

Equation (3.13) is one of the main results of this Chapter, providing a simple explicit formula for the spectral curve in terms of free JNR data. There is an obvious invariance of this formula under permutations of all $N+1$ poles, together with their weights, and it degenerates to the formula (3.11) in the 't Hooft limit $\lambda_0^2=1+|\gamma_0|^2\to\infty$. An obvious consequence of equation (3.13)

is that the spectral curve contains all geodesics that connect any pair of JNR poles. Before we go on to present some example spectral curves using this formula, we shall first consider the construction of rational maps from JNR data.

The rational map takes a particularly simple form for 't Hooft data, because M is diagonal in the ADHM matrix (3.6). Applying (1.37) in this case yields

$$\mathcal{R} = \sum_{j=1}^{N} \frac{\lambda_j^2}{z - \gamma_j}, \tag{3.14}$$

which reveals that the interpretation of the 't Hooft parameters as poles and weights in the harmonic function that determines the instanton conveniently extends to the same interpretation of poles and weights for the rational map.

The generalization of the rational map formula (3.14) to the JNR case is more complicated. In particular, it cannot be obtained using the same rotation trick that we used to obtain the JNR spectral curve from the 't Hooft case, because the rational map involves scattering along geodesics that originate at ∞ and only rotations that leave this point fixed can be applied. We therefore use the following alternative strategy to determine the JNR rational map. The denominator is obtained by using the fact that it is equal (up to a constant multiple) to the spectral curve (3.13) evaluated at $(\eta, \zeta) = (0, z)$. The numerator is then obtained by the requirement that the rational map must be invariant under any permutation of the $N+1$ poles and weights, together with the fact that it must reduce to the 't Hooft rational map (3.14) in the limit $\lambda_0^2 = 1 + |\gamma_0|^2 \to \infty$. A natural candidate is

$$\mathcal{R} = \left\{ \sum_{i=0}^{N} \sum_{j=i+1}^{N} \lambda_i^2 \lambda_j^2 (\gamma_i - \gamma_j)^2 \prod_{\substack{k=0 \\ k \neq i,j}}^{N} (z - \gamma_k) \right\} \Big/ \left\{ \left(\sum_{i=0}^{N} \lambda_i^2 \right) \left(\sum_{j=0}^{N} \lambda_j^2 \prod_{\substack{k=0 \\ k \neq j}}^{N} (z - \gamma_k) \right) \right\}. \tag{3.15}$$

The conditions we used to derive this formula are not really sufficient to prove it; they are consistent with the appearance in the numerator of any symmetric polynomial in the λ_j of degree less than $4N$, for example. Below we give a direct proof of this formula using the definition (1.37) together with the ADHM matrix (3.7) and the change of basis matrices (3.9) and (3.10). This proof was my contribution to our joint paper [BCS15], along with the proof in Appendix A.

Proof. The proof involves a formal expansion in z^{-1}. The coefficients q_I are defined by

$$L(z-M)^{-1}L^t = \sum_{I=1}^{\infty} q_I z^{-I}, \tag{3.16}$$

and we define Q_I similarly to be the coefficient of z^{-I} in the expansion of (3.15).

To prove the rational map formula we need to show that $q_I = Q_I$, which we accomplish by proving that both sets of coefficients satisfy the same inductive relation, together with $q_1 = Q_1$.

To begin, we expand the left hand side of (3.16) to give

$$q_I = LM^{I-1}L^t.$$

From the $(N+1)\times(N+1)$ matrix S, given by (3.10), we define the $N\times(N+1)$ matrix S' by removing the top row of S. Furthermore, we define this removed row to be S''. With this decomposition of S and the corresponding decomposition (1.7) of the ADHM matrix, equation (3.7) becomes

$$L = S''\Gamma V \quad \text{and} \quad M = S'\Gamma V,$$

and therefore

$$q_{I+1} = LM^I L^t = S''\Gamma(VS'\Gamma)^I VV^t\Gamma^t(S'')^t.$$

Note that

$$\begin{aligned}(VS')_{ab} &= \sum_{i=1}^{N} V_{ai}S_{i+1,b} = \sum_{i=1}^{N}\frac{1}{\lambda_0}S_{i+i,a+1}S_{i+1,b}\\ &= \frac{1}{\lambda_0}(\delta_{a+1,b} - S_{1,a+1}S_{1b}) \quad \text{(since } S \text{ is an orthogonal matrix)}\\ &= \frac{1}{\lambda_0}(U^t - (S''')^t S'')_{ab},\end{aligned} \tag{3.17}$$

and similarly

$$VV^t = \frac{1}{\lambda_0^2}(1 - (S''')^t S'''), \tag{3.18}$$

where U is the $(N+1)\times N$ matrix obtained from the $N\times N$ identity matrix by adding an extra top row of zeros, and we have defined the N-component row vector S''' by $(S''')_i = (S'')_{i+1}$. The next step is to prove the following

induction relation for the q_I:

$$q_I = \sum_{J=1}^{I-1} a_J q_{I-J} + b_I, \tag{3.19}$$

where we have introduced

$$a_I = -\frac{1}{\lambda_0^I} S''\Gamma(U^t\Gamma)^{I-1}(S''')^t,$$

and

$$b_I = \frac{1}{\lambda_0^{I-1}} S''\Gamma(U^t\Gamma)^{I-1}VV^t\Gamma^t(S'')^t.$$

We will use another inductive argument to prove (3.19). Suppose that for some K with $1 \leq K \leq I-1$ we have

$$q_I = \frac{1}{\lambda_0^{K-1}} S''\Gamma(U^t\Gamma)^{K-1}(VS'\Gamma)^{I-K}VV^t\Gamma^t(S'')^t + \sum_{J=1}^{K-1} a_J q_{I-J}. \tag{3.20}$$

Then using (3.17):

$$\begin{aligned} q_I =& \frac{1}{\lambda_0^K} S''\Gamma(U^t\Gamma)^{K-1}(U^t - (S''')^t S'')\Gamma(VS'\Gamma)^{I-K-1}VV^t\Gamma^t(S'')^t + \sum_{J=1}^{K-1} a_J q_{I-J} \\ =& \frac{1}{\lambda_0^K} S''\Gamma(U^t\Gamma)^{K}(VS'\Gamma)^{I-K-1}VV^t\Gamma^t(S'')^t + \sum_{J=1}^{K} a_J q_{I-J}. \end{aligned}$$

The relation (3.20) is trivially true for $K = 1$, so by induction it must be true for $K = I$, and this proves the induction relation (3.19).

The key point is that $U^t\Gamma$ is diagonal, so a_I can be calculated to be

$$a_I = -p_N^2 \sum_{j=1}^{N} \lambda_j^2 \gamma_j^{I-1}(\gamma_j - \gamma_0),$$

and using (3.18) we can calculate b_I to be

$$\begin{aligned} b_I = \Bigg\{ & \sum_{j=1}^{N} \lambda_j^2 \gamma_j^{I-1}(\gamma_j - \gamma_0)^2 \\ & - p_N^2 \left(\sum_{j=1}^{N} \lambda_j^2 \gamma_j^{I-1}(\gamma_j - \gamma_0) \right) \left(\sum_{k=1}^{N} \lambda_k^2 (\gamma_k - \gamma_0) \right) \Bigg\} p_N^2. \end{aligned}$$

As the rational map is invariant under permutations of the poles and weights then the coefficients q_I must be too. Taking (3.19), exchanging (γ_0, λ_0) with (γ_k, λ_k) and summing over k from 0 to N yields, after a long but straightforward manipulation,

$$(N+1)q_I = \sum_{J=1}^{I-1} \alpha_J q_{I-J} + \beta_I, \tag{3.21}$$

where

$$\alpha_I = -p_N^2 \sum_{j=0}^{N} \sum_{k=0}^{N} \lambda_j^2 \gamma_j^{I-1} (\gamma_j - \gamma_k),$$

and

$$\beta_I = p_N^4 \sum_{j=0}^{N} \sum_{k=j+1}^{N} \lambda_j^2 \lambda_k^2 (\gamma_j - \gamma_k) \left((N+1)(\gamma_j^I - \gamma_k^I) - \left(\sum_{l=0}^{N} \gamma_l \right) (\gamma_j^{I-1} - \gamma_k^{I-1}) \right).$$

We now show that the induction relation (3.21) is also true for the Q_I. From (3.15), after multiplying by the denominator of the left hand side and cancelling an overall factor of $\prod_{j=0}^{N}(z - \gamma_j)$, we find that

$$p_N^2 \sum_{i=0}^{N} \sum_{j=i+1}^{N} \lambda_i^2 \lambda_j^2 (\gamma_i - \gamma_j) \left(\frac{1}{z - \gamma_i} - \frac{1}{z - \gamma_j} \right) = \left(\sum_{I=1}^{\infty} Q_I z^{-I} \right) \left(\sum_{j=0}^{N} \frac{\lambda_j^2}{z - \gamma_j} \right).$$

Expanding this relation in z^{-1} and comparing coefficients produces the induction relations

$$Q_{I-1}\widetilde{\alpha}_1 + Q_{I-2}\widetilde{\alpha}_2 + \cdots + Q_1 \widetilde{\alpha}_{I-1} = \widetilde{\beta}_I p_N^2, \tag{3.22}$$

where

$$\widetilde{\alpha}_I = \sum_{j=0}^{N} \lambda_j^2 \gamma_j^{I-1} \quad \text{and} \quad \widetilde{\beta}_I = \sum_{j=0}^{N} \sum_{k=j+1}^{N} \lambda_j^2 \lambda_k^2 (\gamma_j - \gamma_k)(\gamma_j^{I-1} - \gamma_k^{I-1}).$$

We will call (3.22) the I-th of these induction relations. The $\widetilde{\alpha}_I$ are related to the α_I by

$$(N+1)\widetilde{\alpha}_{I+1} = \widetilde{\alpha}_I \left(\sum_{k=0}^{N} \gamma_k \right) - \frac{\alpha_I}{p_N^2}.$$

Substituting this identity into (3.22) gives

$$\sum_{J=1}^{I-1} Q_{I-J} \left(p_N^2 (N+1) \widetilde{\alpha}_{J+1} + \alpha_J \right) = \left(\sum_{k=0}^{N} \gamma_k \right) \widetilde{\beta}_I p_N^4.$$

Subtracting this from $p_N^2(N+1)$ times the $(I+1)$-th of the induction relations (3.22), gives

$$(N+1)Q_I - \sum_{J=1}^{I-1} \alpha_J Q_{I-J} = p_N^4 \left((N+1)\widetilde{\beta}_{I+1} - \left(\sum_{k=0}^{N} \gamma_k \right) \widetilde{\beta}_I \right) = \beta_I.$$

This shows that Q_I and q_I satisfy the same induction relation.

It is easy to check that

$$q_1 = Q_1 = p_N^4 \sum_{i=0}^{N} \sum_{j=i+1}^{N} \lambda_i^2 \lambda_j^2 (\gamma_i - \gamma_j)^2,$$

so $q_I = Q_I$ for all I, and this completes the proof. □

In the following Section we illustrate the use of our spectral curve and rational map formulae by calculating some examples with Platonic symmetry. However, we first conclude this Section by considering the single monopole and the axial N-monopole.

For $N = 1$ the 't Hooft form gives all 1-monopoles and the spectral curve is the star (1.27) with point $x_1 + ix_2 = \gamma_1$ and $r = \lambda_1$. In particular, taking $\gamma_1 = 0$ with canonical weight gives the spectral curve $\eta - \zeta = 0$, for a 1-monopole at the origin, with rational map $\mathcal{R} = 1/z$.

Taking canonical weights and $\gamma_j = \omega^j$, for $j = 0, \ldots, N$, where $\omega = e^{\frac{2\pi i}{N+1}}$, yields the axially symmetric spectral curve

$$\mathcal{A}_N = \sum_{i=0}^{N} (-1)^i \eta^i \zeta^{N-i} = 0 \tag{3.23}$$

and the rational map $\mathcal{R} = 1/z^N$. Although the set of poles appears to have only a dihedral D_{N+1} symmetry, the enhancement to axial symmetry is a consequence of the previously mentioned fact that when all poles lie on a circle there is an action of the conformal group that moves the poles around the circle and acts on their weights. The axial symmetry is manifest in the spectral curve (3.23) as the invariance under $(\eta, \zeta) \to (e^{i\theta}\eta, e^{i\theta}\zeta)$, corresponding to a rotation around the X_3-axis by an arbitrary angle θ. The symmetry is evident in the rational map as the relation $\mathcal{R}(e^{i\theta}z) = e^{-iN\theta}\mathcal{R}(z)$, where we recall that a rational map is defined modulo multiplication by a constant phase.

This is one of the few examples in which the full symmetry of the monopole is apparent from the rational map, because the action of this symmetry group

happens to fix the point $z = \infty$. If a monopole is symmetric under a transformation that moves the point ∞ on the Riemann sphere boundary of hyperbolic space, then the rational map cannot detect this symmetry, because in general it is not known how to explicitly relate the based rational map $\mathcal{R}(z)$, with $\mathcal{R}(\infty) = 0$, to a rational map that is based at a different point than ∞.

Note that if the monopole is of JNR type then the formula (3.15) allows the calculation of the rational map based at an arbitrary point z_∞, since we know how the Möbius transformation that moves z_∞ to ∞ acts on the JNR poles and weights. We can then apply (3.15) to the rotated poles and weights and finally obtain the rational map based at z_∞ by replacing z by its image under the Möbius transformation. In principle this means we could calculate the required line in $\mathbf{CP}^N$ on which to project the holomorphic sphere to obtain the rational maps based at z_∞.

The above axial monopoles are positioned at the point $(X_1, X_2, X_3) = (0, 0, 0)$, but for future reference it will be useful to have the spectral curve of the axial 2-monopole with position $(X_1, X_2, X_3) = (0, 0, b)$. This is obtained by taking canonical weights with poles $\gamma_j = \frac{(1+b)}{(1-b)}\omega^j$ for $j = 0, 1, 2$, where $\omega = e^{2\pi i/3}$. The resulting spectral curve is

$$(1+b)^4\eta^2 + (1-b)^4\zeta^2 - (1-b^2)^2\eta\zeta = 0. \tag{3.24}$$

3.3 PLATONIC SPECTRAL CURVES

In this Section we use the explicit formulae derived in the previous one to present the spectral curves and rational maps of some Platonic examples. The monopoles are obtained by placing the poles on the boundary with the same symmetries as the Platonic solid, and with canonical weight. The Higgs field magnitudes and energy densities of these monopoles were presented in [MS14], so the results of this Section are complementary to that study.

A convenient choice for the positions of the poles is given by the standard Klein polynomials, which are defined to be the polynomials with roots at the stereographic projections of the vertices or edge/face centres. The lowest charge example of a Platonic monopole is the tetrahedral 3-monopole, obtained by taking the roots of the Klein polynomial associated with the vertices of a tetrahedron:

$$\mathcal{T}_v(\gamma) = \gamma^4 + 2i\sqrt{3}\gamma^2 + 1.$$

Explicitly, the poles are $\gamma_0 = \frac{1+i}{\sqrt{3}+1}$, $\gamma_1 = -\gamma_0$, $\gamma_2 = \gamma_0^{-1}$, $\gamma_3 = -\gamma_0^{-1}$, and equation (3.13) with canonical weights gives the spectral curve

$$(\eta - \zeta)^3 + \frac{i}{\sqrt{3}}(\eta + \zeta)(\eta\zeta + 1)(\eta\zeta - 1) = 0. \tag{3.25}$$

This spectral curve was derived previously in [NR07] by imposing invariance under generators of the tetrahedral group

$$(\eta, \zeta) \mapsto (-\eta, -\zeta), \qquad (\eta, \zeta) \mapsto \left(\frac{\eta - i}{\eta + i}, \frac{\zeta - i}{\zeta + i}\right) \tag{3.26}$$

and using Atiyah's algebro-geometric constraints to fix the remaining parameters. Note that restricting the curve (3.25) to the diagonal $\eta = \zeta$ determines the spectral geodesics that pass through the origin as

$$\mathcal{T}_e(\zeta) = \zeta(\zeta^4 - 1) = 0,$$

where we recognize $\mathcal{T}_e$ as the Klein polynomial for the edges of the tetrahedron. Applying formula (3.15) allows us to obtain the associated rational map

$$\mathcal{R} = \frac{5iz^2 + \sqrt{3}}{\sqrt{3}z^3 + iz}, \tag{3.27}$$

where the C_2 symmetry $\mathcal{R}(-z) = -\mathcal{R}(z)$ is manifest, but not the full tetrahedral symmetry.

The octahedral 5-monopole is obtained from six poles (with canonical weights) on the vertices of an octahedron, given by the roots of the Klein polynomial

$$\mathcal{O}_v(\gamma) = \gamma(\gamma^4 - 1),$$

including the root at ∞. As one pole is at ∞ this example is of 't Hooft form and applying formula (3.11) results in the spectral curve

$$(\eta - \zeta)\Big((\eta^4 - 1)(\zeta^4 - 1) + 8\eta\zeta(\eta^2 + \zeta^2)\Big) = 0, \tag{3.28}$$

which is invariant under the generators of the octahedral group

$$(\eta, \zeta) \mapsto (i\eta, i\zeta), \qquad (\eta, \zeta) \mapsto \left(\frac{\eta - i}{\eta + i}, \frac{\zeta - i}{\zeta + i}\right). \tag{3.29}$$

Restricting to the diagonal $\eta = \zeta$ makes the first factor in (3.28) vanish identically but the condition that the second factor also vanishes is

$$\mathcal{O}_f(\zeta) = \zeta^8 + 14\zeta^4 + 1 = 0, \tag{3.30}$$

where $\mathcal{O}_f$ is the Klein polynomial for the face centres of the octahedron. Equation (3.14) for the rational map from 't Hooft data yields

$$\mathcal{R} = \frac{9z^4 - 1}{z^5 - z}, \tag{3.31}$$

with denominator equal to the Klein polynomial $\mathcal{O}_v(z)$. Note that the fact that the denominator of the rational map is the Klein polynomial for the vertices of the polyhedron is generic if the Klein polynomial is in an orientation in which there is a root at ∞. This follows immediately from (3.14).

Our last Platonic example is the remaining JNR-type monopole presented in [MS14], which is the icosahedral 11-monopole. The vertex Klein polynomial for the icosahedron is

$$\mathcal{Y}_v(\gamma) = \gamma^{11} + 11\gamma^6 - \gamma, \tag{3.32}$$

where the orientation is such that one root is at ∞. Taking the canonical weight poles as the roots of (3.32) and using (3.11) we obtain the substantial spectral curve

$$\begin{aligned}
&(\eta - \zeta)\Big(\eta^{10}\zeta^{10} + 11(\eta^{10}\zeta^5 + \eta^5\zeta^{10} - \eta^5 - \zeta^5) \\
&-75(\eta^9\zeta^6 + \eta^6\zeta^9 - \eta^4\zeta - \eta\zeta^4) - 50(\eta^8\zeta^7 + \eta^7\zeta^8 - \eta^3\zeta^2 - \eta^2\zeta^3) \\
&+25(\eta^9\zeta + \eta\zeta^9 - \eta^8\zeta^2 - \eta^2\zeta^8) + 100(\eta^7\zeta^3 + \eta^3\zeta^7) \\
&-225(\eta^6\zeta^4 + \eta^4\zeta^6) + 746\eta^5\zeta^5 - \eta^{10} - \zeta^{10} + 1\Big) = 0,
\end{aligned} \tag{3.33}$$

that is invariant under the following generators of the icosahedral group, where $\omega = e^{2\pi i/5}$,

$$\begin{aligned}
(\eta, \zeta) &\mapsto (\omega\eta, \omega\zeta), \\
(\eta, \zeta) &\mapsto \left(\frac{(\omega^3 - 1)\eta + \omega - \omega^2}{(\omega - \omega^2)\eta + 1 - \omega^3}, \frac{(\omega^3 - 1)\zeta + \omega - \omega^2}{(\omega - \omega^2)\zeta + 1 - \omega^3}\right).
\end{aligned}$$

The first factor in (3.33) automatically vanishes on the diagonal $\eta = \zeta$ and the second factor vanishes when

$$\mathcal{Y}_f(\zeta) = \zeta^{20} - 228\zeta^{15} + 494\zeta^{10} + 228\zeta^5 + 1 = 0,$$

which is the Klein polynomial for the face centres of the icosahedron. For this example the rational map is

$$\mathcal{R} = \frac{26z^{10} + 86z^5 - 1}{z^{11} + 11z^6 - z}, \tag{3.34}$$

where the denominator is indeed $\mathcal{Y}_v(z)$, with the obvious C_5 symmetry $\mathcal{R}(\omega z) = \mathcal{R}(z)/\omega$.

3.4 Dihedral one-parameter families

A number of interesting geodesics in the moduli space of Euclidean monopoles have been found by searching for submanifolds invariant under the action of a discrete symmetry subgroup of the metric. The fixed-point sets of such group actions are necessarily geodesic submanifolds, and we can arrange for these submanifolds to be 1-dimensional by a judicious choice of symmetry group. The aim of this Section is to investigate the parallel story for hyperbolic monopoles by imposing dihedral symmetries. As discussed in the introduction the geodesic approximation is not available for hyperbolic monopoles, so one should simply regard the results in this Section as some interesting one-parameter families of symmetric static hyperbolic monopoles. However, they do bear a striking resemblance to similar symmetric families in Euclidean space that indeed describe symmetric monopole scattering. It seems sensible to regard these families as the hyperbolic versions of corresponding Euclidean scatterings.

Dihedral symmetry is particularly useful in finding these 1-parameter families and is a natural extension of the results in the previous Section, since the Platonic symmetry groups have dihedral subgroups. Of course, we shall actually be imposing the symmetry within the moduli space $\mathbf{M}_N^{\mathrm{JNR}}$, and there are three different ways to obtain symmetric families of JNR data, as follows. The first type of one-parameter family involves moving the positions of the poles around the Riemann sphere with the associated weights at their canonical values. The second type involves fixed positions for the poles but a variation of the weights from their canonical values. Finally, the third type involves

simultaneously varying the positions of the poles together with non-canonical weights. We shall provide examples of all three types of families with dihedral symmetry. Dihedral symmetry is not the only finite symmetry group that is useful in generating families of monopoles, as we illustrate with a cyclic and a tetrahedral example. We will show in Chapter 4 that many of the families presented in this Section admit generalisations to higher charges.

3.4.1 3-MONOPOLES WITH D_2 SYMMETRY

This example is of the first type, which is perhaps the most obvious method to construct a symmetric family, since the symmetry of the monopole is simply the symmetry of the points on the sphere corresponding to the positions of the poles. The one-parameter family is given by $a \in (-1, 1)$ where we take the four poles

$$\gamma_0 = \sqrt{\frac{1+a}{1-a}} e^{i\pi/4},\ \gamma_1 = -\gamma_0,\ \gamma_2 = 1/\gamma_0,\ \gamma_3 = -1/\gamma_0,$$

with canonical weights, giving an obvious dihedral D_2 symmetry. The spectral curve is

$$(\eta - \zeta)\left(\eta^2 + \zeta^2 - \frac{4a^2}{1-a^2}\eta\zeta\right) + ia(\eta+\zeta)(\eta\zeta+1)(\eta\zeta-1) = 0, \qquad (3.35)$$

and is invariant under

$$(\eta, \zeta) \mapsto (-\eta, -\zeta), \qquad (\eta, \zeta) \mapsto \left(\frac{1}{\eta}, \frac{1}{\zeta}\right), \qquad (3.36)$$

which generate the D_2 subgroup of the tetrahedral group (3.26). Note that the change of sign $a \mapsto -a$ is equivalent to the $\pi/2$ rotation $(\eta, \zeta) \mapsto (i\eta, i\zeta)$, which is also clear from considering the positions of the poles.

We can determine the behaviour of this 3-monopole family by looking at particular relevant values of a. If $a = 0$ then the poles are at the vertices of a square, so the configuration is axial, and if $a = 1/\sqrt{3}$ then we obtain the same configuration of poles as for the tetrahedral example in the previous Section. The fact that $a \to -a$ corresponds to a rotation by $\pi/2$ implies that $a = -1/\sqrt{3}$ corresponds to the dual tetrahedral configuration. The spectral curve gives us asymptotic information about the limit $a \to \pm 1$; in this limit the spectral curve tends to the curve $(\eta - \zeta)\eta\zeta = 0$, and we see by comparison with (1.26) that this is the product of three stars for monopoles with positions

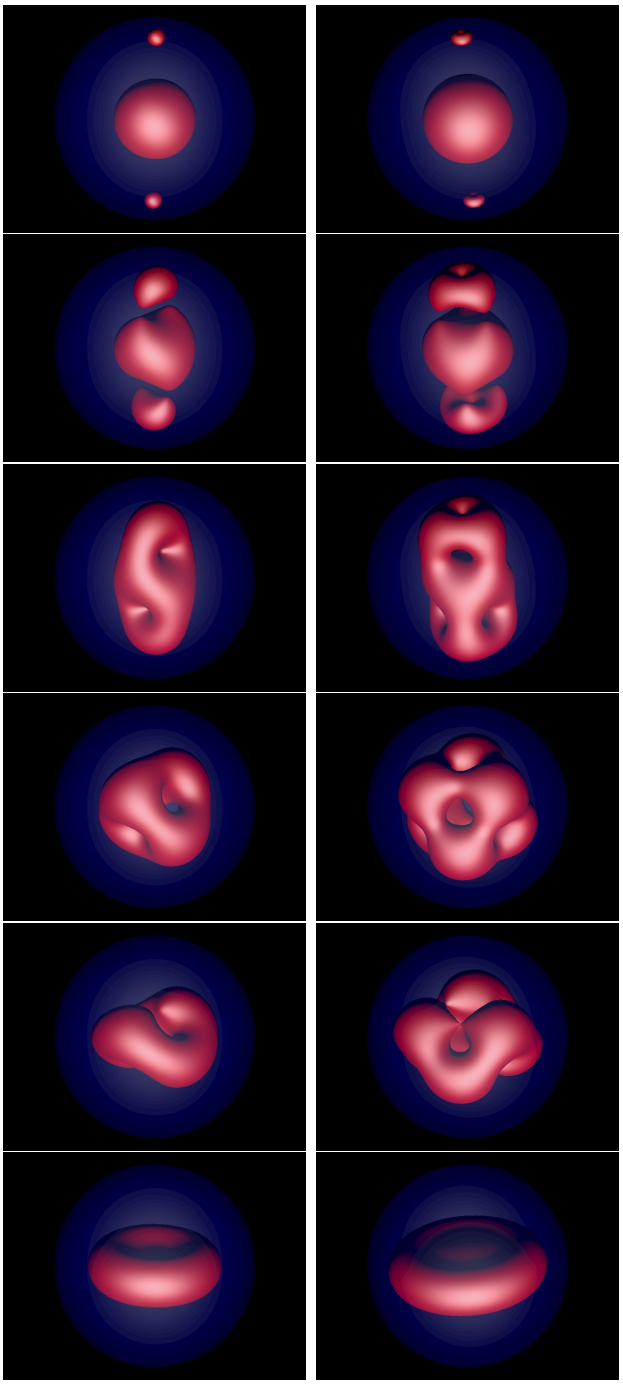

Figure 3.1: Energy density isosurfaces: first column D_2 symmetric 3-monopoles, second column D_3 symmetric 5-monopoles.

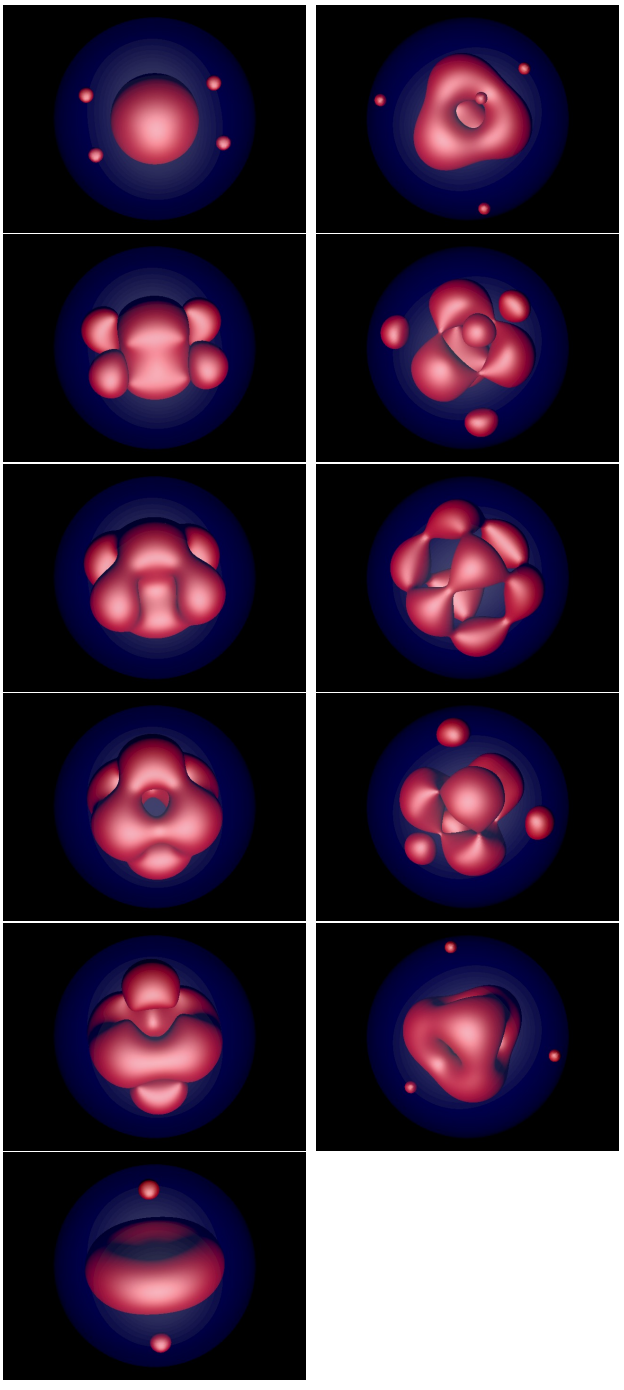

Figure 3.2: Energy density isosurfaces: first column D_4 symmetric 5-monopoles, second column tetrahedrally symmetric 7-monopoles.

(X_1, X_2, X_3) given by $(0, 0, 0)$ and $(0, 0, \pm 1)$. We therefore find that as a is varied from -1 to 1, two monopoles from infinity approach a monopole at the origin from opposite directions along a line, form the tetrahedral 3-monopole, then the axial 3-monopole, and then separate in the same manner along the same line but with a rotation by $\pi/2$ about the line.

Equation (3.2) gives a lengthy but explicit expression for $||\Phi||^2$ for the whole family and hence we can obtain an explicit form for the energy density by applying the Laplace-Beltrami operator. This process generates the energy density isosurfaces displayed in the first column of Figure 3.1, which correspond to increasing values of $a \in (-1, 0]$. Plots for $a > 0$ are not shown since they are simply 90° rotations of the plots for $a < 0$. The blue sphere in the energy density plots represents the boundary of hyperbolic space and, of course, the metric in the ball-model of hyperbolic space appears to shrink the monopoles as they approach the boundary. This one-parameter family is the hyperbolic analogue of the twisted line scattering of three Euclidean monopoles presented in [HS96a], where the spectral curve is known via a solution of the Nahm equation but the Higgs field and energy density is only available by means of a numerical computation of the Nahm transform. A generalisation of this twisted-line family to all N is presented in subsection 4.3.3.

The rational map for this one-parameter family is obtained using equation (3.15) and is given by

$$\mathcal{R} = \frac{ia(3 + a^2)z^2 + 1 - a^2}{(1 - a^2)(z^3 + iaz)}, \tag{3.37}$$

with the manifest C_2 symmetry $\mathcal{R}(-z) = -\mathcal{R}(z)$. In Section 4.3.3 we will present a Jarvis-type rational map for this family.

3.4.2 5-MONOPOLES WITH D_3 SYMMETRY

The 3-monopole twisted line family of the previous subsection can be generalised to N-monopoles with a $D_{(N+1)/2}$ symmetry, for N odd. The canonically weighted poles are taken to be

$$\gamma_j = \sqrt{\frac{1+a}{1-a}} e^{\frac{i\pi(1+4j)}{N+1}}, \quad \gamma_{j+(N+1)/2} = 1/\gamma_j, \quad j = 0, 1, \ldots, (N-1)/2.$$

This configuration has manifest symmetry under the generators of $D_{(N+1)/2}$ consisting of a rotation by $2\pi/(N+1)$ around the X_3-axis, and a rotation by

π around the X_1-axis. The replacement $a \to -a$ corresponds to a rotation by $4\pi/(N+1)$ around the X_3-axis.

In this Section we shall focus on the $N = 5$ family, which was previously identified in the Euclidean context in [HS96a]. The associated spectral curves and energy densities for this geodesic were not investigated, but the hyperbolic version can easily be studied in explicit detail using our new approach.

The spectral curve is

$$\eta^5 - \zeta^5 - \frac{2ia}{\sqrt{1-a^2}}(\eta^5\zeta^3 - \eta^3\zeta^5 + \eta^2 - \zeta^2) - \frac{(1+3a^2)}{(1-a^2)}(\eta^4\zeta - \eta\zeta^4) + \frac{(1+10a^2+5a^4)}{(1-a^2)^2}(\eta^3\zeta^2 - \eta^2\zeta^3) = 0, \quad (3.38)$$

which is invariant under the generators of the D_3 symmetry group:

$$(\eta, \zeta) \mapsto (\omega\eta, \omega\zeta), \qquad (\eta, \zeta) \mapsto \left(\frac{1}{\eta}, \frac{1}{\zeta}\right), \quad (3.39)$$

where $\omega = e^{2\pi i/3}$. There is octahedral symmetry when $a = -\frac{1}{\sqrt{3}}$ and the curve becomes

$$(\eta-\zeta)\big(\eta^4+\zeta^4-2(\eta^3\zeta+\eta\zeta^3)+9\eta^2\zeta^2+\sqrt{2}i(\eta^4\zeta^3+\eta^3\zeta^4+\eta+\zeta)\big) = 0, \quad (3.40)$$

which agrees with the earlier octahedral curve (3.28) after a spatial rotation. The configuration is axial for $a = 0$ as before. In the limit $a \to \pm 1$ the curve becomes $(\eta - \zeta)\eta^2\zeta^2 = 0$, which is the product of a star for a 1-monopole at the origin and the curves (3.24) for two axial 2-monopoles at infinity with positions $(X_1, X_2, X_3) = (0, 0, \pm 1)$. This twisted line family therefore describes two axial 2-monopoles that approach a single monopole at the origin, from either side of the symmetry axis, form the octahedral 5-monopole, then the axial 5-monopole, with the process then reversing with an accompanying rotation by $\pi/3$. Some selected energy density isosurfaces are presented in the second column of Figure 3.1, for increasing values of $a \in (-1, 0]$.

The rational map for this family is

$$\mathcal{R} = \frac{\sqrt{1-a^2} - 4ia\frac{(1+a^2)}{(1-a^2)}z^3}{\sqrt{1-a^2}z^5 - 2iaz^2}, \quad (3.41)$$

with the C_3 symmetry realized as $\mathcal{R}(\omega z) = \mathcal{R}(z)/\omega^2$.

3.4.3 5-MONOPOLES WITH D_4 SYMMETRY

Our second type of family is perhaps less intuitive than the first type, as it involves fixing the positions of the poles but varying the weights away from their canonical values. As an example we present a one-parameter family of 5-monopoles with D_4 symmetry that includes the octahedral 5-monopole.

The six poles are placed at the vertices of an octahedron

$$\gamma_0 = \infty,\ \gamma_1 = 1,\ \gamma_2 = -1,\ \gamma_3 = i,\ \gamma_4 = -i,\ \gamma_5 = 0,$$

so this data is of 't Hooft form as one of the poles is at ∞. The weights of the remaining five poles are taken to be

$$\lambda_5^2 = 1, \qquad \lambda_1^2 = \lambda_2^2 = \lambda_3^2 = \lambda_4^2,$$

with $\lambda_1 \in (0, \infty)$ the parameter of this family. If $\lambda_1 = \sqrt{2}$, then all weights are canonical and there is octahedral symmetry, but otherwise the symmetry is broken to D_4 symmetry.

The spectral curve is

$$(\eta - \zeta)(\eta^4\zeta^4 - \eta^4 + 4\lambda_1^2\eta^3\zeta + 4\lambda_1^2\eta\zeta^3 - \zeta^4 + 1) = 0, \tag{3.42}$$

and is invariant under

$$(\eta, \zeta) \mapsto (i\eta, i\zeta), \qquad (\eta, \zeta) \mapsto \left(\frac{1}{\eta}, \frac{1}{\zeta}\right), \tag{3.43}$$

which generate the D_4 symmetry.

If $\lambda_1 = \sqrt{2}$ then the curve (3.42) reverts to the spectral curve (3.28) of the octahedral 5-monopole. In the limit $\lambda_1 \to 0$ the curve (3.42) becomes

$$(\eta - \zeta)(\eta^4\zeta^4 - \eta^4 - \zeta^4 + 1) = 0 = (\eta - \zeta)\prod_{j=1}^{4}(\eta + i^j)(\zeta - i^j) \tag{3.44}$$

which is the product of stars for five monopoles, with one at the origin $(X_1, X_2, X_3) = (0, 0, 0)$ and the remaining four monopoles at the boundary of hyperbolic space along the Cartesian axes $(\pm 1, 0, 0)$ and $(0, \pm 1, 0)$. In the opposite limit $\lambda_1 \to \infty$ the curve becomes

$$\eta\zeta(\eta^3 - \eta^2\zeta + \eta\zeta^2 - \zeta^3) = 0, \tag{3.45}$$

where the first two factors describe 1-monopoles at the boundary of hyperbolic space with positions $(0, 0, \pm 1)$ and the final factor is the spectral curve of the axial 3-monopole at the origin. Note that the spectral curve of this family (3.42) is equal to the sum of the curve (3.44) and λ_1^2 times the curve (3.45). This feature is generic for JNR-type monopoles obtained by keeping the pole positions fixed and varying the weights, which is clear from the spectral curve formula (3.13).

We therefore see that as λ_1 increases through the interval $(0, \infty)$, four 1-monopoles approach from infinity along the Cartesian axes in the plane $X_3 = 0$ and merge with a 1-monopole at the origin to form the octahedral 5-monopole. The octahedral 5-monopole then splits to produce two 1-monopoles moving in opposite directions along the X_3-axis, leaving behind the axial 3-monopole. Corresponding energy density isosurfaces are displayed in the first column of Figure 3.2. Note that, as with some of the other energy density isosurfaces presented in this Thesis, we often slightly rotate the image to obtain an improved viewing angle, so for example the X_3-axis may not be exactly aligned with the vertical, although the images within each column have the same viewing angle.

The rational map for this one-parameter family is

$$\mathcal{R} = \frac{(4\lambda_1^2 + 1)z^4 - 1}{z^5 - z}, \tag{3.46}$$

with the clear C_4 symmetry $\mathcal{R}(iz) = -i\mathcal{R}(z)$.

3.4.4 7-MONOPOLES WITH TETRAHEDRAL SYMMETRY

Our next example of a family of the second type illustrates the fact that dihedral symmetry, although convenient for producing one-parameter families, is certainly not the only possibility. In this subsection, we construct a one-parameter family of 7-monopoles by imposing tetrahedral symmetry.

The eight poles are taken to be the roots of the Klein polynomial (3.30) for the face centres of the octahedron (or equivalently the vertices of the cube). Explicitly, we label the poles as

$$\gamma_0 = \frac{1+i}{\sqrt{3}+1},\ \gamma_1 = -\gamma_0,\ \gamma_2 = \gamma_0^{-1},\ \gamma_3 = -\gamma_0^{-1}, \gamma_4 = \frac{1-i}{\sqrt{3}+1},$$
$$\gamma_5 = -\gamma_4,\ \gamma_6 = \gamma_4^{-1},\ \gamma_7 = -\gamma_4^{-1},$$

and take λ_j^2 to be canonical weights for $j = 0, 1, 2, 3$ but μ^2 times the canonical weights for $j = 4, 5, 6, 7$. The one-parameter family is given by $\mu \in (0, \infty)$ with the resulting spectral curve taking the form

$$\left((\eta-\zeta)^3 + \frac{i}{\sqrt{3}}(\eta+\zeta)(\eta\zeta+1)(\eta\zeta-1)\right)\prod_{j=4}^{7}(\eta\zeta\bar{\gamma}_j + \zeta - \eta|\gamma_j|^2 - \gamma_j)$$
$$+ \mu^2\left((\eta-\zeta)^3 - \frac{i}{\sqrt{3}}(\eta+\zeta)(\eta\zeta+1)(\eta\zeta-1)\right)\prod_{j=0}^{3}(\eta\zeta\bar{\gamma}_j + \zeta - \eta|\gamma_j|^2 - \gamma_j) = 0.$$

Since this family is obtained by varying only the weights, the spectral curve is again the weighted sum of the two asymptotic curves. The first term is the product of the tetrahedral 3-monopole curve (3.25) and four stars for monopoles on the sphere at infinity on the vertices of the dual tetrahedron. The second term is μ^2 times the first term after the replacement $(\eta, \zeta) \mapsto (i\eta, i\zeta)$. The transformation $\mu \mapsto \mu^{-1}$ is therefore equivalent to a rotation by $\pi/2$ around the X_3-axis.

If $\mu = 1$ then the tetrahedral symmetry is enhanced to cubic symmetry, as there are eight poles with canonical weights on the vertices of a cube. $N = 7$ is not the lowest value of N for which there is a hyperbolic monopole with cubic symmetry. The lowest value is $N = 4$ and the spectral curve can be found in [NR07] with the explicit Higgs field derived in [MS14] using the ADHM construction with circle invariance. This $N = 4$ cubic monopole will appear later in subsection 4.3.3 as a member of a twisted-line symmetric family. However, this monopole is clearly not within the JNR class, as five points cannot be placed on a sphere with cubic symmetry.

We see from the above spectral curve that as μ increases through the interval $(0, \infty)$, four monopoles approach from infinity towards the face centers of the tetrahedral 3-monopole. The monopoles then merge to form a cubic 7-monopole which subsequently splits to leave the dual tetrahedral 3-monopole with four monopoles receding from the face centres towards infinity. Energy density isosurfaces are displayed in the second column of Figure 3.2 for increasing values of μ.

For values of μ around that associated with the second image in the second column of Figure 3.2 (or equivalently the fourth image in this column), we may view this solution as a prototype hyperbolic analogue of the multi-shell Euclidean monopoles suggested in [Man12] within the magnetic bag approximation.

The rational map for the family is

$$\mathcal{R} = \frac{(1-\mu^4)(5z^6 - z^2) - i\sqrt{3}(1+\mu^2)^2(11z^4+1)}{i\sqrt{3}(1+\mu^2)^2(z^7+3z^3) + (1-\mu^4)(5z^5+z)}, \tag{3.47}$$

with the evident C_2 symmetry $\mathcal{R}(-z) = -\mathcal{R}(z)$. For the cubic $\mu = 1$ case the map simplifies to

$$\mathcal{R} = \frac{11z^4+1}{z^7+3z^3}, \tag{3.48}$$

with the manifest C_4 symmetry $\mathcal{R}(iz) = i\mathcal{R}(z)$.

3.4.5 2-MONOPOLES WITH D_2 SYMMETRY

Our first example of a family of the third type, where the positions of the poles vary together with the (generically) non-canonical weights, is a one-parameter family of D_2 symmetric 2-monopoles. Although this is perhaps the simplest family of multi-monopoles, and was studied in [MS14] using the ADHM formalism, its analysis in terms of the JNR approach is a little subtle, and is therefore worth presenting.

The dimensional considerations at the end of Section 3.1 imply that the $N = 2$ moduli space is exhausted by JNR-type monopoles, despite the fact that we cannot place 3 points on the boundary sphere with D_2 symmetry. Clearly we need to exploit the degeneracy that arises when all poles lie on a circle, which we take to be the unit circle in the plane $X_3 = 0$. We can easily impose symmetry under the C_2 subgroup generated by a rotation by π around the X_1-axis, as one of the poles can be placed on the X_1-axis with the two remaining poles placed symmetrically about the axis with equal weights. Explicitly, let $a \in (-1, 1)$ be the parameter of the family and set

$$\gamma_0 = 1, \quad \gamma_1 = \frac{a-1}{2} + \frac{i}{2}\sqrt{3+2a-a^2}, \quad \gamma_2 = \gamma_1^{-1}, \quad \lambda_1^2 = \lambda_2^2 = 1,$$

with the weight λ_0^2 undetermined for the moment.

The spectral curve is

$$\frac{(\lambda_0^2+a-1)}{(2+\lambda_0^2)}(\eta^2\zeta^2+1) + \frac{(\lambda_0^2 - a\lambda_0^2 - a - 1)}{(2+\lambda_0^2)}(\eta^2\zeta - \eta\zeta^2 - \eta + \zeta) + \eta^2 + \zeta^2 - \frac{(2+2a+\lambda_0^2(1-a)^2)}{(2+\lambda_0^2)}\eta\zeta = 0, \tag{3.49}$$

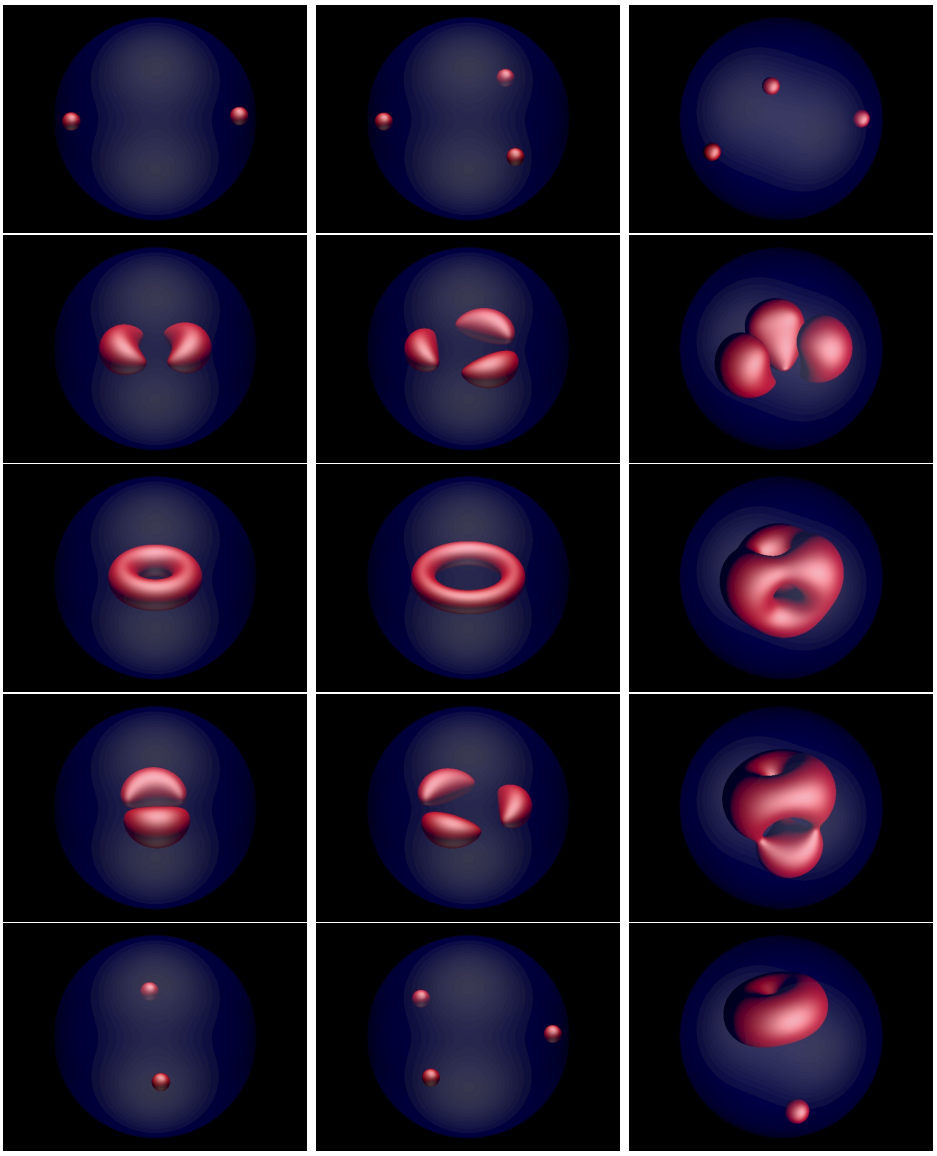

Figure 3.3: Energy density isosurfaces: first column D_2 symmetric 2-monopoles, second column D_3 symmetric 3-monopoles, third column C_3 symmetric 3-monopoles.

and is invariant under the C_2 symmetry $(\eta, \zeta) \mapsto (\eta^{-1}, \zeta^{-1})$. This C_2 symmetry is extended to D_2 symmetry by requiring invariance of the spectral curve (3.49) under the additional generator $(\eta, \zeta) \mapsto (-\eta, -\zeta)$. This extra symmetry requires that the coefficient c_{ij} vanishes unless $(i+j) \bmod 2 = 0$. This is satisfied providing

$$\lambda_0^2 = \frac{1+a}{1-a},$$

which yields the required D_2 invariant spectral curve

$$\eta^2 + \zeta^2 + a(\eta^2\zeta^2 + 1) + (a^2 - 1)\eta\zeta = 0. \tag{3.50}$$

We see from (3.50) that $a \mapsto -a$ is equivalent to the $\pi/2$ rotation $(\eta, \zeta) \mapsto (i\eta, i\zeta)$, and furthermore the axial 2-monopole curve is recovered by setting $a = 0$. This spectral curve was derived for arbitrary mass monopoles in [NR07].

The boundary of hyperbolic space intersects the plane $X_3 = 0$ in the circle given by $(X_1, X_2, X_3) = (\cos\theta, \sin\theta, 0)$, and from (1.26) a monopole at this position corresponds to the star

$$(\eta + e^{i\theta})(\zeta - e^{i\theta}) = 0.$$

In the limit $a \to -1$ the curve (3.50) becomes the product of two stars

$$(\eta + 1)(\zeta - 1)(\eta - 1)(\zeta + 1) = 0$$

for monopoles with positions $(\pm 1, 0, 0)$. Therefore as a increases through $(-1, 1)$ the two monopoles approach along the X_1-axis, merge to form the axially symmetric 2-monopole, and separate along the X_2-axis. This is the hyperbolic analogue of the famous right angle scattering of two Euclidean monopoles discovered by Atiyah and Hitchin [AH88]. Energy density isosurfaces are displayed for increasing values of a in the first column of Figure 3.3.

The rational map for this family is

$$\mathcal{R} = \frac{1 - a^2}{z^2 + a}, \tag{3.51}$$

with the manifest C_2 symmetry $\mathcal{R}(-z) = \mathcal{R}(z)$.

3.4.6 3-MONOPOLES WITH D_3 SYMMETRY

On a Euclidean background, the one-parameter family of D_2 symmetric 2-monopoles studied in the previous subsection is known to have a generalization to a one-parameter family of D_N symmetric N-monopoles. The N monopoles are located on the vertices of a contracting regular N-gon, merge to form the axial N-monopole, and then separate on the vertices of an expanding regular N-gon that is obtained from the incoming polygon by a rotation through $180^\circ/N$.

We illustrate the generalization of this to hyperbolic monopoles by presenting the result for $N = 3$. The four poles are again taken to lie on the unit circle, but this time two of the poles are placed on the X_1-axis to achieve the C_2 symmetry given by a rotation by 180° around the X_1-axis. As before, the two remaining poles are placed symmetrically about this axis with equal weights. In detail, the parameter is $a \in (-1, 1)$ and the poles and weights are

$$\gamma_0 = 1,\ \gamma_1 = -1,\ \gamma_2 = \frac{1}{2}(a + i\sqrt{4 - a^2}),\ \gamma_3 = \gamma_2^{-1},\ \lambda_0^2 = 1,\ \lambda_2^2 = \lambda_3^2,$$

with λ_1 and λ_2 yet to be determined. The D_3 symmetry is obtained by demanding that the spectral curve is invariant under the additional C_3 symmetry $(\eta, \zeta) \mapsto (\omega\eta, \omega\zeta)$, where $\omega = e^{2i\pi/3}$. This results in the requirement that $c_{ij} = 0$ if $(i + j) \bmod 3 \neq 0$, which gives

$$\lambda_1^2 = \frac{(1 - a)(2 - a)}{(1 + a)(2 + a)}, \qquad \lambda_2^2 = \frac{2(1 - a)}{(2 + a)}.$$

The one-parameter family of D_3 symmetric spectral curves is then

$$\eta^3 - \zeta^3 + a(\eta^3\zeta^3 - 1) + (a^2 - 1)(\eta^2\zeta - \eta\zeta^2) = 0, \tag{3.52}$$

which satisfies all the properties expected of this family, as described at the start of this subsection. Some energy density isosurfaces are displayed in the second column of Figure 3.3 for increasing values of $a \in (-1, 1)$.

The rational map is

$$\mathcal{R} = \frac{1 - a^2}{z^3 + a}, \tag{3.53}$$

being the obvious generalization of (3.51). Although we have not been able to provide a proof, all the D_N-symmetric N-monopoles appear to lie within the space of JNR data. For larger values of N the procedure follows the same

process as in this subsection and the previous one, with one pole on the X_1-axis if N is even and two if N is odd. The remaining poles are placed symmetrically in pairs around the unit circle, with equal weights to attain the C_2 symmetry, with the weights then determined by applying an additional C_N generator to enforce the full D_N symmetry. In Section 4.3.1 we shall derive explicit ADHM data for these families using a different method.

3.4.7 3-MONOPOLES WITH C_3 SYMMETRY

Our final example illustrates a phenomenon that appears if cyclic symmetry is imposed, rather than dihedral symmetry. Imposing cyclic symmetry will produce more than a one-parameter family, as there will be an additional degree of freedom associated with a translation of the whole configuration along the symmetry axis.

In Euclidean space, the motion of N monopoles has a natural decomposition into a trivial motion of the centre of mass of the configuration and a non-trivial relative motion between monopoles. In terms of the moduli space approximation, this allows (without loss of generality) a restriction to centered monopoles, in which the centre of mass is fixed at the origin. In hyperbolic space the situation is not so simple, since there is no definition of the centre of mass (even for point particles) that has all the properties that exist in the Euclidean setting. Fortunately there is a definition [MNS01] for a hyperbolic monopole to be centred, so we will apply this definition to restrict to a one-parameter family.

The definition introduced in [MNS01] is purely geometric and relies on the use of the holomorphic sphere. The holomorphic sphere allows us to lift the action of the isometry group of hyperbolic space to a linear action on $\mathbf{C}^N$, and a monopole is defined to be centred if it lies in the zero set of the moment map for the action of $SU(2) \subset SL(2,\mathbf{C})$. This condition maps to the following simple linear relations between the coefficients c_{ij} in the spectral curve:

$$\sum_{j=0}^{N}(-1)^j\frac{(2j-N)j!(N-j)!}{N!}c_{N-j,j}=\sum_{j=0}^{N-1}(-1)^j\frac{(j+1)j!(N-j)!}{N!}c_{N-j,j+1}=0.$$

All the spectral curves that we have presented so far obey these centred conditions, as a result of the symmetries that we have imposed. In particular, the

relations for a 3-monopole are:

$$9c_{30} - c_{21} - c_{12} + 9c_{03} = 3c_{31} - 2c_{22} + 3c_{13} = 0. \tag{3.54}$$

We shall make use of this condition shortly.

The cyclic example we consider is C_3 symmetric 3-monopoles obtained from the following choice of four poles,

$$\gamma_0 = 0, \qquad \gamma_j = \sqrt{\frac{1+a}{1-a}}\omega^j \quad \text{for } j = 1, 2, 3,$$

where $\omega = e^{2\pi i/3}$ and $a \in (-1, 1)$ is the free parameter. The weights λ_j^2 are canonical for $j = 1, 2, 3$ but λ_0^2 is free for the moment. This yields the two-parameter family of C_3 symmetric spectral curves

$$\lambda_0^2\sqrt{\frac{1+a}{1-a}}(\eta^3\zeta^3 - 1) - \lambda_0^2\frac{(1+a)^2}{(1-a)^2}\eta^3 + \frac{6(1+a)}{(1-a)^2}\eta^2\zeta \\ - \frac{6}{(1-a)}\eta\zeta^2 + \frac{(6+\lambda_0^2 - a\lambda_0^2)}{(1+a)}\zeta^3 = 0, \tag{3.55}$$

invariant under the symmetry $(\eta, \zeta) \mapsto (\omega\eta, \omega\zeta)$.

We now reduce this two-parameter family to a one-parameter family by imposing the centered condition (3.54), which determines the weight to be

$$\lambda_0^2 = \frac{9 - 20a + 7a^2}{3a(3 + a^2)}. \tag{3.56}$$

The requirement that $\lambda_0^2 > 0$ imposes the restriction $a \in (0, a_\star)$, where $a_\star = (10 - \sqrt{37})/7$.

Substituting (3.56) into (3.55) produces the centered spectral curve

$$\sqrt{\frac{1+a}{1-a}}(\eta^3\zeta^3 - 1) - \frac{(1+a)^2}{(1-a)^2}\eta^3 + \frac{(9 + 16a + 11a^2)}{(9 - 20a + 7a^2)}\zeta^3 \\ + \frac{18a(3+a^2)(\eta^2\zeta(1+a) - \eta\zeta^2(1-a))}{(1-a)^2(9 - 20a + 7a^2)} = 0. \tag{3.57}$$

The curve has tetrahedral symmetry if $a = \frac{1}{3}$ and becomes

$$\sqrt{2}\eta^3\zeta^3 - 4\eta^3 + 18\eta^2\zeta - 9\eta\zeta^2 + 5\zeta^3 - \sqrt{2} = 0, \tag{3.58}$$

with the extra C_2 symmetry

$$(\eta,\zeta)\mapsto\left(\frac{\sqrt{2}-\eta}{\sqrt{2}\eta+1},\frac{\sqrt{2}-\zeta}{\sqrt{2}\zeta+1}\right).$$

This tetrahedral curve is equal to the earlier tetrahedral curve (3.25) after a suitable rotation. In the limit $a\to 0$ the curve is a product of stars

$$\eta^3\zeta^3-\eta^3+\zeta^3-1=0=\prod_{j=1}^{3}(\eta+\omega^j)(\zeta-\omega^j)$$

for three monopoles on the vertices of an equilateral triangle in the plane $X_3=0$ at the boundary of hyperbolic space. In the limit $a\to a_\star$ the curve becomes

$$\zeta\bigg((1+b)^4\eta^2+(1-b)^4\zeta^2-(1-b^2)^2\eta\zeta\bigg)=0,$$

where b is given by the relation $a_\star=2b/(1+b^2)$, so $b=(7-2\sqrt{5\sqrt{37}-22})/(10-\sqrt{37})\approx 0.3$. This curve is the product of a star for a monopole at $(0,0,-1)$ and the curve (3.24) for an axial 2-monopole at $(0,0,b)$. The interesting new phenomenon here is that the single monopole is at infinity when the axial 2-monopole is at a finite distance from the origin, despite the fact that the total configuration is centered. This contrasts with the Euclidean situation, where an N-monopole cannot be centered if it consists of two clusters with only one cluster at infinity, as is self-evident from the properties of the centre of mass in Euclidean space.

A possible physical understanding of this new phenomenon in hyperbolic space is that the condition for a hyperbolic monopole to be centered should be similar to a requirement that the magnetic field on the sphere at infinity has a vanishing dipole. A definition of this sort would be quite natural, given that the abelian magnetic field on the sphere at infinity completely determines the monopole. A single monopole has a finite dipole even as its position tends to the sphere at infinity in hyperbolic space, so this can indeed be cancelled by a non-zero dipole of a cluster in the interior of hyperbolic space. At the moment this is nothing more than an attempt at a potential physical understanding of this surprising phenomenon, but it at least suggests why the result is not unreasonable.

In summary, the one-parameter family described in this subsection consists of three monopoles that approach on the vertices of a contracting triangle, merge to form the tetrahedral 3-monopole, which then splits into a single

monopole that travels down the symmetry axis of the triangle, leaving an axial 2-monopole at a finite distance up the symmetry axis. A selection of the corresponding energy density isosurfaces are displayed in the third column of Figure 3.3. This process is a hyperbolic analogue of the C_3-symmetric scattering of three Euclidean monopoles, for which similar energy density isosurfaces can be seen in [Sut97]; except that the axial 2-monopole continues to travel along the axis. These Euclidean results involve a numerical computation of the relevant solution of the Nahm equation, as the associated genus four curve is the Galois cover of a genus two curve (rather than an elliptic curve). Progress has been made in computing the spectral curve for this Euclidean case [BDE11], but it is significantly more complicated than the hyperbolic spectral curve (3.57).

The rational map for the centered C_3 symmetric 3-monopole family is

$$\mathcal{R} = \frac{18a(3+a^2)\sqrt{\frac{1+a}{1-a}}z}{(1-a)(11a^2+16a+9)z^3 - \sqrt{1-a^2}(7a^2-20a+9)}, \tag{3.59}$$

with the symmetry realized as $\mathcal{R}(\omega z) = \omega\mathcal{R}(z)$. Note that this is a different realization of the C_3 symmetry than for the rational map (3.53) of the D_3 symmetric 3-monopole of the previous subsection, where $\mathcal{R}(\omega z) = \mathcal{R}(z)$. Although both families involve three monopoles on the vertices of a contracting triangle, the subsequent different configurations are a result of different arrangements of the relative phases, which are captured by the above rational map realizations of the C_3 symmetry.

3.5 A metric on the space of JNR data

A natural metric on the moduli space of hyperbolic monopoles is given by the L^2-metric on the the space of abelian connections induced by hyperbolic monopoles at infinity. This metric is also invariant under the isometries of hyperbolic space, and in the case of a single monopole the moduli space equipped with this metric is simply hyperbolic space itself. Applying the moduli space approximation with this metric therefore yields the natural result that a slowly moving single hyperbolic monopole follows a geodesic in hyperbolic space.

In this Section we provide a simple integral formula for the above metric restricted to the space of JNR data and illustrate its application by explicit

computation to confirm that hyperbolic space is obtained as the moduli space for a single monopole.

To present the metric it is most convenient to use the upper half space model of hyperbolic space, where the boundary is given by $r = 0$ and we set $z = x_1 + ix_2$ to be the complex coordinate on the boundary. As shown in [MNS01], the required connection on the sphere at infinity can be written in terms of a hermitian metric obtained by evaluating the spectral curve on the antidiagonal. Explicitly, the abelian connection $\mathcal{A}_z = \frac{1}{2}(\mathcal{A}_1 - i\mathcal{A}_2)$ is given in terms of the hermitian metric $h(z, \bar{z})$ by

$$\mathcal{A}_z = \frac{1}{2}\partial_z \log h, \tag{3.60}$$

where $h(z, \bar{z})$ is the polynomial in z and $\bar{z}$ obtained as $\bar{z}^N$ times the spectral curve evaluated on the antidiagonal $\zeta = z$ and $\eta = -1/\bar{z}$. Using (3.13) gives the hermitian metric in terms of the JNR data as

$$h(z, \bar{z}) = \sum_{j=0}^{N} \lambda_j^2 \prod_{\substack{k=0 \\ k\neq j}}^{N} |z - \gamma_k|^2 = \psi|_{r=0} \prod_{k=0}^{N} |z - \gamma_k|^2. \tag{3.61}$$

Let t_μ for $\mu = 1, \ldots, \dim(\mathbf{M}_N^{\mathrm{JNR}})$ be real independent coordinates on the JNR moduli space. The metric is the L^2 metric of the abelian connection

$$g_{\mu\nu} = K \int \frac{\partial \mathcal{A}_i}{\partial t_\mu} \frac{\partial \mathcal{A}_i}{\partial t_\nu} \, d^2x = K \int \left(\frac{\partial}{\partial t_\mu}\left(\frac{\partial_i h}{h}\right)\right)\left(\frac{\partial}{\partial t_\nu}\left(\frac{\partial_i h}{h}\right)\right) d^2x, \tag{3.62}$$

where K is a normalization constant.

As an example, consider the case $N = 1$, where the three real independent coordinates may be taken to be those in the 't Hooft data, that is, $t_1 + it_2 = \gamma_1$ and $t_3 = \lambda_1$. The hermitian metric is then

$$h = |z - \gamma_1|^2\left(1 + \frac{\lambda_1^2}{|z - \gamma_1|^2}\right) = t_3^2 + (x_1 - t_1)^2 + (x_2 - t_2)^2, \tag{3.63}$$

and the above formula, with normalization constant $K = 3/(8\pi)$, gives the moduli space metric

$$g_{\mu\nu} dt_\mu dt_\nu = \frac{dt_1^2 + dt_2^2 + dt_3^2}{t_3^2}. \tag{3.64}$$

As advertised, this is indeed the metric of hyperbolic space, in upper half space coordinates.

The moduli space of inversion symmetric hyperbolic 2-monopoles is four-dimensional and is obtained from the action of $SO(3)$ on the one-parameter family of D_2 symmetric 2-monopoles described earlier. It would be interesting to use the above approach to compute the metric on this moduli space and to compare with both the Atiyah-Hitchin metric for Euclidean 2-monopoles and Hitchin's metric, with $k = 6$ in the notation of [Hit96], which is an algebraic metric on the spectral curves of precisely these hyperbolic 2-monopoles.

As the moduli space metric is invariant under $SO(3)$ spatial rotations then the one-parameter dihedral families discussed in the previous Section, being obtained as fixed point sets of a finite subgroup of this $SO(3)$ action, are automatically geodesics with respect to this metric. This relies on the fact that, for the examples considered, there are no hyperbolic monopoles with the given symmetry and charge that lie outside the JNR ansatz, which follows from known results on the dimensions of spaces of symmetric Euclidean monopoles.

3.6 Summary

For a specific relation between the curvature of hyperbolic space and the magnitude of the Higgs field at infinity, we have been able to obtain a complete description of a large class of hyperbolic N-monopoles. We have presented simple explicit formulae for the spectral curve and the rational map in terms of free data given by $N + 1$ points on the sphere together with positive real weights. This complements recent work [MS14] that provided an explicit formula for the Higgs field in terms of the same data. A number of symmetric examples have been presented, including one-parameter families that are hyperbolic analogues of geodesics that describe Euclidean monopole scattering. We have derived an integral expression for an interesting metric on the space of this data. There remain many open questions about this metric; for example, we would like to calculate the metric on non-trivial geodesic submanifolds of higher charge moduli spaces, and to clarify the connection between this metric and the other geometric structures that have been defined on hyperbolic monopole moduli spaces.

4

Hyperbolic monopoles from symmetric ADHM data

In this Chapter we give more $p = 1/2$ hyperbolic monopole solutions together with their associated spectral curves and rational maps. The new examples are found by deforming the axial monopole ADHM data while imposing judiciously chosen discrete symmetries. This approach requires that we have axial monopole ADHM data in a particularly convenient form. One could obtain axial monopole ADHM data by placing JNR poles of equal weight at the vertices of a regular polygon and using the matrices (3.9) and (3.10) to bring the data into standard form, but the resulting data will be messy and unnatural. Moreover, this approach will not give us the explicit action of the axial symmetry group on the data. In Section 4.2 we give a different, indirect derivation of axial monopole ADHM data via the Braam-Austin construction. The ADHM data so obtained follows a simple pattern and one can clearly see the action of the axial symmetry. This approach also allows us to write down the explicit fields for all the axial monopoles. In Section 4.3 we will deform the axial monopole data to give families of dihedral and twisted-line symmetric monopoles. Some of these families are generalisations of 1-parameter families in the previous Chapter to all values of the magnetic charge. The work in this Chapter was published in J. Phys. A under the title *Symmetric hyperbolic monopoles* [Coc14].

4.1 THE MANTON-SUTCLIFFE FORMALISM

We begin this Chapter by reviewing the Manton-Sutcliffe approach to finding circle-symmetric instantons, as described in [MS14]. Manton and Sutcliffe considered a circle action which leads to the ball model of hyperbolic space, and found many solutions with commuting Platonic symmetries. In particular they found that many previously discovered instantons [Hou99] [SS99] satisfy their constraints, if the scale of the instanton is chosen appropriately.

We can write conformal transformations of $\mathbf{R}^4$ as quaternionic Möbius transformations

$$x \to x' = (Ax + B)(Cx + D)^{-1}.$$

The circle action Manton and Sutcliffe use is

$$\begin{pmatrix} A & B \\ C & D \end{pmatrix} = \begin{pmatrix} \cos\frac{\alpha}{2} & \sin\frac{\alpha}{2} \\ -\sin\frac{\alpha}{2} & \cos\frac{\alpha}{2} \end{pmatrix}. \tag{4.1}$$

If we repeat the conformal equivalence (1.28) with the circle direction defined by this action, then we obtain a conformal equivalence between $\mathbf{R}^4 \setminus S^2$ and $\mathbf{H}^3 \times S^1$, where $\mathbf{H}^3$ is now in the ball model with metric (1.22). In terms of the notation for ADHM data introduced in (1.7), the Manton-Sutcliffe constraints for an instanton to be invariant under this action are:

1. M is pure quaternion and symmetric,
2. $\widehat{M}^\dagger \widehat{M} = 1_N$,
3. $LM = \mu L$, where μ is a pure quaternion, and L is non-vanishing.

ADHM data satisfying these constraints will correspond to a hyperbolic monopole with $p = 1/2$. All of the new monopole solutions in this Chapter will be given in terms of ADHM matrices satisfying the Manton-Sutcliffe constraints.

To calculate the Higgs field and energy density, suppose that the pure quaternion $X = X_1 i + X_2 j + X_3 k$ represents a point in the unit ball. Let $V(X)$ be a unit vector satisfying

$$V^\dagger \Delta(X) = 0,$$

where $\Delta(x)$ was defined by (1.10). The Higgs field is then

$$\Phi = \frac{1}{2} V^\dagger \begin{pmatrix} -\mu & L \\ -L^\dagger & M \end{pmatrix} V.$$

We will be interested in subgroups of the $SO(3)$ group of transformations of the form

$$\begin{pmatrix} A & B \\ C & D \end{pmatrix} = \begin{pmatrix} k & 0 \\ 0 & k \end{pmatrix},$$

where k is a unit quaternion. These transformations commute with the circle action (4.1) and will correspond, after dimensional reduction, to the group of rotations of $\mathbf{H}^3$ fixing the origin. Recalling the redundancy (1.9), we require that for an instanton to be symmetric under these transformations:

$$\begin{pmatrix} q & 0 \\ 0 & \mathcal{O} \end{pmatrix} \begin{pmatrix} L \\ M \end{pmatrix} \mathcal{O}^{-1} = k \begin{pmatrix} L \\ M \end{pmatrix} k^{-1}, \tag{4.2}$$

where q is a unit quaternion, and $\mathcal{O} \in \mathrm{O}(N)$. As k runs over the elements of some symmetry subgroup of $SO(3)$, the corresponding matrices $\mathcal{O}(k)$ will furnish a real I-dimensional representation of the symmetry group, while $q(k)$ will give a 2-dimensional complex representation.

An advantage of the Manton-Sutcliffe approach is that it appears to be particularly convenient for calculating a rational map of Jarvis type. If we have ADHM data satisfying the Manton-Sutcliffe constraints for circle-invariance, as well as $\mu = 0$, a candidate Jarvis-type rational map is [MS14]:

$$f(X) = L(M - X)^{-1} L^{\dagger}, \tag{4.3}$$

where X is a unit pure quaternion representing a point on the boundary. One obtains a rational map by writing both X and its image $f(X)$ in Riemann sphere coordinates. It is not known if this rational map is the same as the one defined by Jarvis using radial scattering [JN97]. For all the known examples of monopoles in the Manton-Sutcliffe formalism, the rational map (4.3) has the same symmetry as the corresponding monopole. We shall see that this is also true of all the monopoles in this Chapter with $\mu = 0$.

4.2 Axial Hyperbolic Monopoles

The first new result of this Chapter uses a correspondence between axial $p = 1/2$ N-monopoles and $p = N/2$ 1-monopoles to derive explicit axial monopole fields. To see this correspondence, start with a $p = N/2$ 1-monopole. This monopole is equivalent to a charge N instanton invariant under rotations in the x_3x_4-plane. However, 1-monopoles have an $SO(3)$-symmetry group of

rotations about their centres, and in particular are symmetric under the $SO(2)$ subgroup of rotations in the x_1x_2 plane. This $SO(2)$ symmetry lifts to a second independent circle-invariance of the underlying instanton. The idea is now to swap the roles of these two circle actions, so we quotient by rotations in the x_1x_2-plane and view rotations in the x_3x_4-plane as a physical symmetry of the resulting monopole. The axially symmetric monopole one obtains after this swap will have charge N and $p = 1/2$.

This observation is useful because 1-monopoles are particularly simple. The Bogomolny equation can be solved for all values of p [Nas86] by a spherically-symmetric ansatz similar to the ansatz for Euclidean monopoles (1.18):

$$A_i^a = \frac{2(P(R)-1)}{R^2}\varepsilon_{iak}X^k \text{ and } \Phi^a = \frac{Q(R)X_a}{R}, \tag{4.4}$$

where

$$P(R) = \frac{B\sinh s}{\sinh Bs},\ Q(R) = \coth s - B\coth Bs,$$

and $s = 2\tanh^{-1} R$, $B = 2p+1$. If p is a half-integer, then P and Q are rational functions of R.

To obtain axial monopole fields, one first performs a coordinate transformation of the fields (4.4) to half-space $(A_{X_1}, A_{X_2}, A_{X_3}, \Phi) \to (A_1, A_2, A_r, \Phi)$. To lift to the instanton, we interpret (A_r, Φ) as radial and angular components respectively of A in the x_3x_4-plane. This instanton is invariant under rotations in the x_1x_2 plane, but to dimensionally reduce along this direction we must first put it in a gauge in which it is independent of these rotations. This process gives the Higgs field magnitude of an axial $2p$-monopole, written in ball model coordinates:

$$||\Phi||^2 = (P(S)-1)^2\frac{(1-R^2)^2(R^2-\rho^2)}{((1+R^2)^2-4\rho^2)^2} + \frac{1}{4}\left((P(S)-1)\frac{(1-R^2)^2}{(1+R^2)^2-4\rho^2}+1\right)^2, \tag{4.5}$$

where $\rho^2 = X_1^2 + X_2^2$ and $S = 2\sqrt{\frac{1+R^2-2\rho}{1+R^2+2\rho}}$.

4.2.1 Axial monopole ADHM data from the Braam-Austin construction

The real usefulness of this 'swap' of the roles of the circle actions is that it gives the axial monopole ADHM data in a simple, natural form. Carrying out the swap at the ADHM level means that the Braam-Austin data for a 1-monopole written as a standard-form ADHM matrix is precisely the same as

the Braam-Austin data for the corresponding axial monopole. Braam-Austin data for a 1-monopole is trivial to write down, so the matrix one obtains this way is much simpler than the one coming from the JNR ansatz.

To implement this 'swap' at the ADHM level, one has to write the ADHM construction in the abstract, coordinate-independent way it was originally introduced. In this formulation, ADHM data defining an instanton of charge I is a linear map $A(z) : W \to V$ depending linearly on $z \in \mathbf{C}^4$, where W is an I-dimensional complex vector space with an antilinear map σ_W satisfying $\sigma_W^2 = 1$, and V is a $(2I + 2)$-dimensional complex vector space with another antilinear map σ_V satisfying $\sigma_V^2 = -1$. If we identify $\mathbf{C}^4$ with $\mathbf{H}^2$ in the standard way, $(z_1, z_2, z_3, z_4) \to (z_1 + jz_2, z_3 + jz_4) = (x, y)$, then we define a map σ on $\mathbf{C}^4$ to be right multiplication by j. To define an instanton, A must then satisfy:

1. $A(\sigma z)(\sigma_W w) = \sigma_V(A(z)w)$,
2. $A(z)$ is injective and $A(z)W \subset \text{Ker } \sigma_V$ for all $z \in \mathbf{C}^4 \setminus \{0\}$.

There is a prescription for turning this into the standard quaternionic matrix form of ADHM data (see for example [Ati79], [WW90]). First, we can write W as $W_{\mathbf{R}} \otimes_{\mathbf{R}} \mathbf{C}$, where $W_{\mathbf{R}}$ is the subspace of W left fixed by σ_W. We can also identify V with an $(I + 1)$-dimensional right quaternionic vector space $V_{\mathbf{H}}$, with multiplication by j given by σ_V. Condition 1 above means that we can consider A to be a quaternionic linear map $\mathbf{H^2} \otimes_{\mathbf{R}} W_{\mathbf{R}} \to V_{\mathbf{H}}$. To write out the corresponding matrix, we first choose a basis for the vector space $W_{\mathbf{R}}$ (a so-called 'real basis'), and a basis for $V_{\mathbf{H}}$ which is unitary with the respect to the standard quaternion inner product. Now with respect to these bases, define a matrix C whose columns are the images under A of $(1, 0) \otimes$ (basis vectors of $W_{\mathbf{R}}$), so C is an $(I + 1) \times I$ quaternionic matrix. Similarly define a matrix D whose columns are the images under A of $(0, 1) \otimes$ (basis vectors of $W_{\mathbf{R}}$). Then A is described by a quaternionic matrix function of the coordinates x, y on $\mathbf{H}^2$:

$$A(x, y) = Cx + Dy.$$

Condition 2 above is equivalent to requiring that $A(x, y)^\dagger A(x, y)$ be a real non-singular matrix for all x, y. We can obtain standard form ADHM data by

setting $y = 1$ and finding $R \in Sp(I+1, \mathbf{H})$ and $S \in GL(I, \mathbf{R})$ such that

$$RCS = \begin{pmatrix} 0 \\ 1_I \end{pmatrix}.$$

Then the standard quaternionic matrix defining an instanton is RDS.

We will illustrate the 'swap' at the ADHM level by writing $p = 3/2$ Braam-Austin data in standard quaternionic matrix form. Using the results of [BA90], if the hyperbolic monopole has charge N then in the $p = 3/2$ case W has complex dimension $3N$ and V has complex dimension $6N + 2$. Under the circle action, W breaks up into subspaces $W_{-1} \oplus W_0 \oplus W_1$ where each W_i has dimension N, while V breaks up into subspaces $V_{-3} \oplus V_{-1} \oplus V_1 \oplus V_3$, where V_3, V_{-3} are $N+1$-dimensional and V_1, V_{-1} are $2N$-dimensional. The subscripts here refer to the weights of the circle action on these spaces. We can write $A(z) = \sum_{i=1}^{4} A_i z_i$, so the A_i are matrix components of the map A. One can choose bases for W and V such that:

$$A_1 = \begin{array}{c} \\ V_{-3} \\ \\ V_{-1} \\ \\ V_1 \\ \\ V_3 \\ \\ \end{array} \begin{array}{c} \begin{array}{ccc} W_{-1} & W_0 & W_1 \end{array} \\ \begin{pmatrix} I_N & & \\ 0 & & \\ & I_N & \\ & 0_N & \\ & & 0_N \\ & & I_N \\ & & 0_N \\ & & 0 \end{pmatrix} \end{array}$$

$$A_3 = \begin{pmatrix} \beta_{-2} & & & \\ v & & & \\ & \beta_0 & & \\ & \gamma_{-1} & & \\ & & -\gamma_1 & \\ & & \beta_2 & \\ & & 0_N & \\ & & 0 & \end{pmatrix}$$

where β_i, γ_i are complex $N \times N$ matrices and v is a complex N-row vector. These matrices will correspond to the quaternionic matrices C, D described above, after we make our quaternionic identifications.

First we need to identify a real basis for W. Suppose that A_1, A_3 above are defined with respect to bases $\{\mathbf{e}^j_\alpha\}_{1\leq\alpha\leq N}$ for each W_j. These bases are chosen in such a way that the real structure $\sigma_W : W_j \to W_{-j}$ is just conjugation. With respect to this real structure, a real basis for $W_{-1}\oplus W_1$ is $\{\mathbf{e}^{-1}_\alpha \oplus \mathbf{e}^1_\alpha\}_{1\leq\alpha\leq N} \cup \{i\mathbf{e}^{-1}_\alpha \oplus -i\mathbf{e}^1_\alpha\}_{1\leq\alpha\leq N}$, while $\{\mathbf{e}^0_\alpha\}_{1\leq\alpha\leq N}$ is already a real basis for W_0. The prescription above says that we need to find the images of these vectors in V and then use the antilinear map on V to identify these images with quaternionic row vectors. The basis of V used to define A_1, A_3 above is chosen such that σ_V acts on $V_{-j}\oplus V_j$ by $(\mathbf{w},\mathbf{v}) \to (-\overline{\mathbf{v}}, \overline{\mathbf{w}})$. This means we should identify $(\mathbf{w},\mathbf{v}) \in V_{-j}\oplus V_j$ with the quaternionic vector $\mathbf{w} + j\mathbf{v}$. The map σ_V now corresponds to multiplication by j on the right. Using the matrices A_1, A_3 to determine the images of the real basis vectors gives:

$$Cx + Dy = \begin{pmatrix} 0 & 0 & 0 \\ I_N & 0_N & iI_N \\ 0_N & I_N & 0_N \\ jI_N & 0_N & kI_N \end{pmatrix} x + \begin{pmatrix} v & 0 & iv \\ \beta_{-2} & 0_k & i\beta_{-2} \\ -j\gamma_1 & \beta_0 & -k\gamma_1 \\ j\beta_2 & \gamma_{-1} & k\beta_2 \end{pmatrix} y \tag{4.6}$$

Multiplying on the left by

$$\begin{pmatrix} 1 & 0 & 0 & 0 \\ 0 & 1/\sqrt{2} & 0 & -j/\sqrt{2} \\ 0 & 0 & 1 & 0 \\ 0 & -i/\sqrt{2} & 0 & -k/\sqrt{2} \end{pmatrix} \tag{4.7}$$

and on the right by

$$-\begin{pmatrix} 1/\sqrt{2} & & \\ & 1 & \\ & & 1/\sqrt{2} \end{pmatrix} \tag{4.8}$$

and setting $y = 1$ gives ADHM data in standard form:

$$\Delta(x) = \begin{pmatrix} -v/\sqrt{2} & 0 & -iv/\sqrt{2} \\ -(\beta_{-2}+\beta_2)/2 & j\gamma_{-1}/\sqrt{2} & -i(\beta_{-2}-\beta_2)/2 \\ j\gamma_1/\sqrt{2} & -\beta_0 & k\gamma_1/\sqrt{2} \\ i(\beta_2-\beta_{-2})/2 & k\gamma_{-1}/\sqrt{2} & -(\beta_{-2}+\beta_2)/2 \end{pmatrix} - \begin{pmatrix} 0 & 0 & 0 \\ 1 & & \\ & 1 & \\ & & 1 \end{pmatrix} x \tag{4.9}$$

Imposing the usual ADHM constraint that $\Delta(x)^\dagger\Delta(x)$ be a real non-singular matrix gives exactly the Braam-Austin equations for the $p = 3/2$ system.

Now we specialise to the case of a charge 1 $p = 3/2$ monopole. As described

in Section 1.7, we can choose our gauge such that $\gamma_i = \gamma \in \mathbf{R}^+$, $\beta_i = \beta$, $v = q\gamma$ are constant for all i. We can then interpret (β, γ) as centre of mass coordinates for the 1-monopole in the half-space model. We choose our monopole to sit at $\beta = 0, \gamma = 1$, and we also choose $q = -j$. Then (4.9) gives us ADHM data in standard form:

$$\frac{1}{\sqrt{2}} \begin{pmatrix} j & 0 & -k \\ 0 & j & 0 \\ j & 0 & k \\ 0 & k & 0 \end{pmatrix} \tag{4.10}$$

Note that the resulting ADHM matrix only has non-zero j, k-parts, which shows that this data is invariant under rotations in the x_1x_2 plane. This example illustrates how to interpret the 'swap' at the level of ADHM data. We arranged the Braam-Austin data for a 1-monopole of mass 3/2, which is a set of matrices defined on a lattice with 3 sites, into a single 4×3 matrix with pure j, k entries. The Braam-Austin data for a $p = 1/2$ monopole just consists of a single complex matrix satisfying the ADHM constraints, which, up to an overall factor of j, is what we obtained in (4.10). This whole construction generalises straightforwardly to give the data for higher charge axial monopoles, which we shall give explicitly in the next subsection.

The construction also gives the matrices compensating for axial symmetry. One can see from (4.9) that the rotation $x \to e^{i\theta/2} x e^{-i\theta/2}$ acts on the Braam-Austin data as:

$$\beta_j \to \beta_j, \gamma_j \to e^{i\theta}\gamma_j, v \to v. \tag{4.11}$$

Recalling the gauge freedom (1.34) we can compensate for this by the gauge transformation

$$\begin{aligned} g_2 &= e^{-i\theta} \\ g_0 &= 1 \\ g_{-2} &= e^{i\theta} \\ q &= e^{i\theta} \end{aligned} \quad . \tag{4.12}$$

We need to understand how to interpret gauge transformations in terms of compensating matrices for standard ADHM data. Gauge transformations act on both V and W; in terms of the bases chosen above, the gauge transformation acts on V by:

$$\begin{array}{c} \\ V_{-3} \\ \\ V_{-1} \\ \\ V_1 \\ \\ V_3 \\ \\ \end{array} \begin{array}{c} \begin{array}{cccccccc} V_{-3} & & V_{-1} & & V_1 & & V_3 & \end{array} \\ \begin{pmatrix} g_{-2} & & & & & & & \\ & q & & & & & & \\ & & g_0 & & & & & \\ & & & g_{-2} & & & & \\ & & & & g_0 & & & \\ & & & & & g_2 & & \\ & & & & & & g_2 & \\ & & & & & & & q \end{pmatrix} \end{array} \tag{4.13}$$

and on W by:

$$\begin{array}{c} \\ W_{-1} \\ W_0 \\ W_1 \end{array} \begin{array}{c} \begin{array}{ccc} W_{-1} & W_0 & W_1 \end{array} \\ \begin{pmatrix} g_{-2}^{-1} & & \\ & g_0^{-1} & \\ & & g_2^{-1} \end{pmatrix} \end{array} \tag{4.14}$$

Using our quaternionic identifications above, (4.13) becomes:

$$\begin{pmatrix} q & & & \\ & g_{-2} & & \\ & & g_0 & \\ & & & g_{-2} \end{pmatrix}$$

while (4.14) becomes:

$$\begin{pmatrix} \cos\theta & 0 & \sin\theta \\ 0 & 1 & 0 \\ -\sin\theta & 0 & \cos\theta \end{pmatrix}$$

and one can check that these matrices will compensate for the transformations (4.11) applied to the data (4.6). Using our transformations (4.7) and (4.8) gives the compensating matrices for the axial symmetry:

$$\begin{pmatrix} e^{-2i\theta} & & \\ & \cos\theta & 0 & -\sin\theta \\ & 0 & 1 & 0 \\ & \sin\theta & 0 & \cos\theta \end{pmatrix} \frac{1}{\sqrt{2}} \begin{pmatrix} j & 0 & -k \\ 0 & j & 0 \\ j & 0 & k \\ 0 & k & 0 \end{pmatrix} \begin{pmatrix} \cos\theta & 0 & \sin\theta \\ 0 & 1 & 0 \\ -\sin\theta & 0 & \cos\theta \end{pmatrix}$$
$$= e^{i\theta} \frac{1}{\sqrt{2}} \begin{pmatrix} j & 0 & -k \\ 0 & j & 0 \\ j & 0 & k \\ 0 & k & 0 \end{pmatrix} \quad (4.15)$$

and this construction generalises straightforwardly to higher charges.

4.2.2 General Axial N-monopole ADHM data

The ADHM data for the axial charge N, $p = 1/2$ monopole is best given inductively. The data for the 2-monopole is

$$\widehat{M}_2^{\rm ax} = \frac{1}{2} \begin{pmatrix} j\sqrt{2} & -k\sqrt{2} \\ -j & -k \\ -k & j \end{pmatrix} \quad (4.16)$$

while the data for the 3-monopole (4.10) was given in the previous subsection.

Now suppose that

$$\widehat{M}_N^{\rm ax} = \begin{pmatrix} L_N^{\rm ax} \\ M_N^{\rm ax} \end{pmatrix}$$

is the ADHM data for an axial N-monopole for $N \geq 2$. Then

$$\widehat{M}_{N+2}^{\rm ax} = \begin{pmatrix} j/\sqrt{2} & 0 & 0 & \cdots & 0 & 0 & -k/\sqrt{2} \\ 0 & j/2 & 0 & \cdots & 0 & -k/2 & 0 \\ j/2 & & & & & & k/2 \\ 0 & & & & & & 0 \\ \vdots & & & M_N^{\rm ax} & & & \vdots \\ 0 & & & & & & 0 \\ -k/2 & & & & & & j/2 \\ 0 & k/2 & 0 & \cdots & 0 & j/2 & 0 \end{pmatrix} \quad (4.17)$$

For axial symmetry, the matrices $\widehat{M}_N^{\rm ax}$ satisfy

$$\begin{pmatrix} q_N & 0 \\ 0 & \mathcal{O}_N \end{pmatrix} \widehat{M}_N^{\rm ax} \mathcal{O}_N^{-1} = e^{-i\theta} \widehat{M}_N^{\rm ax}, \quad (4.18)$$

where

$$q_N(\theta) = e^{-i\theta(N+1)/2} \tag{4.19}$$

and we define $\mathcal{O}_N$ inductively. Firstly,

$$\mathcal{O}_1(\theta) = 1 \text{ and } \mathcal{O}_2(\theta) = \begin{pmatrix} \cos\theta/2 & -\sin\theta/2 \\ \sin\theta/2 & \cos\theta/2 \end{pmatrix}$$

and, for $N \geq 3$,

$$\mathcal{O}_{N+2}(\theta) = \begin{pmatrix} \cos(N+1)\theta/2 & 0 & \cdots & 0 & -\sin(N+1)\theta/2 \\ 0 & & & & 0 \\ \vdots & & \mathcal{O}_N(\theta) & & \vdots \\ 0 & & & & 0 \\ \sin(N+1)\theta/2 & 0 & \cdots & 0 & \cos(N+1)\theta/2 \end{pmatrix} \tag{4.20}$$

One can check that the matrices defined by (4.17) satisfy the Manton-Sutcliffe constraints for circle invariance. This is actually unsurprising. We would obtain the same instantons by placing the poles of the JNR ansatz at the roots of unity with equal weight in the jk-plane. But then the poles will lie on the fixed-point set of the Manton-Sutcliffe circle action, which is the 2-sphere of unit-norm pure imaginary quaternions, so the instanton must also be invariant under this action as well.

In the next Section we will be interested in subgroups of the symmetry group of the axial monopoles. Axial monopoles are invariant under reflection in the X_2X_3-plane

$$I : X \to iXi$$

since $i\widehat{M}_N i = \widehat{M}_N$, and the compensating transformation is just the identity. Axial N-monopoles are also symmetric under rotations by π around the X_2-axis,

$$R_2 : X \to -jXj$$

since

$$-j\widehat{M}_N j = \begin{pmatrix} 1 & 0 \\ 0 & \mathcal{O}_N^R \end{pmatrix} \widehat{M}_N (\mathcal{O}_N^R)^{-1}, \tag{4.21}$$

where

$$(\mathcal{O}_N^R)_{ab} = \begin{cases} 1 & \text{if } a = b \text{ and } 1 \leq a \leq (N+1)/2 \\ -1 & \text{if } a = b \text{ and } (N+1)/2 < a \leq N \\ 0 & \text{otherwise} \end{cases}$$

Since $\mu = 0$ for the axial monopoles, one can calculate their Jarvis rational maps to be $1/z^N$.

4.3 Deforming the axial monopole

In this Section we derive circle-invariant ADHM data corresponding to families of dihedral and twisted-line symmetric hyperbolic monopoles. Our data will satisfy the Manton-Sutcliffe constraints for circle invariance. To find symmetric ADHM data, one can take representations of the symmetry groups in $\mathbf{C}^2$ and $\mathrm{O}(N)$, and use them as constraints on ADHM data via (4.2). For low charges, solving for ADHM data constrained by the dihedral and twisted line symmetries as well as the Manton-Sutcliffe conditions is tractable, and the solutions can be easily generalised to higher charges. This Section contains the results of this approach for some dihedral and twisted-line symmetry groups. The representations (4.20) are key for this derivation, since we are using subrepresentations of these to constrain the data.

4.3.1 D_N symmetric N-monopoles

The dihedral group D_N is generated by rotations by $2\pi/N$ around the X_1-axis, and the rotation R_2 given above. Using the representations of these symmetries given in Section 4.2.1 leads to the following family of D_N symmetric N-monopoles, for $N > 2$:

$$\widehat{M}_N = \frac{1}{2} \begin{pmatrix} j\sqrt{2(1-\alpha^2)} & 0 & & \cdots & & 0 & -k\sqrt{2(1-\alpha^2)} \\ (-1)^N j\alpha & j & 0 & \cdots & 0 & -k & (-1)^{N+1} k\alpha \\ j & & & & & & k \\ 0 & & & & & & 0 \\ \vdots & & & 2M^{\mathrm{ax}}_{N-2} & & & \vdots \\ 0 & & & & & & 0 \\ -k & & & & & & j \\ (-1)^{N+1} k\alpha & k & 0 & \cdots & 0 & j & (-1)^{N+1} j\alpha \end{pmatrix} \tag{4.22}$$

for $\alpha \in (-1, 1)$. It is straightforward to check that the above data also satisfies the Manton-Sutcliffe constraints, and in particular that $\mu = (-1)^N \alpha j$ for all N.

Symmetry and dimensional considerations imply that for $N = 2$ and 3 these families are the same as the dihedral families derived in subsections 3.4.5 and 3.4.6 respectively. For higher charges these families appear to be the appropriate generalisation of the D_N symmetric N-monopoles mentioned in subsection 3.4.6. Strictly speaking we have not been able to prove this because the data (4.22) was derived within the Manton-Sutcliffe formalism, and it is not known how to calculate spectral curves and rational maps in this setting. However, the numerics are extremely suggestive that this is the correct generalisation. Assuming this interpretation is correct, the explicit data (4.22) is an improvement on the Euclidean case, where these families of monopoles are known only from their Donaldson rational maps.

If we multiply by j on the left, then the data (4.22) is purely complex, so we can think of it as $p = 1/2$ Braam-Austin data and use the spectral curve (1.36) and rational map (1.37). For $N = 3$, the spectral curve is

$$\eta^3 - \zeta^3 - \alpha(\eta^3\zeta^3 - 1) + (\alpha^2 - 1)(\eta^2\zeta - \eta\zeta^2) = 0, \tag{4.23}$$

If we make the identification $\alpha = -a$, then (4.23) is the same as the spectral curve (3.52) of the D_3-symmetric 3-monopole family discussed in subsection 3.4.6. It is actually unsurprising that for $N = 3$ the data (4.22) gives the same monopole in either the Braam-Austin or Manton-Sutcliffe approaches; just as for the axial monopoles, the JNR poles lie on the fixed-point sets of both circle actions. This seems likely to extend to higher charges, since D_N symmetric N-monopoles appear to lie within the space of JNR data for all N with the poles lying on both fixed-point sets, although the required configuration of poles and weight would be rather messy. Here these monopoles appear as simple, natural deformations of axial monopole ADHM data.

The Donaldson-type rational map corresponding to the data (4.22) is

$$\mathcal{R}(z) = \frac{1 - \alpha^2}{z^N + \alpha}. \tag{4.24}$$

We can prove this straightforwardly using a formal expansion in powers of z^{-1}. The expansion of (4.24) is

$$\sum_{j=0}^{\infty}(1-\alpha^2)\frac{(-\alpha)^j}{z^{N(j+1)}},$$

while the expansion of the general rational map formula is

$$L(z-M)^{-1}L^t = \sum_{k=0}^{\infty}\frac{LM^kL^t}{z^{k+1}},$$

where for the rest of this Section L and M are the top row and bottom N rows respectively of (4.22) multiplied on the left by j. The coefficients LM^kL^t can be calculated explicitly. Note that for $1 \leq k < N/2-1$,

$$\begin{aligned}(0,\ldots,0,\underbrace{1}_{k\text{-th}},0,\ldots,0,\underbrace{-i}_{(N-k+1)\text{-th}},\ldots,0)M_N \\ = (0,\ldots,0,\underbrace{1}_{(k+1)\text{-th}},0,\ldots,0,\underbrace{-i}_{(N-k)\text{-th}},\ldots,0) \quad (4.25)\end{aligned}$$

so we have, for $0 \leq k \leq N/2-1$,

$$LM^k = \sqrt{\frac{1-\alpha^2}{2}}(0,\ldots,0,\underbrace{1}_{(k+1)\text{-th}},0,\ldots,0,\underbrace{-i}_{(N-k)\text{-th}},\ldots,0).$$

Similarly, for $N/2 \leq k \leq N-1$, if N is even,

$$LM^k = \sqrt{\frac{1-\alpha^2}{2}}(0,\ldots,0,\underbrace{-1}_{(N-k)\text{-th}},0,\ldots,0,\underbrace{-i}_{(k+1)\text{-th}},\ldots,0),$$

and if N is odd,

$$LM^{(N-1)/2} = \sqrt{\frac{1-\alpha^2}{2}}(0,\ldots,0,\underbrace{1}_{(N+1)/2\text{-th}},0,\ldots,0),$$

and

$$LM^k = \sqrt{\frac{1-\alpha^2}{2}}(0,\ldots,0,\underbrace{1}_{(N-k)\text{-th}},0,\ldots,0,\underbrace{i}_{(k+1)\text{-th}},\ldots,0)$$

$$\text{for } (N+1)/2 \leq k \leq N-1.$$

This shows that $LM^kL^t = 0$ for $0 \leq k < N-1$, and $LM^{N-1}L^t = (-1)^N(\alpha^2-1)$. Also

$$LM^N = -\alpha\sqrt{\frac{1-\alpha^2}{2}}(1,0,\ldots,0,-i) = -\alpha L,$$

and so

$$LM^kL^t = \begin{cases} 0 & \text{if } (k+1) \bmod N \neq 0 \\ (-1)^N(-\alpha)^{(k+1)/N-1}(\alpha^2-1) & \text{if } (k+1) \bmod N = 0. \end{cases}$$

so the coefficients of the two expansions are equal up to an overall phase of $(-1)^N$, proving the rational map formula (4.24). The rational map formula also makes the cyclic symmetry $z \to e^{2\pi i/N}z$ manifest.

The generalisation of the spectral curve formula (4.23) to arbitrary N appears to be, using the definition (3.23) of $\mathcal{A}_N$,

$$\mathcal{A}_N + \alpha(1-(-\eta\zeta)^N) + \alpha^2(\zeta^N + (-\eta)^N - \mathcal{A}_N) = 0. \tag{4.26}$$

We have not been able to prove this formula from the data (4.22), although it has been checked for a large range of values of N.

4.3.2 D_{N-M}-SYMMETRIC N-MONOPOLES

We can generate another interesting family by imposing D_{N-1} symmetry together with the constraint $\mu = 0$. For $N > 2$, the resulting ADHM data is

$$\frac{1}{2}\begin{pmatrix} j\sqrt{2}f_{N+1}(\alpha) & 0 & 0 & \cdots & 0 & 0 & -k\sqrt{2}f_N(\alpha) \\ 0 & jf_N(\alpha) & 0 & \cdots & 0 & -kf_N(\alpha) & 0 \\ jf_N(\alpha) & & & & & & kf_{N+1}(\alpha) \\ 0 & & & & & & 0 \\ \vdots & & & 2M^{\mathrm{ax}}_{N-2} & & & \vdots \\ 0 & & & & & & 0 \\ -kf_N(\alpha) & & & & & & jf_{N+1}(\alpha) \\ 0 & kf_{N+1}(\alpha) & 0 & \cdots & 0 & jf_{N+1}(\alpha) & 0 \end{pmatrix} \tag{4.27}$$

for $\alpha \in (-1,1)$, where

$$f_N(\alpha) = \sqrt{1+(-1)^N\alpha}.$$

For α close to 1, the configuration consists of $N-1$ monopoles at the roots of unity, and one monopole at the origin. As α decreases, the outer monopoles approach the origin from infinity, while a 1-monopole stays at the origin throughout. The configuration becomes axial for $\alpha = 0$, and as α becomes negative the same process happens in reverse, with the configuration rotated by an angle of $\pi/(N-1)$. The first column of Figure 4.1 shows energy density isosurfaces of D_2 symmetric 3-monopoles at several different values of α between 1 and -1, decreasing down the column.

This family can be generalised to give families with two or three monopoles at the origin. Other families with more than three at the origin must exist, but we have not been able to find them with our methods. All these D_{N-M}-symmetric N-monopole families follow the same pattern as the D_{N-1}-symmetric N-monopole families. For α close to 1, $(N-M)$ 1-monopoles are arranged in a regular polygon around an axial M-monopole at the origin. As α decreases, the 1-monopoles move radially inwards, 'scattering' through the axial configuration at $\alpha = 0$, and coming out again rotated by an angle of $\pi/(N-M)$.

The data corresponding to a D_2 symmetric 4-monopole is

$$\frac{1}{2}\begin{pmatrix} j\sqrt{2} & 0 & 0 & -k\sqrt{2} \\ -j\alpha & j\sqrt{1-\alpha^2} & -k\sqrt{1-\alpha^2} & -k\alpha \\ j\sqrt{1-\alpha^2} & j(-1+\alpha) & k(-1-\alpha) & k\sqrt{1-\alpha^2} \\ -k\sqrt{1-\alpha^2} & k(-1-\alpha) & j(1-\alpha) & j\sqrt{1-\alpha^2} \\ -k\alpha & k\sqrt{1-\alpha^2} & j\sqrt{1-\alpha^2} & j\alpha \end{pmatrix} \tag{4.28}$$

The second column of Figure 4.1 shows energy density isosurfaces for this family for different values of α between 1 and -1, decreasing down the column.

For $N > 4$, the data corresponding to a D_{N-2} symmetric N-monopole is

$$\frac{1}{2}\begin{pmatrix}
j\sqrt{2} & 0 & & & \dots & & & 0 & -k\sqrt{2} \\
(-1)^{N+1}j\alpha & jf_1(\alpha^2) & 0 & & \dots & & 0 & -kf_1(\alpha^2) & (-1)^{N+1}k\alpha \\
jf_1(\alpha^2) & (-1)^N j\alpha & j & 0 & \dots & 0 & -k & (-1)^{N+1}k\alpha & kf_1(\alpha^2) \\
0 & j & & & & & & k & 0 \\
0 & 0 & & & & & & 0 & 0 \\
\vdots & \vdots & & & 2M^{\mathrm{ax}}_{N-4} & & & \vdots & \vdots \\
0 & 0 & & & & & & 0 & 0 \\
0 & -k & & & & & & j & 0 \\
-kf_1(\alpha^2) & (-1)^{N+1}k\alpha & k & 0 & \dots & 0 & j & (-1)^{N+1}j\alpha & jf_1(\alpha^2) \\
(-1)^{N+1}k\alpha & kf_1(\alpha^2) & 0 & & \dots & & 0 & jf_1(\alpha^2) & (-1)^N j\alpha
\end{pmatrix} \tag{4.29}$$

For $N > 4$, the data corresponding to a D_{N-3} symmetric N-monopole is

$$\frac{1}{2}\begin{pmatrix}
j\sqrt{2} & 0 & & & \dots & & & 0 & -k\sqrt{2} \\
0 & jf_1(\alpha) & 0 & & \dots & & 0 & -kf_0(\alpha) & 0 \\
jf_1(\alpha) & 0 & jf_0(\alpha) & 0 & \dots & 0 & -kf_0(\alpha) & 0 & kf_1(\alpha) \\
0 & jf_0(\alpha) & & & & & & kf_1(\alpha) & 0 \\
0 & 0 & & & & & & 0 & 0 \\
\vdots & \vdots & & & 2M^{\mathrm{ax}}_{N-4} & & & \vdots & \vdots \\
0 & 0 & & & & & & 0 & 0 \\
0 & -kf_0(\alpha) & & & & & & jf_1(\alpha) & 0 \\
-kf_0(\alpha) & 0 & kf_1(\alpha) & 0 & \dots & 0 & jf_1(\alpha) & 0 & jf_0(\alpha) \\
0 & kf_1(\alpha) & 0 & & \dots & & 0 & jf_0(\alpha) & 0
\end{pmatrix} \tag{4.30}$$

The signs of α in (4.22), (4.27), (4.28), and (4.29) were chosen to ensure that the outer monopoles lie near roots of unity for α close to 1. For (4.30), the outer monopoles will lie near roots of unity for α close to 1 if N is even, and on the dual regular polygon if N is odd. Replacing α by $(-1)^N\alpha$ would ensure that the outer monopoles lie near the roots of unity for all N, but this would make the matrix (4.30) more cumbersome.

As in Section 4.3.1, we can think of all the data in this Section as defining monopoles in either the half-space or ball models. The generalisation of the

spectral curve (4.26) to D_{N-M}-symmetric N-monopoles appears to be

$$\mathcal{A}_N - \alpha\mathcal{A}_M\left((-1)^{M+1} + (-1)^N(\eta\zeta)^{N-M}\right) + \alpha^2\left(\mathcal{A}_M(\zeta^{N-M} + (-\eta)^{N-M}) - \mathcal{A}_N\right) = 0. \quad (4.31)$$

This formula has been checked for a large range of values of N for each M in the range $0 \leq M \leq 3$. We have not been able to check (4.31) for $M > 3$, because the required ADHM data is not known. One can check that as $|\alpha| \to 1$ this curve becomes a product of $\mathcal{A}_M$ and stars for monopoles arranged in a regular polygon on the boundary. (4.31) has the rotation symmetries $(\eta, \zeta) \to (e^{2\pi i/(N-M)}\eta, e^{2\pi i/(N-M)}\zeta)$ and $(\eta, \zeta) \to (1/\eta, 1/\zeta)$, so the data (4.27)-(4.30), all correspond to D_{N-M}-symmetric N-monopoles in either Braam-Austin or Manton-Sutcliffe formalisms. The corresponding Donaldson-type rational maps are

$$\mathcal{R}(z) = \frac{1 + \alpha z^{N-M}}{\alpha z^M + z^N},$$

with manifest rotational symmetry $\mathcal{R}(e^{2\pi i/(N-M)}z) = e^{-2\pi i/(N-M)}\mathcal{R}(z)$. These can be proved in the same way as the D_N symmetric N-monopole rational map (4.24). If $M > 0$, then $\mu = 0$ for all values of N and α (recall from Section 4.3.1 that $\mu = (-1)^N\alpha j$ if $M = 0$). This is to be expected, because μ is related to the Higgs field at the origin by $-2\mu = \Phi(0)$ [MS14]. Since there is an approximately axial M-monopole at the origin for $M > 0$ the Higgs field should vanish there, and this means that we can calculate the Jarvis rational maps for these families. Interestingly, if one replaces $i \to k, j \to i, k \to j$ in the data above to ensure the monopole is in the correct orientation, then the Jarvis-type rational maps are precisely the same as the Donaldson-type maps, with the other D_{N-M} symmetry generator manifesting itself as $\mathcal{R}(1/z) = 1/\mathcal{R}(z)$.

4.3.3 TWISTED-LINE SYMMETRIC MONOPOLES

In this subsection we will consider monopoles symmetric under a 'twisted inversion symmetry'. The symmetry I_N acts by the reflection I in the X_2X_3 plane combined with a rotation of $2\pi/N$ around the X_1-axis:

$$I_N : X \to ie^{\frac{2i\pi}{N}}Xe^{-\frac{2i\pi}{N}}i.$$

We shall consider N-monopoles invariant under an I_{2N-2} symmetry. This was the symmetry originally considered in the Euclidean space context in [HS96a].

The first example is a 3-monopole with I_4 symmetry, given by the matrix

$$\frac{1}{\sqrt{2}}\begin{pmatrix} j\sqrt{1-\alpha^2} & i\sqrt{2}\alpha & -k\sqrt{1-\alpha^2} \\ i\sqrt{2}\alpha & j\sqrt{1-\alpha^2} & 0 \\ j\sqrt{1-\alpha^2} & 0 & k\sqrt{1-\alpha^2} \\ 0 & k\sqrt{1-\alpha^2} & -i\sqrt{2}\alpha \end{pmatrix} \tag{4.32}$$

for $\alpha \in (-1, 1)$. This is exactly the same as the D_2-symmetric 3-monopole family considered in 3.4.1. The parameter α here plays the same role as a in (3.4.1), and the scattering takes place along the X_1-axis. When $\alpha = 1/\sqrt{3}$, (4.32) becomes equal to (a rotated version of) the tetrahedrally symmetric ADHM data given in [MS14].

The generalisation of (4.32) to all N is

$$\widehat{M}_N^I = \frac{1}{2}\begin{pmatrix} j\sqrt{2}f_1(\alpha^2) & -i\alpha\sqrt{2} & 0 & \cdots & 0 & \alpha\sqrt{2} & -k\sqrt{2}f_1(\alpha^2) \\ -2i\alpha & jf_1(\alpha^2) & 0 & \cdots & 0 & -kf_1(\alpha^2) & 0 \\ jf_1(\alpha^2) & & & & & & kf_1(\alpha^2) \\ 0 & & & & & & 0 \\ \vdots & & & 2M_{N-2}^{\mathrm{ax}} & & & \vdots \\ 0 & & & & & & 0 \\ -kf_1(\alpha^2) & & & & & & jf_1(\alpha^2) \\ 0 & kf_1(\alpha^2) & 0 & \cdots & 0 & jf_1(\alpha^2) & 2i\alpha \end{pmatrix} \tag{4.33}$$

As α varies, the process consists of two 1-monopoles moving along the X_1-axis towards a central approximately axial cluster of $(N-2)$ monopoles at the origin. In contrast to the dihedral families, the outer monopoles lie on the symmetry axis of the central cluster, rather than perpendicular to it. The configuration becomes axial as α passes through zero, and then as α decreases the process happens in reverse, but rotated by $\pi/(N-1)$ around the X_1-axis.

Since $\mu = 0$ for all members of the family (4.33), we can calculate their Jarvis rational maps. We again substitute $i \to k, j \to i, k \to j$ in the data to put the rational maps into a simpler form. For $N = 3$, the rational map is

$$\frac{2\alpha z^2 + 1 - \alpha^2}{(1-\alpha^2)z^3 - 2\alpha z} \tag{4.34}$$

which has the I_4 symmetry $R(i/\overline{z}) = i/\overline{R(z)}$. For $N = 4$, the rational map is

$$\frac{2\alpha z^3 + 1 - \alpha^2}{(1-\alpha^2)z^4 - 2\alpha z}, \tag{4.35}$$

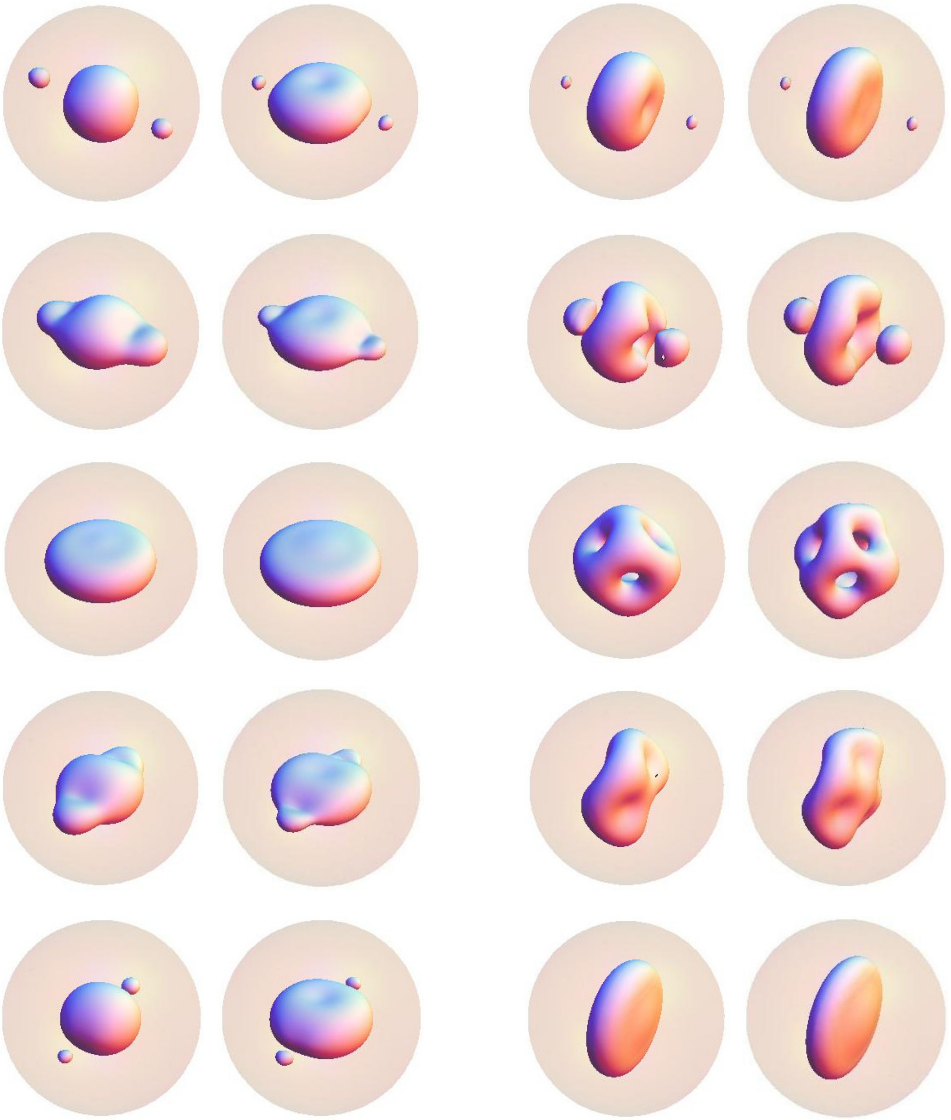

Figure 4.1: Energy density isosurfaces: first column D_2-symmetric 3-monopoles, second column D_2-symmetric 4-monopoles, third column I_6-symmetric 4-monopoles, fourth column I_8-symmetric 5-monopoles. The energy densities were calculated using the formula (3.3).

with the I_6 symmetry $R(e^{i\pi/3}/\overline{z}) = e^{i\pi/3}/\overline{R(z)}$. The third and fourth columns of Figure 4.1 show energy density isosurfaces of twisted-line symmetric monopoles of charges 4 and 5 respectively, for different values of α between 1 and 0 decreasing down the column.

For the $N = 4$ family, one can check that if $\alpha = \pm 1/\sqrt{2}$ the rational map (4.35) is equivalent to the degree 4 cubically symmetric rational map given in [MS14], combined with a rotation to bring the cube into the correct orientation. Note that for $N > 3$, all members of these twisted-line symmetric families (apart from the axial monopoles) lie outside the space of JNR-type monopoles, because it is impossible to arrange $N + 1$ distinct points on the 2-sphere with I_{2N-2}-symmetry.

4.4 Summary

Using an equivalence between hyperbolic $p = 1/2$ axial N-monopoles and $p = N/2$ 1-monopoles, we have given an explicit formula for the Higgs field magnitude of axial $p = 1/2$ monopoles, as well as their circle-invariant ADHM data. We have deformed the axial monopole data to give 1-parameter families with various kinds of dihedral and twisted-line symmetry, for all values of the topological charge.

The dihedral families presented here should extend to D_{N-M}-symmetric N-monopole configurations with M monopoles at the origin for $M > 3$, although we have not been able to find the explicit ADHM data for these with our methods. Another approach would be to look for JNR-type monopoles with the right poles and weights to give the conjectured spectral curves (4.31). For M and $(N-M)$ both large, this should give a hyperbolic prototype of Manton's multi-shell magnetic bags [Man12], although these bags would be degenerate, in the sense that the volume of their interiors would be zero.

Finally, it would be interesting to compare the metric on the space of D_2 symmetric 3-monopoles presented in this Chapter with the metric on the space of D_2 symmetric 2-monopoles presented in the previous one, since in the Euclidean case these are known to be the same.

5

Vortices and magnetic impurities

The work in this Chapter was inspired by [TW14], in which Tong and Wong discussed BPS vortices in the presence of both electric and magnetic impurities. At the classical level, electric impurities were shown to leave the moduli space of static solutions unchanged, but the usual geodesic approximation to the dynamics is supplemented by a connection term. This observation allowed a complete analysis of both the classical and quantum dynamics of a single vortex in the presence of a delta-function electric impurity. The purpose of this Chapter is to investigate the less well-understood effect of magnetic impurities on vortex dynamics.

Magnetic impurities do not introduce any connection term, but instead deform the static solutions and the corresponding moduli space metric, assuming they exist. [TW14] gives a number of different arguments for the existence of a moduli space, which this paper complements with some numerical evidence in Section 5.1. To illustrate the generic effect of magnetic impurities on vortex dynamics, we also give numerical examples of moduli space metrics for a single vortex in the presence of axially-symmetric, localised lump-like impurities.

In Chapter 2 we described how analytic progress can be made by making a judicious choice of background. In Section 5.2 we will show that the vortex equations on the hyperbolic plane of curvature $-1/2$ remain integrable when delta-function magnetic impurities are introduced, and we will present an explicit 1-vortex moduli space metric. In Section 5.3 we will extend the work of Baptista and Manton on vortices on the 2-sphere near the Bradlow limit to the introduction of impurities.

5.1 FLAT SPACE VORTICES WITH IMPURITIES

The deformation of the action (2.1) suggested in [TW14] to include magnetic impurities is:

$$\int \left(-\frac{1}{4} F_{\mu\nu} F^{\mu\nu} + \frac{1}{2} \overline{D_\mu \phi} D^\mu \phi - \frac{1}{8} (1 + \sigma - |\phi|^2)^2 + \frac{1}{2} \sigma B \right) d^3x, \tag{5.1}$$

where σ is a static source for the magnetic field $B = F_{12}$. Applying the usual Bogomolny argument gives first-order equations:

$$D_1 \phi + i D_2 \phi = 0 \tag{5.2}$$

$$B - \frac{1}{2}(1 + \sigma - |\phi|^2) = 0, \tag{5.3}$$

and we still have the topological bound $E \geq \frac{1}{2} \int B \, d^2x = \pi N$, where N is the asymptotic winding of ϕ. Two arguments are given in [TW14] for the existence of a $2N$-dimensional moduli space of solutions to these equations. Firstly, the linearisation of equations (5.2) and (5.3) and Gauss's law is independent of the impurity σ, so the usual index theorem [Wei79a] counting the number of linearised deformations goes through unchanged. Secondly, the magnetic impurities above can be shown to arise as the limit of vortices in product gauge groups, and these systems can be realised as D-brane configurations. The aim of this Section is to complement these arguments with some numerical examples. We will obtain numerical solutions for the case where σ is an axially-symmetric localised impurity of the form $\sigma = ce^{-d(x^2+y^2)}$, where $c \in \mathbf{R}$ and $d \in \mathbf{R}_+$. We will also give numerical evidence for the existence of a 1-vortex moduli space and adapt the methods of Samols to calculate the metric numerically for various impurities.

We can straightforwardly rewrite (5.2) and (5.3) as a modified version of Taubes' equation:

$$\nabla^2 f + 1 + \sigma - e^f = 4\pi \sum_{r=1}^{N} \delta^2(z - z_r). \tag{5.4}$$

The function f has singularities, so for numerical work we solve for the function

$$\Phi = f - \sum_{r=1}^{N} \log |z - z_r|^2,$$

so that (5.4) becomes

$$\nabla^2\Phi + 1 + \sigma - \prod_{r=1}^{N} |z - z_r|^2 e^{\Phi} = 0, \tag{5.5}$$

with boundary conditions

$$\Phi \sim -\sum_{r=1}^{N} \log|z - z_r|^2 \text{ as } |z| \to \infty. \tag{5.6}$$

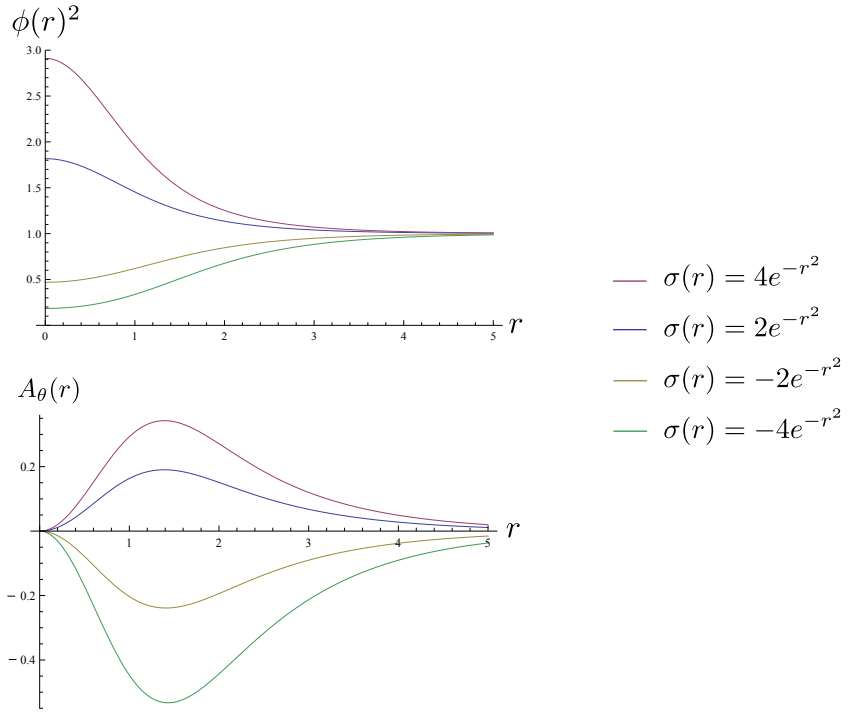

Figure 5.1: Higgs and gauge field profiles for vacua in the presence of impurities.

The first step is to solve for the vacuum. Plots of ϕ, A_θ are given in Fig. 5.1 for various values of c, d. For these plots we have chosen an axial gauge where $A_r = 0$ and ϕ is real on the whole plane, which is only possible for these vacuum solutions with zero asymptotic winding. The solutions were found using an over-relaxation method on the interval $[0, 5]$ by imposing the Neumann boundary condition that $\Phi'(0) = 0$ and the Dirichlet condition (5.6) at $r = 5$. The solutions illustrate the important fact that the response of the fields to a localised impurity is also localised. These plots also indicate that $\phi(0) \to 0$ as $c \to -\infty$, while $\phi(0) \to \infty$ as $c \to \infty$, and this seems to hold true over a much greater range of values of c than those plotted here.

Just as for impurity-free vortices, the energy density is defined to the static part of the Lagrangian (5.1). Plots of the energy density and magnetic field are shown in Fig. 5.2. Note that there is a range of values for which the energy density is negative. In contrast to the standard abelian-Higgs system (2.1), the integrand of the the potential energy functional for the system with magnetic impurities is not a sum of total squares, so there is nothing to prevent this. The plot of the magnetic field illustrates the general observation that reversing the sign of the impurity appears to approximately reverse the sign of B.

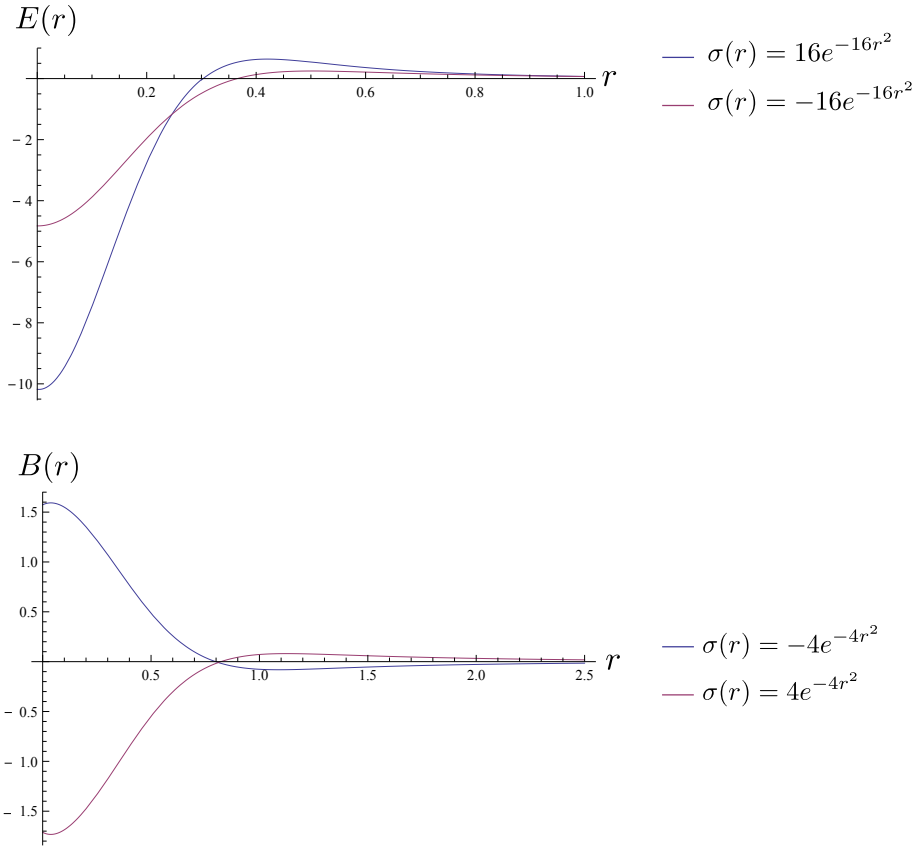

Figure 5.2: Energy densities and magnetic fields for vacua in the presence of impurities.

To find 1-vortex solutions, we can numerically solve (5.5) with $N = 1$ by over-relaxing from an initial configuration

$$\Phi_0 = \log\left(\mu(|z - z_1|)\right)^2 - \log|z - z_1|^2 + \Phi_{\text{vac}},$$

where we have approximated the 1-vortex profile by $\mu(r) = \tanh(0.6r)$ and Φ_{vac} is one of the vacuum impurity solutions found above. Some solutions for $\sigma(r) = \pm e^{-r^2}$ and z_1 placed on the x-axis and varying by intervals of 0.5

between -2.5 and 0 are plotted in Fig. 5.3. The fact that solutions appear to exist wherever one puts the vortex zero provides evidence of a 1-vortex moduli space. The energies of these solutions are within 1% of the Bogomolny bound, giving a good check on the numerics. As one would expect, the solution looks like a superposition of the vacuum solution and an ordinary 1-vortex when the vortex zero is placed far from the impurity, but the vortex appears to 'screen' the impurity as it approaches the origin.

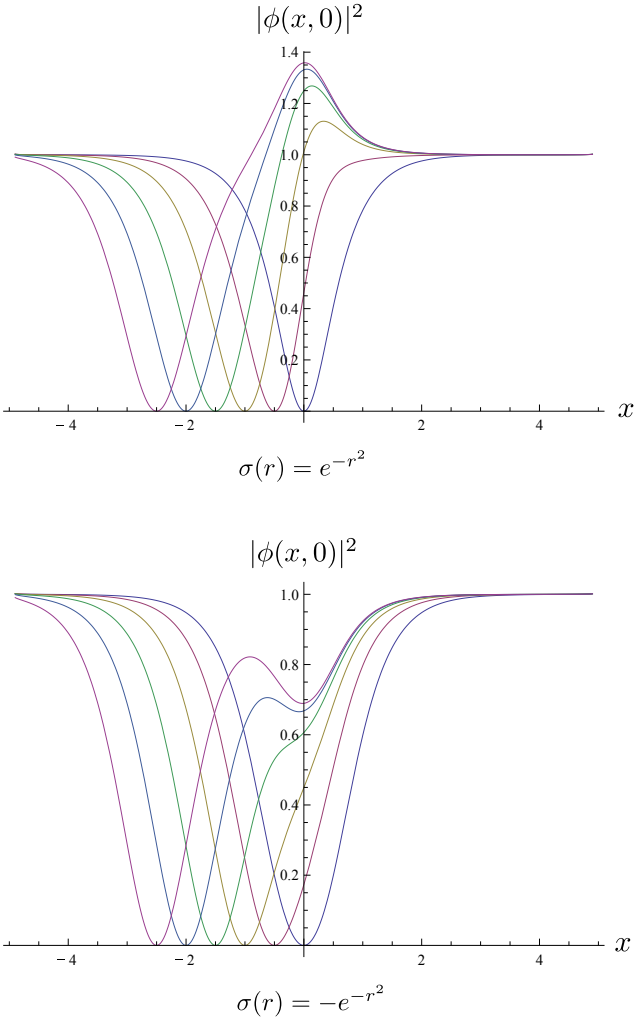

Figure 5.3: Higgs fields for families of 1-vortices in the presence of two different axial impurities.

5.1.1 Moduli space metrics

Samols' formula (2.10) generalises easily to magnetic impurities. The only difference is due to the fact the quantity d_r defined in (2.9), which in the

impurity-free case is $-1/4$, must be equal to $-\frac{1}{4}(1+\sigma(z_r))$ to satisfy (5.5). The rest of the derivation goes through as in the impurity-free case [Sam92], and the general expression for the metric is:

$$ds^2 = \pi \sum_{r,s=1}^{N} \left(\delta_{rs}(1+\sigma(z_r)) + 2\frac{\partial \bar{b}_s}{\partial z_r} \right) dz_r d\bar{z}_s. \tag{5.7}$$

Our numerical metrics will be for 1-vortices in the presence of axially symmetric impurities. If $z_1 = \rho e^{i\theta}$ is the position of the vortex zero, then by rotational symmetry and the fact that the metric is Hermitian b_1 must take the form $b_1 = b(\rho)e^{-i\theta}$, and the metric is

$$\begin{aligned} ds^2 &= \pi \left(1 + \sigma(\rho) + 2\frac{\partial \bar{b}_1}{\partial z_1} \right) dz_1 d\bar{z}_1 \\ &= \pi \left(1 + \sigma(\rho) + \frac{1}{\rho}\frac{d(\rho b)}{d\rho} \right) \left(d\rho^2 + \rho^2 d\theta^2 \right) \qquad (5.8) \\ &\equiv \pi F^2(\rho) \left(d\rho^2 + \rho^2 d\theta^2 \right). \qquad (5.9) \end{aligned}$$

For the 1-vortex, $b_1 = 2\partial_z \Phi(z_1)$, so $b = \partial_\rho \Phi(z_1)$. Fig. 5.4 illustrates the results of this for different impurities. It is straightforward to numerically calculate geodesics for these metrics, and they show that in general a slow-moving vortex is repelled from the impurity if $c < 0$, and attracted if $c > 0$.

We can obtain a more physical understanding of this behaviour using a point particle approximation of both the vortex and the impurity. Just as for impurity-free vortices [MS03], this gives analytic information about the moduli space metric when the vortex is far from the impurity. Suppose we have either an axial impurity on its own or a single vortex at the origin. Provided the impurity decays sufficiently rapidly, then in either case (5.4) linearises at large ρ to

$$\frac{d^2 f_0}{d\rho^2} + \frac{1}{\rho}\frac{df_0}{d\rho} - f_0 = 0, \tag{5.10}$$

the modified Bessel equation of zeroth order, and this is independent of the impurity. f_0 must therefore have the asymptotic form

$$f_0(\rho) \sim \frac{q}{\pi} K_0(\rho)$$

for some constant q. The interpretation of this is that at large ρ, the vortex or impurity can be thought of as a composite of a scalar monopole of charge q and a magnetic dipole of moment q perpendicular to the plane. We shall

therefore refer to q as the point charge of the vortex or impurity. Manton and Speight used this point particle model to explicitly calculate the asymptotic N-vortex moduli space metric [MS03].

For a 1-vortex, the point charge was first calculated numerically by Speight [Spe97] to be -10.6, and later Tong gave a string theory argument suggesting that the point charge is $-2\pi 8^{\frac{1}{4}}$ [Ton02]. The point charges of impurities are straightforward to calculate numerically, and the derivation of the asymptotic 1-vortex metric goes through in almost exactly the same way as the asymptotic 2-vortex metric in [MS03], giving

$$\frac{\pi}{2}\left(2-\frac{qq'}{\pi^2}K_0(\rho)\right)(d\rho^2+\rho^2 d\theta^2), \tag{5.11}$$

where q, q' are the point charges of the vortex and the impurity respectively.

The explicit form of (5.11) allows us to calculate exactly the difference in volume between (5.8) and the metric on the impurity-free 1-vortex moduli space $\pi dz_1 d\bar{z}_1$, which (5.8) approaches asymptotically. The exponential decay of K_0 as $\rho \to \infty$ and the form of (5.8) imply that b also decays exponentially, and so one can easily calculate this difference in volume to be $\pi \int \sigma \, d^2x$.

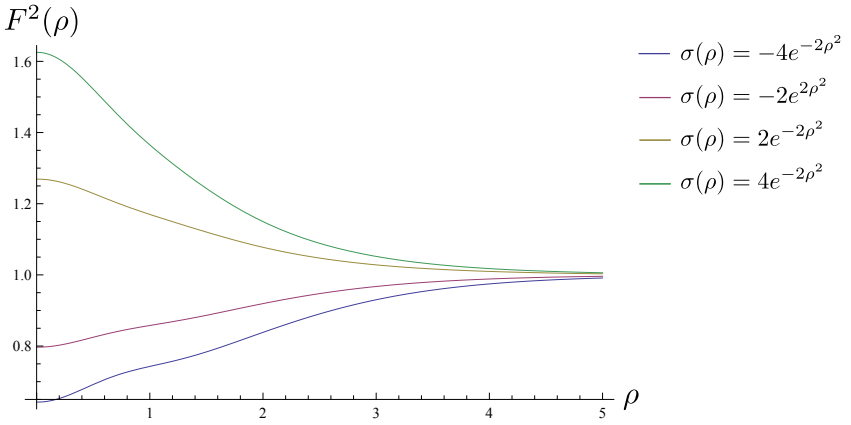

Figure 5.4: Moduli space metric profiles for 1-vortices in the presence of various impurities.

5.1.2 Delta-function impurities

It is natural to consider what happens in the limit where σ approaches a delta-function. Unfortunately this introduces the square of a delta-function into the Lagrangian (5.1), which is not defined. However, it does make sense to replace

σ with a delta-function in (5.3), and we can consider this to be a limit of impurities for which there is a Lagrangian description.

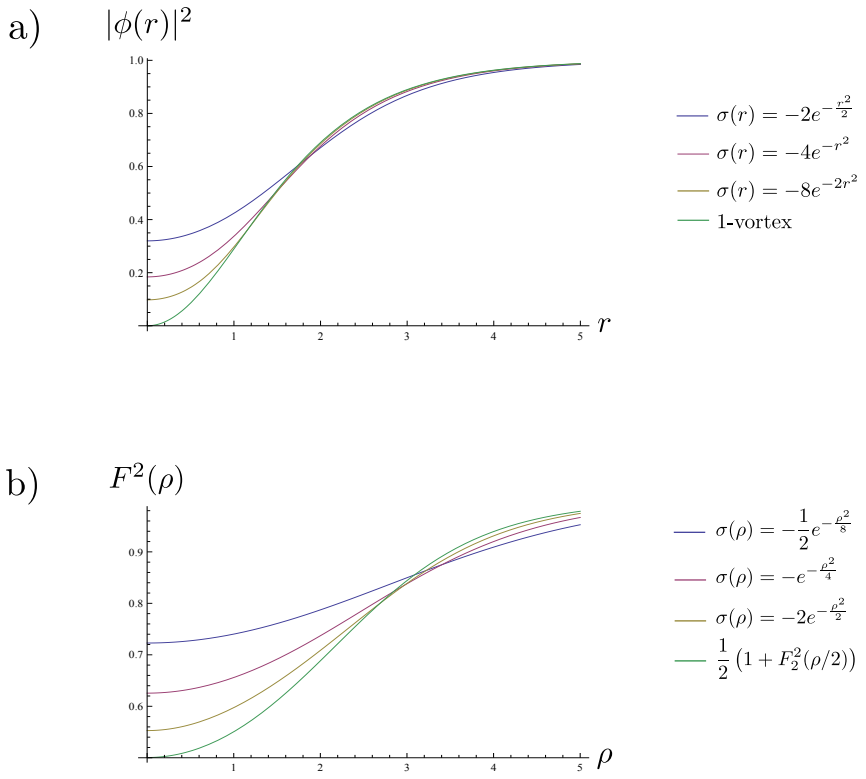

Figure 5.5: a) Higgs field profiles for vacua converging to the 1-vortex profile in the delta-function limit. b) Moduli space metric profiles for 1-vortices in the presence of impurities converging to a shifted version of the impurity-free 2-vortex metric in the delta-function limit.

Suppose we replace σ by a delta-function of the form $-4\pi\alpha\delta(z)$ where $\alpha \in \mathbf{N}$, and we look for solutions with winding number N. In this case (5.4) becomes the impurity-free Taubes equation for $N + \alpha$ vortices with α vortices constrained to lie at $z = 0$. This corresponds to applying the singular gauge transformation $\phi \to e^{-i\alpha\theta}\phi$ to this $(N + \alpha)$-vortex solution, so the winding number of ϕ at infinity is still N. In a formal sense, we could solve (5.2) and (5.3) by taking any $(N + \alpha)$-vortex solution with a single vortex at the origin and applying this singular gauge transformation, but if $\alpha > 1$ numerical investigations suggest that this does not correspond to the limit of solutions to Bogomolny equations with finite impurities. Instead the correct moduli space of solutions with winding number N is the submanifold of the impurity-free $(N + \alpha)$-vortex moduli space with α vortices fixed at the origin. Fig. 5.5 a)

shows vacua with winding number zero converging to the 1-vortex solution in the delta-function limit.

The global gauge transformation relating an N-vortex (ϕ, A_i) in the presence of an α-impurity to an impurity-free $(N+\alpha)$-vortex (ϕ', A_i') is the same for every vortex, which means that the corresponding map between the moduli space of N-vortices in the presence of an α-impurity and the moduli space of $(N+\alpha)$-vortices with α vortices constrained to lie at the origin is a diffeomorphism. Gauss's law is unchanged by the impurity, so $(\delta\phi, \delta A_i) = (\delta\phi', \delta A_i')$ and using (2.8) we see that this diffeomorphism of moduli spaces is an isometry. This implies that the metric on the moduli space of vortices in the presence of delta-function impurities with $\alpha \in \mathbf{N}$ is just the restriction of the usual impurity-free vortex metric to the submanifold of solutions where α vortices are fixed at the origin. As one would expect, the numerics suggest that the moduli space metric for finite impurities converges to the metric on this submanifold in the delta-function limit. In particular, the metric for a 1-vortex moving in the presence of an impurity $\sigma = -4\pi\delta(z)$ should be related to the impurity-free 2-vortex metric by a simple shift of coordinates. The impurity-free metric for two vortices at positions $z_1 = Z + W$ and $z_2 = Z - W$ has the form

$$ds^2 = 2\pi dZ d\bar{Z} + 2\pi F_2^2(|W|)\, dW d\overline{W}.$$

The submanifold defined by the constraint $z_2 = 0$ therefore has metric

$$\frac{\pi}{2}\left(1 + F_2^2(\rho/2)\right)(d\rho^2 + \rho^2 d\theta^2), \tag{5.12}$$

where $z_1 = \rho e^{i\theta}$ as before. Fig. 5.5 b) shows moduli space metrics for 1-vortices in the presence of impurities converging to (5.12), as expected.

We can also find numerical solutions in the case where α is any positive real number by solving

$$\nabla^2\Phi + 1 - |z|^\alpha \prod_{r=1}^{N} |z - z_r|^2 e^\Phi = 0$$

with the same boundary conditions as before. Near the origin the Higgs field of the solution will vanish to order α, and the interpretation is that α vortices are pinned at the origin. The next Section shows that we can find explicit static solutions and 1-vortex metrics for all $\alpha > 0$ if we move to a hyperbolic space background.

5.2 HYPERBOLIC VORTICES WITH DELTA-FUNCTION IMPURITIES

Just as for impurity-free vortices, it is straightforward to generalise (5.1) to a spacetime of the form $X \times \mathbf{R}$, where X is an arbitrary Riemann surface. Locally we choose isothermal coordinates so that the metric on X is of the form $ds^2 = \Omega(x_1, x_2)(dx_1^2 + dx_2^2)$ and the Bogomolny equations (5.2), (5.3) become

$$D_1\phi + iD_2\phi = 0 \tag{5.13}$$

$$B - \frac{\Omega}{2}(1 + \sigma - |\phi|^2) = 0, \tag{5.14}$$

and (5.4) generalises to

$$\nabla^2 f + \Omega(1 + \sigma - e^f) = 4\pi \sum_{r=1}^{N} \delta^2(z - z_r). \tag{5.15}$$

As described in Chaper 2, the vortex equations are integrable if X is hyperbolic space with constant curvature $-1/2$, which has metric

$$\Omega(z, \bar{z}) = \frac{8}{(1 - |z|^2)^2}, \tag{5.16}$$

where $|z| < 1$. If we make the substitution $f = 2g + 2\log\frac{1}{2}(1 - |z|^2)$, then (5.15) becomes

$$\nabla^2 g + \frac{1}{2}\Omega\sigma - e^{2g} = 2\pi \sum_{r=1}^{N} \delta^2(z - z_r). \tag{5.17}$$

When $\sigma = 0$, this is Liouville's equation with sources, whose solution is

$$g = -\log\frac{1}{2}\left(1 - |h|^2\right) + \frac{1}{2}\log\left|\frac{dh}{dz}\right|^2,$$

where $h(z)$ is an analytic function of the form

$$h(z) = \prod_{i=1}^{N+1}\left(\frac{z - \beta_i}{1 - \bar{\beta}_i z}\right). \tag{5.18}$$

The β_i are complex numbers in the unit disc chosen so that $\frac{dh}{dz}$ vanishes at the vortex positions z_r. The corresponding Higgs and gauge fields are

$$\phi = \frac{1-|z|^2}{1-|h|^2}\frac{dh}{dz} \text{ and } A_{\bar{z}} = -i\frac{\partial}{\partial \bar{z}} \log\left(\frac{1-|z|^2}{1-|h|^2}\right)$$

where $A_{\bar{z}} = \frac{1}{2}(A_1 + iA_2)$.

If we choose $\sigma(z) = -4\pi\alpha\Omega(0)^{-1}\delta(z)$ for any α, then the equations (5.13) and (5.14) can still be solved by a rational map ansatz of exactly the same type which constrains α of the vortices to lie at the origin. We let

$$g = -\log\frac{1}{2}\left(1-|z|^{2(\alpha+1)}|k|^2\right) + \frac{1}{2}\log\left|z\frac{dk}{dz} + (\alpha+1)k\right|^2 - \frac{1}{2}\log|z|^{2\alpha}, \quad (5.19)$$

where we take $k(z) = \prod_{i=1}^{N}\left(\frac{z-\beta_i}{1-\bar{\beta}_i z}\right)$ and choose the β_i so that the N zeroes of $z\frac{dk}{dz} + (\alpha+1)h$ lie at the vortex positions z_r. The corresponding fields are

$$\phi = |z|^\alpha\left(\frac{1-|z|^2}{1-|z|^{2(\alpha+1)}|k|^2}\right)\left((\alpha+1)k + z\frac{dk}{dz}\right) \text{ and } A_{\bar{z}} = -i\partial_{\bar{z}}\log\phi. \quad (5.20)$$

It turns out that just as in the impurity-free case, these solutions have a four-dimensional interpretation [Har]. They can be thought of as multi-instantons on $\mathbf{H}^3 \times S^1$, generalising 1-instanton solutions on the same space given in [Har08].

The static solutions can be calculated explicitly when $N = 1$. In this case we take

$$k(z) = \frac{z-\beta}{1-\bar{\beta}z},$$

where β is given by solving the quadratic equation obtained by setting the numerator of the expression for ϕ in (5.20) to zero:

$$\beta = z_1\frac{(\alpha+1)(1+|z_1|^2) - \sqrt{(\alpha+1)^2(1-|z_1|^2)^2 + 4|z_1|^2}}{2\alpha|z_1|^2}.$$

To calculate the 1-vortex moduli space metrics, one can use the straightforward generalisation of Samols' formula on a general background (2.13) to include impurities:

$$ds^2 = \pi\sum_{r,s=1}^{n}\left(\Omega(z_r)\delta_{rs}(1+\sigma(z_r)) + 2\frac{\partial\bar{b}_s}{\partial z_r}\right)dz_r d\bar{z}_s. \quad (5.21)$$

For the 1-vortex, if we Taylor expand around the vortex position z_1:

$$(\alpha+1)k + z\frac{dk}{dz} = k^{(1)}(z-z_1) + \frac{k^{(2)}}{2!}(z-z_1)^2 + \dots$$

then it is straightforward to show that (5.21) becomes

$$ds^2 = 4\pi \frac{\partial}{\partial z_1}\left(\frac{\overline{k}^{(2)}}{2\overline{k}^{(1)}}\right) dz_1\, d\bar{z}_1,$$

which can be calculated to be

$$\begin{aligned} ds^2 &= 4\pi \frac{2+2|z_1|^2 + \sqrt{(1+\alpha)^2(1+|z_1|^2)^2 - 4\alpha(2+\alpha)|z_1|^2}}{(1-|z_1|^2)^2\sqrt{(1+\alpha)^2(1+|z_1|^2)^2 - 4\alpha(2+\alpha)|z_1|^2}} dz_1 d\bar{z}_1 \qquad (5.22)\\ &\equiv \frac{G(|z_1|)}{(1-|z_1|^2)^2} dz_1 d\bar{z}_1. \end{aligned}$$

As $\alpha \to \infty$, the factor G tends pointwise to the constant function 4π. The limit $\alpha \to \infty$ corresponds to a fixed 'bag' of hyperbolic vortices at the origin of the type considered in [Sut12]. The Higgs field is very close to zero inside the bag, whose radius grows with α, and very close to 1 outside the bag. The thickness of the bag's surface depends only on the Higgs mass.

We can see this bag structure in the metric (5.22). The disc model coordinate z_1 is not convenient for analysing the large α limit, because it has finite range. If we change coordinates $|z_1| = \tanh(r/2^{3/2})$, then the hyperbolic plane metric (5.16) is

$$ds^2 = dr^2 + 2\sinh^2(r/\sqrt{2})d\theta^2$$

and r has infinite range. The radius of the bag is given approximately by $R = \sqrt{2}\log(2\alpha)$. If we scale coordinates $r' = r/R$ to keep this radius at the same position as α changes, then it is easy to check that as $\alpha \to \infty$, $G(\tanh(Rr'/2^{3/2}))$ tends pointwise to the step function

$$G_\infty(r') = \begin{cases} 4\pi & \text{if } r' < 1 \\ 12\pi & \text{if } r' > 1 \end{cases}$$

This shows that a slow-moving vortex moves along the geodesics of hyperbolic space both inside and outside the bag, but with effective inertial masses $\pi/2$ inside the bag and $3\pi/2$ outside.

5.3 Vortices on the 2-sphere with impurities

In this Section we adapt the results of Baptista and Manton on vortices on the 2-sphere near the Bradlow limit [BM03] to the inclusion of delta-function magnetic impurities. Since the background is a closed manifold, we think of ϕ as a Section of a complex line bundle $E \to S^2 \cong \mathbf{CP}^1$ equipped with a Hermitian metric h. The bundle $E \to S^2$ can now have non-trivial topology and we identify its first Chern class with the topological charge N. The gauge potentials are local 1-form representatives of an h-compatible connection D on E, and the magnetic field is identified with the curvature $F \in \Omega^2(X, \mathbf{R})$ of D. The Bogomolny equations can be written in covariant form as

$$D^{0,1}\phi = 0 \tag{5.23}$$

$$F - \frac{1}{2}(1 + \sigma - |\phi|_h^2)\mathrm{vol}_X = 0 \tag{5.24}$$

where the impurity σ is some smooth real-valued function on S^2.

We will take the usual atlas on $\mathbf{CP}^1$ consisting of the two open sets $U_1 = \mathbf{CP}^1 \backslash \{[0,1]\}$ and $U_2 = \mathbf{CP}^1 \backslash \{[1,0]\}$ and the charts $\varphi_i : U_i \to \mathbf{C}$ with transition function $\varphi_1 \circ \varphi_2^{-1}(z) = 1/z$. We will consider spheres of varying radius with metric defined by $g_R = R^2 \times$ (standard round sphere metric). The line bundle $\pi : E \to S^2$ is defined by the transition functions $g_{ij} : U_i \cap U_j \to U(1)$ where

$$g_{21} \circ \varphi_2^{-1}(z) = (z/|z|)^N, \quad g_{12} = 1/g_{21}, \quad g_{11} = g_{22} = 1$$

It is straightforward to check that these transition functions satisfy the cocycle conditions and that the corresponding bundle has degree N. If $\psi_i : \pi^{-1}(U_i) \to U_i \times \mathbf{C}$ are the associated trivialisations, then one can define a metric h by setting $|\psi_i^{-1}(p, y)|_h^2 = |y|^2$. This is the bundle and metric we shall take throughout this Section.

The Bradlow bound (2.14) on the 2-sphere is modified by the presence of an impurity to:

$$R^2 + \frac{1}{4\pi}\int \sigma \, \mathrm{vol}_R \geq N. \tag{5.25}$$

Suppose we have a delta-function impurity σ defined by $\sigma(\phi_1(z)) = -\frac{\pi\alpha}{R^2}\,\delta^2(z)$ on U_1 and $\sigma(\phi_2(z)) = 0$ on U_2, so that $\int \sigma \, \mathrm{vol}_R = -4\pi\alpha$. We can explicitly solve the Bogomolny equations at the Bradlow limit $R^2 = N + \alpha$ for this choice of impurity. The Higgs field must vanish everywhere if the bound is saturated,

and one can check that the gauge potentials $A_i \in \Omega^1(U_i, \mathbf{R})$ defined by

$$A_1 = \phi_1^* A + \frac{i\alpha}{2|z|^2}(\bar{z}dz - zd\bar{z})$$
$$A_2 = \phi_2^* A,$$

where

$$A = -i\frac{N+\alpha}{2(1+|z|^2)}(\bar{z}dz - zd\bar{z})$$

give a connection $D_{N+\alpha}$ on E with $F_{N+\alpha} = \frac{1}{2}(1+\sigma)\mathrm{vol}_{\sqrt{N+\alpha}}$ as required.

Now we move away from the Bradlow limit, taking R^2 to be slightly greater than $N+\alpha$. We shall make similar assumptions to Baptista and Manton; namely, $D \approx D_{N+\alpha}$ for these vortices, and ϕ satisfies the conditions:

1. $D^{0,1}_{N+\alpha}\phi = 0$,
2. $\int_{\mathbf{CP}^1} \left(F_{N+\alpha} - \frac{1}{2}(1+\sigma-|\phi|_h^2)\mathrm{vol}_R\right) = 0$.

We shall work on the coordinate patch U_1 and take a representative $\phi_1 = \phi \circ \varphi_1^{-1}$ of ϕ. In these coordinates condition 1 becomes

$$\frac{\partial \phi_1}{\partial \bar{z}} = z\left(-\frac{\alpha+N}{2(1+|z|^2)} + \frac{\alpha}{2|z|^2}\right)\phi_1,$$

which has general solution

$$\phi_1 = \frac{f(z)|z|^\alpha}{(1+|z|^2)^{(N+\alpha)/2}},$$

where f is holomorphic on $\mathbf{C}$. This must be extensible to a solution $\phi_2 = g_{12}(z)\phi_1(\frac{1}{z})$ of condition 1 on U_2, which forces f to be a polynomial in z of degree N. If we write $f(z) = a_0 z^N + a_1 z^{N-1} + \cdots + a_N$, then condition 2 becomes

$$4\pi(R^2 - N - \alpha) = \int_{\mathbf{CP}^1} |\phi|_h^2 \,\mathrm{vol}_R = \int_{\mathbf{C}} |\phi_1|^2 \frac{2iR^2}{(1+|z|^2)^2} dz \wedge d\bar{z} \tag{5.26}$$

$$= \sum_{k=0}^{N} |a_k|^2 \int_{\mathbf{C}} \frac{|z|^{2(N-k+\alpha)} 2iR^2}{(1+|z|^2)^{N+\alpha+2}} dz \wedge d\bar{z} \tag{5.27}$$

$$= 4\pi R^2 \sum_{k=0}^{N} |a_k|^2 \frac{\Gamma(k+\alpha+1)(N-k)!}{\Gamma(N+\alpha+2)} \tag{5.28}$$

Just as for impurity-free vortices, there is a bijection between the space of solutions to conditions 1, 2 and S^{2N+1} given by

$$\phi_1 \to \left(1 - \frac{N+\alpha}{R^2}\right)^{-1/2} \left(\dots, \left(\frac{\Gamma(N+\alpha+2)}{\Gamma(k+\alpha+1)(N-k)!} \right)^{1/2} a_k, \dots \right)_{0 \leq k \leq N} \tag{5.29}$$

The rest of the derivation of the moduli space metric in [BM03] goes through unchanged; the only difference is the sphere identification (5.29). The fact that we have fixed the gauge field means that the remaining gauge freedom is multiplication of ϕ by a constant phase, so identifying gauge-equivalent points in S^{2N+1} corresponds to the usual $U(1)$-principal bundle $S^{2N+1} \to \mathbf{CP}^N$. The geodesic approximation can be implemented in just the same way as in the impurity-free case, and the metric on $\mathbf{CP}^N$ is again the Fubini-Study metric. In particular, the 1-vortex metric is

$$(2\pi - N - \alpha) \frac{1+\alpha}{(1+\alpha+|z|^2)^2} dz d\bar{z}.$$

It is easy to see from this that the vortex is pushed away from the impurity for $\alpha > 0$, as one would expect from the results of the previous Sections. The same effect is visible for higher charge vortices; Fig. 5.6 shows two vortices scattering off the impurity for different values of α.

5.4 Summary

In this Chapter we investigated the effect of magnetic impurities on vortex dynamics in various models. A natural extension of this work would be to try to generalise to monopoles and instantons. Monopoles in the presence of a point-like Dirac monopole have been investigated previously [CD09], and it would be interesting to explore the connections between this system and the delta-function singularities described in this Chapter.

The existence result for impurity-free vortices on compact surfaces is easier than the corresponding result on flat space, and has been proved under quite general conditions. Another promising future direction would be to try to prove existence results for vortices on compact surfaces with impurities, and to investigate the conditions on the impurity for solutions to exist.

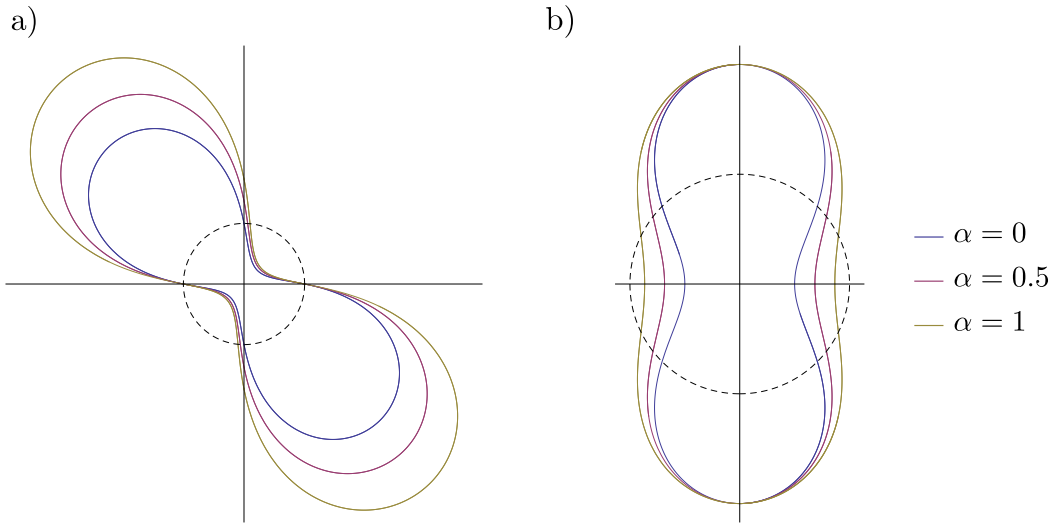

Figure 5.6: Geodesics corresponding to slow-motion scattering of two vortices off a delta-function impurity at the south pole. The southern hemisphere has been stereographically projected to the interior of the unit disc. The vortices in a) have initial positions $z_1 = 1$, $z_2 = -1$, and velocities $\dot{z}_1 = -1 + 0.2i$, $\dot{z}_2 = 1 - 0.2i$. The vortices in b) have initial positions $z_1 = 2$, $z_2 = 2$, and velocities $\dot{z}_1 = 2$, $\dot{z}_2 = 2$.

6

Conclusions and Outlook

We began this thesis with two introductory Chapters on monopoles and vortices. The first Chapter discussed the difficulty of solving the Bogomolny equation for monopoles on flat space and finding associated holomorphic objects. This motivated a change of background from Euclidean to hyperbolic space, because hyperbolic monopoles are known to be equivalent to Euclidean instantons if a discrete relationship exists between the Higgs mass and the curvature of the background. In Chapter 2 we gave some basic results for BPS vortices, setting the scene for the introduction of magnetic impurities in Chapter 5.

The main results of Chapter 3 were explicit formulae for the spectral curve and rational map of a JNR-type monopole in terms of its free JNR data. We used these to present the spectral curves and rational maps of some Platonic hyperbolic monopoles as well as some interesting 1-parameter families resembling scattering events. In Chapter 4 we derived explicit fields and ADHM data for axial hyperbolic monopoles and deformed them to give symmetric 1-parameter families generalising some of those given in Chapter 3. Finally, in Chapter 5 we adapted previous work on BPS vortices to the introduction of magnetic impurities of various kinds.

The work in this thesis raises some interesting questions which could provide the basis for future research. We observed that for the C_3 symmetric 3-monopole family in Section (3.4.7) a hyperbolic monopole can be 'centred' in the sense of [MNS01] even if one monopole is on the boundary and the other is not. It would be interesting to obtain a physical understanding of this phenomenon. Another problem raised by the work in Chapter 3 is that we were unable to perform the integral (3.62) to find the metric on the space of centred

2-monopoles in a simple, closed form. A deeper knowledge of the geometric properties of this metric might make the integral more tractable.

Even if we cannot calculate it explicitly, this integral may still yield interesting information. For example, one could see if the integral simplifies in the asymptotic regime where the monopoles are well-separated. One could then try to adapt the derivation of the Gibbons-Manton metric for well-separated monopoles [GM95] on Euclidean space to this hyperbolic case, and compare it with the asymptotic metric defined by (3.62).

All the monopoles in Chapters 3 and 4 were constructed by imposing symmetry. The Nahm data for an interesting family of Euclidean monopoles without symmetry was discovered by Ercolani and Sinha in [ES89]; the configuration consists of N equidistant monopoles along a line. The original motivation for deriving the axial hyperbolic monopole data (4.17) was to see if a simple deformation of the data gives a hyperbolic version of the Ercolani-Sinha data. Unfortunately we were not able to find such a deformation. It seems quite possible that such monopoles could lie in the space of JNR-type monopoles, but it is much harder to find these than the symmetric examples, because we do not know the constraints on the spectral curve.

We concentrated on localised impurities in Chapter 5, but we could explore the opposite extreme where the impurity is very spread out. The case where σ is a constant greater than -1 just corresponds to a rescaling of the Higgs field, but clearly the case of constant $\sigma \leq -1$ is qualitatively different. It might also be interesting to consider non-constant impurities which integrate to zero, or non-axially symmetric impurities. Another interesting direction might be to try to calculate the volume of the moduli space of vortices on the 2-sphere in the presence of impurities, since this is known to be possible in the impurity-free case [MN99].

Appendix A

Standard form ADHM data from the JNR ansatz

A.1 Proof of equation (3.8)

In this Section we will prove the formula (3.8), showing that the matrices V and S defined by (3.9) and (3.10) respectively do perform the required change of basis. In the next Section of this appendix we will show that $S \in \mathrm{O}(N+1)$.

We will prove (3.8) using induction on N. The identity (3.8) can be written as

$$\sum_{j=1}^{N} \sum_{i=1}^{N+1} S_{ai} Q_{ij} V_{jb} = \delta_{a-1,b} \tag{A.1}$$

where

$$Q = \begin{pmatrix} \lambda_1 & \lambda_2 & \cdots & \lambda_N \\ \lambda_0 & & & \\ & \lambda_0 & & \\ & & \ddots & \\ & & & \lambda_0 \end{pmatrix}$$

The $N = 1$ case is trivial. Suppose for induction that (A.1) holds at charge $N-1$, denoting the relevant matrices at this step by S', V'. We can relate S', V' to the corresponding matrices S, V at the N-th step by

$$S_{1b} = S'_{1b} p_N / p_{N-1} \tag{A.2}$$

$$S_{ab} = S'_{ab} \tag{A.3}$$

for $1 \leq b \leq N$, $2 \leq a \leq N$, and

$$V_{ab} = V'_{ab} \tag{A.4}$$

for $1 \leq a, b \leq N-1$.

We can write

$$\sum_{j=1}^{N}\sum_{i=1}^{N+1} S_{ai}Q_{ij}V_{jb} = \sum_{j=1}^{N-1}\sum_{i=1}^{N} S_{ai}Q_{ij}V_{jb} + \sum_{i=1}^{N+1} S_{ai}Q_{iN}V_{Nb} + \sum_{j=1}^{N} S_{a,N+1}Q_{N+1,j}V_{jb} - S_{a,N+1}Q_{N+1,N}V_{Nb} \tag{A.5}$$

Suppose first that $a < N+1$ and $b < N$. Then by induction and the relations (A.2)-(A.4), the first term in the right-hand side of (A.5) is equal to $\delta_{a-1,b}$. Also $V_{Nb} = 0$, so the second and fourth terms give zero, while the third term is

$$\sum_{j=1}^{N} S_{a,N+1}Q_{N+1,j}V_{jb} = S_{a,N+1}Q_{N+1,N}V_{Nb} = 0$$

so we have shown that (A.1) is true for $a < N+1$ and $b < N$. We now prove (A.1) for the remaining possible values of a, b. We can write the sum (A.1) as

$$\begin{aligned}\sum_{j=1}^{N}\sum_{i=1}^{N+1} S_{ai}Q_{ij}V_{jb} &= \sum_{j=1}^{N}\left(S_{a1}Q_{1j}V_{jb} + \sum_{i=2}^{N+1} S_{ai}Q_{ij}V_{jb}\right) \\ &= S_{a1}\sum_{j=1}^{N}\lambda_j V_{jb} + \sum_{j=1}^{N}\sum_{i=2}^{N+1} S_{ai}\lambda_0\delta_{i-1,j}V_{jb} \\ &= S_{a1}\sum_{j=1}^{N}\lambda_j V_{jb} + \lambda_0\sum_{j=1}^{N} S_{a,j+1}V_{jb}\end{aligned} \tag{A.6}$$

and then the first term can be calculated to be:

$$\begin{aligned}S_{a1}\sum_{j=1}^{N}\lambda_j V_{jb} &= \lambda_{a-1}p_{a-1}p_{a-2}\left(-\sum_{j=1}^{b-1}\lambda_j^2\lambda_b p_b p_{b-1} + \frac{\lambda_b p_b}{p_{b-1}}\right) \\ &= \lambda_{a-1}\lambda_b p_{a-1}p_{a-2}p_b\left(p_{b-1}\left(\lambda_0^2 - \frac{1}{p_{b-1}^2}\right) + \frac{1}{p_{b-1}}\right) \\ &= \lambda_0^2\lambda_b\lambda_{a-1}p_{a-1}p_{a-2}p_b p_{b-1}\end{aligned} \tag{A.7}$$

We now examine the remaining cases in turn.

$b = N,\ a = 1$

The sum (A.6) now becomes

$$\lambda_0^3 \lambda_N p_0 p_N^2 p_{N-1} + \lambda_0 \left(\sum_{j=1}^{N-1} S_{1,j+1} V_{jN} + S_{1,N+1} V_{NN} \right) = \lambda_0^2 \lambda_N p_N^2 p_{N-1} + \sum_{j=1}^{N-1} \lambda_j^2 \lambda_N p_N^2 p_{N-1} - \frac{\lambda_N p_N^2}{p_{N-1}} \quad \text{(A.8)}$$

since $\lambda_0 p_0 = 1$. We can write this as

$$\lambda_0^2 \lambda_N p_N^2 p_{N-1} + \lambda_N p_N^2 p_{N-1} \left(\frac{1}{p_{N-1}^2} - \lambda_0^2 \right) - \frac{\lambda_N p_N^2}{p_{N-1}} = 0$$

as required.

$b = N,\ 1 < a \leq N + 1$

The second term in (A.6) is now

$$\lambda_0^2 \sum_{j=1}^{N} V_{j,a-1} V_{jN} = \lambda_0^2 \sum_{j=1}^{a-2} V_{j,a-1} V_{jN} + \lambda_0^2 V_{a-1,a-1} V_{a-1,N} \quad \text{(A.9)}$$

At this point we must distinguish the cases $a < N + 1$, and $a = N + 1$. If $2 < a < N + 1$, then (A.9) is

$$\begin{aligned} &\sum_{j=1}^{a-2} \lambda_j^2 \lambda_N \lambda_{a-1} p_{a-1} p_{a-2} p_N p_{N-1} - \lambda_{a-1} \lambda_N p_{a-1} p_N p_{N-1} / p_{a-2} \\ &\quad = \lambda_{a-1} \lambda_N p_{a-1} p_{a-2} p_N p_{N-1} \left(\frac{1}{p_{a-2}^2} - \lambda_0^2 \right) - \lambda_{a-1} \lambda_N p_{a-1} p_N p_{N-1} / p_{a-2} \\ &\quad = -\lambda_0^2 \lambda_{a-1} p_{a-1} p_{a-2} \lambda_N p_N p_{N-1} \quad \text{(A.10)} \end{aligned}$$

and if $a = 2 < N + 1$ then it is easy to check that (A.9) is still equal to (A.10). (A.6) is the sum of (A.7) and (A.10), and this is equal to zero as required.

Now suppose that $a = N + 1$. Then using (A.7) and (A.9) the sum (A.6) becomes

$$\begin{aligned}\sum_{j=1}^{N}\sum_{i=1}^{N+1} S_{N+1,i}Q_{ij}V_{jN} &= \lambda_0^2\lambda_N^2 p_N^2 p_{N-1}^2 + \sum_{j=1}^{N-1}\lambda_j^2\lambda_N^2 p_N^2 p_{N-1}^2 + p_N^2/p_{N-1}^2 \\ &= \lambda_0^2\lambda_N^2 p_N^2 p_{N-1}^2 + p_N^2\lambda_N^2 p_{N-1}^2\left(\frac{1}{p_{N-1}^2} - \lambda_0^2\right) + \frac{p_N^2}{p_{N-1}^2} \\ &= p_N^2\left(\lambda_N^2 + \frac{1}{p_{N-1}^2}\right) \\ &= 1 \end{aligned} \tag{A.11}$$

as required.

$a = N + 1,\ b < N$

Using (A.7), we can write the sum as

$$\sum_{j=1}^{N}\sum_{i=1}^{N+1} S_{N+1,i}Q_{ij}V_{jb} = S_{N+1,1}\sum_{j=1}^{N}\lambda_j V_{jb} + \lambda_0\sum_{j=1}^{N} S_{N+1,j+1}V_{jb} \tag{A.12}$$

$$= \lambda_0^2\lambda_b\lambda_N p_N p_{N-1} p_b p_{b-1} + \lambda_0^2\sum_{j=1}^{N} V_{j,N}V_{jb} \tag{A.13}$$

The second term in (A.12) is the same as (A.9) with $b = a - 1 < N$, so using (A.10) the sum (A.12) is equal to 0, as required.

A.2 Proof that S is orthogonal

To show that $S \in \mathrm{O}(N + 1)$, we will use induction and the fact that a matrix is orthogonal if its rows are orthonormal.

The $N = 1$ step is trivial. Suppose for the induction step that $S' \in \mathrm{O}(N)$. Then, since $S_{a,N+1} = 0$ for $2 \le a \le N$,

$$\sum_{j=1}^{N+1} S_{aj}S_{bj} = \delta_{ab} \tag{A.14}$$

for $2 \le a, b \le N$. Also, for $2 \le b \le N$,

$$\sum_{j=1}^{N+1} S_{1j}S_{bj} = \frac{p_N}{p_{N-1}}\sum_{j=1}^{N} S'_{1j}S'_{bj} + S_{1,N+1}S_{b,N+1} = 0$$

and

$$\begin{aligned}\sum_{j=1}^{N+1} S_{1j}^2 &= \frac{p_N^2}{p_{N-1}^2}\sum_{j=1}^{N}(S'_{1j})^2 + S_{1,N+1}^2 \\ &= \frac{p_N^2}{p_{N-1}^2} + \lambda_N^2 p_N^2 \\ &= 1\end{aligned}$$

by (A.2) and induction. The only thing left to prove is that

$$\sum_{j=1}^{N+1} S_{N+1,j}S_{bj} = \delta_{N+1,b}$$

for $1 \leq b \leq N+1$. We distinguish the cases $b = 1$, $1 < b < N+1$ and $b = N+1$.

$b = 1$

We have

$$\begin{aligned}\sum_{j=1}^{N+1} S_{N+1,j}S_{1j} &= S_{N+1,1}S_{11} + \sum_{j=2}^{N+1} S_{N+1,j}S_{1j} \\ &= \lambda_0^2\lambda_N p_N^2 p_{N-1} + \sum_{j=1}^{N-1}\lambda_j^2\lambda_N p_N^2 p_{N-1} - \frac{\lambda_N p_N^2}{p_{N-1}} \\ &= \lambda_0^2\lambda_N p_N^2 p_{N-1} + \lambda_N p_N^2 p_{N-1}\left(\frac{1}{p_{N-1}^2} - \lambda_0^2\right) - \frac{\lambda_N p_N^2}{p_{N-1}} \\ &= 0\end{aligned}$$

$1 < b < N+1$

$$\begin{aligned}\sum_{j=1}^{N+1} S_{N+1,j}S_{bj} &= S_{N+1,1}S_{b1} + \sum_{j=2}^{N+1} S_{N+1,j}S_{bj} \\ &= \lambda_0^2\lambda_N\lambda_{b-1}p_N p_{N-1}p_{b-1}p_{b-2} + \lambda_0^2\sum_{j=1}^{N} V_{j,N}V_{j,b-1} \\ &= 0\end{aligned}$$

using the expression (A.10) we derived in the previous Section for the second term in (A.15).

$b = N + 1$

$$\sum_{j=1}^{N+1} S_{N+1,j}^2 = S_{N+1,1}^2 + \sum_{j=2}^{N+1} S_{N+1,j}^2 \tag{A.15}$$

$$= (\lambda_0 \lambda_N p_N p_{N-1})^2 + \lambda_0^2 \sum_{j=1}^{N} V_{jN}^2 \tag{A.16}$$

At this point we can see that (A.16) is the same as (A.11), which we calculated to be 1.

Bibliography

[AH88] M. F. Atiyah and N. J. Hitchin. *The Geometry and Dynamics of Magnetic Monopoles*. Princeton University Press, 1988.

[AHDM78] M. F. Atiyah, N. J. Hitchin, V. G. Drinfeld, and Y. I. Manin. Construction of Instantons. *Phys. Lett.*, A65:185, 1978.

[AHS77] M. F. Atiyah, N. J. Hitchin, and I. M. Singer. Deformations of instantons. *Proc. Natl. Acad. Sci. USA*, 74:2662, 1977.

[AS13] J. Allen and P. M. Sutcliffe. ADHM Polytopes. *JHEP*, 1305:63, 2013.

[Ati79] M. F. Atiyah. *Geometry of Yang-Mills fields*. Fermi lectures (Scuola Normale Superiore, Pisa), 1979.

[Ati84] M. F. Atiyah. Magnetic monopoles in hyperbolic space. *Proc. Bombay Colloq. on Vector Bundles*, pages 1–34, 1984.

[BA90] P. J. Braam and D. M. Austin. Boundary values of hyperbolic monopoles. *Nonlinearity*, 3(3):809, 1990.

[BC89] M. S. Berger and Y. Y. Chen. Symmetric vortices for the ginzburg-landau equations of superconductivity and the nonlinear desingularization phenomenon. *J. Func. Anal.*, 82:259, 1989.

[BCS15] S. Bolognesi, A. H. Cockburn, and P. M. Sutcliffe. Hyperbolic monopoles, JNR data and spectral curves. *Nonlinearity*, 28:211, 2015.

[BDE11] H.W. Braden, A. D'Avanzo, and V.Z. Enolski. On Charge-3 Cyclic Monopoles. *Nonlinearity*, 24:643, 2011.

[BM03] J. M. Baptista and N. S. Manton. The Dynamics of vortices on S**2 near the Bradlow limit. *J. Math. Phys.*, 44:3495, 2003.

[BPST75] A. A. Belavin, A. M. Polyakov, A. S. Schwartz, and Yu. S. Tyupkin. Pseudoparticle Solutions of the Yang-Mills Equations. *Phys. Lett.*, B59:85, 1975.

[Bra90] S.B. Bradlow. Vortices in holomorphic line bundles over closed Kähler manifolds. *Commun. Math. Phys.*, 135:1, 1990.

[BvB89] P. J. Braam and P. van Baal. Nahm's Transformation for Instantons. *Commun. Math. Phys.*, 122:267, 1989.

[CD09] S. A. Cherkis and B. Durcan. The 't hooftpolyakov monopole in the presence of a 't hooft operator. *Phys. Lett.*, B 671(1):123, 2009.

[CF77] E. Corrigan and D.B. Fairlie. Scalar Field Theory and Exact Solutions to a Classical SU(2) Gauge Theory. *Phys. Lett.*, B67:69, 1977.

[Coc14] A. H. Cockburn. Symmetric Hyperbolic Monopoles. *J. Phys. A: Math. Theor.*, 47:395, 2014.

[CWS78] N. H. Christ, E. J. Weinberg, and N. K. Stanton. General self-dual yang-mills solutions. *Phys. Rev.*, D18:2013, Sep 1978.

[Dir31] P. A. M. Dirac. Quantised singularities in the electromagnetic field. *Proc. R. Soc. Lond. A*, 38:60, 1931.

[Don84] S. K. Donaldson. Nahm's equations and the classification of monopoles. *Commun. Math. Phys.*, 96(3):387, 1984.

[ES89] N. Ercolani and A. Sinha. Monopoles and Baker Functions. *Commun. Math. Phys.*, 125:385, 1989.

[FOG14] J. Figueroa-O'Farrill and M. Gharamti. Supersymmetry of hyperbolic monopoles. *JHEP*, 1404:74, 2014.

[GM95] G.W. Gibbons and N.S. Manton. The Moduli space metric for well separated BPS monopoles. *Phys. Lett.*, B356:32, 1995.

[GS00] S. Gustafson and I. M. Sigal. The stability of magnetic vortices. *Commun. Math. Phys.*, 212:257, 2000.

[Har] D. Harland. Personal communication.

[Har08] D. Harland. Hyperbolic calorons, monopoles, and instantons. *Commun. Math. Phys.*, 280:727, 2008.

[Hit82] N. J. Hitchin. Monopoles and geodesics. *Commun. Math. Phys.*, 83(4):579, 1982.

[Hit96] N. J. Hitchin. *A new family of Einstein metrics*. Cambridge University Press, 1996.

[HMM95] N. J. Hitchin, N. S. Manton, and M. K. Murray. Symmetric monopoles. *Nonlinearity*, 8:661, 1995.

[Hou99] C. J. Houghton. Instanton vibrations of the three Skyrmion. *Phys. Rev.*, D60:105003, 1999.

[HS96a] C. J. Houghton and P. M. Sutcliffe. Monopole scattering with a twist. *Nucl. Phys.*, B464:59, 1996.

[HS96b] C. J. Houghton and P. M. Sutcliffe. Tetrahedral and cubic monopoles. *Commun. Math. Phys.*, 180:343, 1996.

[HS96c] Conor J. Houghton and Paul M. Sutcliffe. Octahedral and dodecahedral monopoles. *Nonlinearity*, 9:385, 1996.

[Jar00] S. Jarvis. A rational map for euclidean monopoles via radial scattering. *J. reine angew. Math.*, 524:17, 2000.

[JN97] S. Jarvis and P. Norbury. Zero and infinite curvature limits of hyperbolic monopoles. *Bull. London Math. Soc.*, 29:737, 1997.

[JNR77] R. Jackiw, C. Nohl, and C. Rebbi. Conformal Properties of Pseudoparticle Configurations. *Phys. Rev.*, D15:1642, 1977.

[JT80] A. Jaffe and C. Taubes. *Vortices and monopoles*. Birkhäuser, 1980.

[KS83] V. E. Korepin and S. L. Shatashvili. Rational parametrization of the three-instanton solutions of the yang-mills equations. *Sov. Phys. Dokl.*, 28:1018, 1983.

[Man78] N.S. Manton. Complex Structure of Monopoles. *Nucl. Phys.*, B135:319, 1978.

[Man82] N.S. Manton. A Remark on the Scattering of BPS Monopoles. *Phys. Lett.*, B110:54, 1982.

[Man12] N.S. Manton. Monopole Planets and Galaxies. *Phys. Rev.*, D85:045022, 2012.

[MN99] N.S. Manton and S.M. Nasir. Volume of vortex moduli spaces. *Commun. Math. Phys.*, 199:591, 1999.

[MNS01] M. K. Murray, P. Norbury, and M. A. Singer. Hyperbolic monopoles and holomorphic spheres. *Ann. Global Anal. Geom.*, 23:101, 2001.

[MS00] M. K. Murray and Michael A. Singer. On the complete integrability of the discrete Nahm equations. *Commun. Math. Phys.*, 210:497, 2000.

[MS03] N.S. Manton and J.M. Speight. Asymptotic interactions of critically coupled vortices. *Commun. Math. Phys.*, 236:535, 2003.

[MS04] N. S. Manton and P. M. Sutcliffe. *Topological Solitons*. Cambridge University Press, 2004.

[MS14] N. S. Manton and P. M. Sutcliffe. Platonic hyperbolic monopoles. *Commun. Math. Phys.*, 325:821, 2014.

[Nah80] W. Nahm. A Simple Formalism for the BPS Monopole. *Phys. Lett.*, B90:413, 1980.

[Nas86] C. Nash. Geometry of hyperbolic monopoles. *J. Math. Phys.*, 27:2160, 1986.

[Nas07] O. Nash. A new approach to monopole moduli spaces. *Nonlinearity*, 20(7):1645, 2007.

[NR07] P. Norbury and N. M. Romao. Spectral curves and the mass of hyperbolic monopoles. *Commun. Math. Phys.*, 270:295, 2007.

[Osb81] H. Osborn. Semiclassical Functional Integrals for Selfdual Gauge Fields. *Annals Phys.*, 135:373, 1981.

[Pra81] M. K. Prasad. Yang-mills-higgs monopole solutions of arbitrary topological charge. *Commun. Math. Phys.*, 80(1):137, 1981.

[PS75] M. K. Prasad and C. M. Sommerfield. Exact solutions for the 't hooft monopole and the julia-zee dyon. *Phys. Rev. Lett.*, 35:760, 1975.

[Sam92] T.M. Samols. Vortex scattering. *Commun. Math. Phys.*, 145:149, 1992.

[Sch77] A. S. Schwarz. On regular solutions of euclidean yang-mills equations. *Phys. Lett.*, B67:172, 1977.

[Spe97] J. M. Speight. Static intervortex forces. *Phys. Rev.*, D55:3830, 1997.

[SS99] M. A. Singer and P. M. Sutcliffe. Symmetric instantons and Skyrme fields. *Nonlinearity*, 12:987, 1999.

[Str92] I. A. B. Strachan. Low velocity scattering of vortices in a modified Abelian Higgs model. *J. Math. Phys.*, 33:102, 1992.

[Stu94a] D. Stuart. Dynamics of abelian higgs vortices in the near bogomolny regime. *Commun. Math. Phys.*, 159(1):51, 1994.

[Stu94b] D. Stuart. The Geodesic approximation for the Yang-Mills Higgs equations. *Commun. Math. Phys.*, 166:149, 1994.

[Sut97] P. M. Sutcliffe. Cyclic monopoles. *Nucl. Phys.*, B505:517, 1997.

[Sut12] P. M. Sutcliffe. Hyperbolic vortices with large magnetic flux. *Phys. Rev.*, D85:125015, 2012.

[tH] G. 't Hooft. unpublished.

[Ton02] D. Tong. NS5-branes, T duality and world sheet instantons. *JHEP*, 0207:013, 2002.

[TW14] D. Tong and K. Wong. Vortices and Impurities. *JHEP*, 1401:090, 2014.

[War77] R. S. Ward. On Selfdual gauge fields. *Phys.Lett.*, A61:81, 1977.

[War82] R. S. Ward. A yang-mills-higgs monopole of charge 2. *Commun. Math. Phys.*, 86:437, 1982.

[War99] R. S. Ward. Two integrable systems related to magnetic monopoles. *Asian J. Math.*, 3:325, 1999.

[Wei79a] E. J. Weinberg. Multivortex solutions of the ginzburg-landau equations. *Phys. Rev. D*, 19:3008, May 1979.

[Wei79b] E. J. Weinberg. Parameter counting for multimonopole solutions. *Phys. Rev. D*, 20:936, Aug 1979.

[WG76] E. J. Weinberg and A. H. Guth. Nonexistence of spherically symmetric monopoles with multiple magnetic charge. *Phys. Rev.*, D 14:1660, 1976.

[Wit76] E. Witten. Some exact multi-pseudoparticle solutions of classical yang-mills theory. *Phys. Rev. Lett.*, 1976.

[WW90] R. S. Ward and R. O. Wells. *Twistor Geometry and Field Theory.* Cambridge University Press, 1990.